POLITECNICO DI TORINO
III FACOLTÀ INGEGNERIA DELL'INFORMAZIONE

PONTIFICIA UNIVERSIDAD JAVERIANA COLOMBIA
ELECTRONIC ENGINEERING DEPARTMENT

HARDWARE IMPLEMENTATION OF A MEASUREMENT UNIT FOR BOREA QUADRICOPTER

Corso di Laurea Magistrale in Ingegneria elettronica(electronic engineering)

Relatore
Prof. Enrico Canuto

Co-relatore
Carlos Norberto Perez
Montenegro

Laureando
Santiago Andres Lopez Carmona

Anno Accademico 2011-2012

Table of Contents

LIST OF FIGURES

LIST OF TABLES

Acknowledgments

1. INTRODUCTION

In this thesis is presented the behavior and the work analysis of the IMU's sensors that are, with the microcontroller, within a development board UBD4, along with the simulation of the lectures of the sensors. The purpose of this work is to show that is possible to obtain in a synchronous way the lecture of all the sensors, with different acquisition time, to use them in the control of the quadricopter Borea. With the term quadricopter is indicated to an Unmanned Aerial Vehicle" (UAV), usually called drone and as the name implies, it is an aircraft without a human pilot on board. On the other hand, with the term Borea is indicated the project development by the team "The Space and Precision Automatics" (S&PA) of the Politecnico di Torino led by the professor Enrico Canuto. UAVs are currently used for a number of missions, including reconnaissance and attack roles, remote sensing, commercial aerial surveillance, gas and mineral exploration and production, transport, scientific research and conservation. However, especially talking of quadricopter Borea, it is developed to simulate control algorithms for a soft landing.

In the first chapter of the thesis is introduced the fundamental definitions to describe the quadricopter Borea, along with necessary theoretical explications to understand the results of the sensors. In first place is necessary to talk about the UVA's to be aware that are aircraft without a human pilot on board that can be either remote controlled aircraft or can fly autonomously based on computers on the vehicle. Therefore, to be able to fly autonomously based on computers on the vehicle, the IMU concept has to be introduced. Inertial measurement unit IMU is an electronic device that measures and reports the velocity, orientation, and gravitational forces of the aircraft. The IMU is composed of accelerometers, gyroscopes, and sometimes also of magnetometers, and it has to be on board of UVA's because the information that different sensors provides is required to make the control of the vehicle. Right away are presented the sensors that could be present on board the UAV. Due to there are many sensors, for the purpose of UAVs, the attitude determination would be the criteria that I use to show the sensors. Within this category, I classify the sensors in inertial sensors, attitude sensors and position sensors. However the most important sensors for this thesis work are the accelerometers, gyroscopes and magnetometers. In the next part of the chapter is presented the basic definition of power spectral density, average and deviation standard. These concepts are important because they are calculated from the simulation of the sensor's lectures and they are used to analyze if the sensor gives an optimum response to be use in the quadricopter Borea. At the end of the chapter is presented the quadricopter Borea with its features and spatial distribution of its components.

The aim the second chapter is to describe all the hardware that is necessary to obtain the sensor's lectures. In first place is presented the UDB4 that is the latest UAV Development Board that comes with a dsPIC33FJ256 CPU, an MMA7361 three axis accelerometer, a dual axis IDG500 gyroscope, and a single axis ISZ500 gyroscope. It was selected for this project because the board can be used to develop a three axis IMU controller. The MMA7361 accelerometer consists of a surface micro machined, capacitive sensing cell (g-cell) and a signal conditioning ASIC contained in a single package. The g-cell is a mechanical structure formed from semiconductor materials (polysilicon). The accelerometer can be modeled as

a set of beams attached to a movable central mass that move between fixed beams, making that the distance from them to the fixed beams on one side will increase by the same amount that the distance to the fixed beams on the other side decreases. This change in distance is a measure of acceleration. The IDG-500 consists of two independent vibratory MEMS gyroscopes. One detects rotation about the X-axis; the other detects rotation about the Y-axis. When the sensor is rotated about the X- or Y axis, the Coriolis effect causes a vibration that can be detected by a capacitive pickoff that produce an analog voltage that is proportional to the angular rate. Lastly the ISZ-500 is a single-axis Z-gyroscope designed specifically for complex motion sensing in 3D-input devices and gaming controllers. However it has the same principle of operation of The IDG-500. Right away is presented the HMC5883L magnetometer, it is not within the UDB4; however the board has the connection for the magnetometer. The Honeywell HMC5883L is a surface-mount, multi-chip module designed for low-field magnetic sensing with a digital interface. It consists in a magneto resistive sensor circuit that measure magnetic fields. So the sensor converts any incident magnetic field in the sensitive axis directions to a differential voltage output. In other words, in the presence of a magnetic field, a change in the bridge resistive elements causes a corresponding change in voltage across the bridge outputs. In the second part of the chapter I present the dsPIC33FJ256GP710A that is the microcontroller integrated in the UBD4. It is a 16-bit digital signal controller, with flash program memory of 256Kb and special for embedded applications. In order to obtain the lecture of the sensors is needed the configuration of the oscillator, the timer, the I/O port, the ADC and the I2C module of the microcontroller. The frequency of the oscillator, that is called FOSC, can be generated by 6 different sources: the primary oscillator, the second oscillator, the internal fast RC oscillator, the internal low-power RC oscillator, the primary oscillator with PLL and the internal fast RC oscillator with PLL. The next module is the timer. There are 3 different types of timer: type A, B and C. They are classify according to their functional differences like; the type A is the only one that can be used for Real-Time Clock (RTC) applications; Type C timer has the ability to trigger an Analog-to-Digital (A/D) conversion; and the type B can be concatenated with a Type C timer to form a 32-bit timer. Moreover, there are four different modes in which the timer module can operate: Timer mode, Gated Timer mode, Synchronous Counter mode Asynchronous Counter mode where just for type A. All the microcontroller device pins can be used for general purpose of Input/output (I/O) ports. The I/O port registers are in charge of determine whether each pin associated with the I/O port is an input or an output and to read or write in the pin. The next module is the ADC. The microcontroller has up to 32 A/D input channels, the analog inputs are multiplexed to four Sample/Hold amplifiers, where one, two, or four of the Sample/Hold amplifiers can be enabled for acquiring input data. The ADC is connected to a single-word result buffer. Each conversion result is converted to one of four 16-bit output formats when it is read from the buffer. Finally, the last module is the I^2C module. I^2C Stands for inter-Integrated circuit module. This module is a serial interface very useful for communicating with others peripherals; it can operate as a slave, as a master or as a master/slave device in a multi-master system. It contains a Baud Rate Generator that does not consume other timer resources in the microcontroller.

The third chapter introduces the configurations of every device on the UDB4 and every module in the microcontroller, along with the explication of why is configure

in that way. First, the oscillator is configured to operate as fast as it possible could go in order to obtain a high frequency operation of instructions. To this aim, the internal fast RC is selected to work with the PLL. As a result the microcontroller runs at 40 MIPS (80 MHz). However the clock frequency is half of oscillator's frequency therefore the clock frequency is 40MHz. I use two timers type A in a counter mode. The first timer is use to generate an interruption every 1ms and the second timer is use to generate an interruption every 20ms. The first timer is use to run the instruction where all data output of the ADC is save. In the other hand, the second timer is use to run the instruction where all the data output of the magnetometer is save. For the I/O ports, just the ports where the outputs of the sensors are connected are configured as an input of the microcontroller. The ADC module is configured in 12-bit mode and operates as fast as it can. The conversion clock (TAD) is 75ns because is the minimum possible. The A/D conversion requires minimum 14 clock periods (14 TAD) because there are 12-bit. Therefore the conversion time for each channel is 14*75ns, this is 1.05us. There are 9 channels, each one is an axis of the sensor, and they are selected manually to convert. Finally the I^2C module is use to communicate the microcontroller, as a master, with the magnetometer, as a slave. In this communication there are two main types of operations, the write command to configure 3 registers of the magnetometer, and the read command to obtain the data value of the three axes of the magnetometer.

In the last chapter are presented all the results and the simulation of the sensor's lectures. The sensors were subjected to a test that consists in measure the data output of every sensor in an uncontrolled environment and then make the same measures on a controlled environment in order to compare the noise and the power spectral density on each one. Every sensor has its own method to be measure for instance the accelerometer has three axes, and then every single axis has to be subjected to positive gravity and negative gravity. The magnetometer has its own self test, where a current is forced to pass in positive and negative way. Therefore there will be a known electromagnetic field in each axis for positive and negative way. And finally, the gyroscope is measure without any gyro or disturbance just to see the noise in each axis. The controlled environment was possible to obtain with a "StableTop 450 Optical tabletops " which is an optical table enhanced with proprietary tuned and broadband dampers, moreover, the table has self-leveling vibration isolator and super damp isolators, that provides total vertical and horizontal isolation with extremely low resonant frequency and constant height. The optical table was provided by Thales Alenia space. Throughout the chapter is presented the simulations in time of every axis of every sensor along with the power spectral density and the values of average and deviation standard.

At the end of the work are presented the conclusions. After all, it was possible to obtain all the sensors lectures with different acquisition time, however, is better to analyze the sensors in a controlled environment due to there are not present external vibrations or aliasing errors. The sensors are optimum for use in the control of the quadricopter Borea.

2. STATE OF ART

This work contains an analysis of the operation and behavior of three sensors for the inertial navigation system of the quadricopter Borea. These sensors are accelerometer, gyroscope and magnetometer. First I present some fundamental definitions related to UAVs, IMU and sensors clarify basic content. Then I introduce the hardware used by the quadricopter Borea. At this point I discuss about the configuration implemented in the hardware in order to achieve the requirements desired. Finally I will present all the results of the sensors. These results show the noise power spectral density of every sensor. Also I present the difference between the results of an uncontrolled environment and a controlled environment. The goal of this work is to help the reader to become familiar with the development sensors firmware.

2.1 UAV

The Unmanned Aerial Vehicle (UAV). UAVs can be either remote controlled aircraft (e.g. pilot on the ground) or can fly autonomously based on computers on the vehicle. UAVs are currently used for a number of missions, including reconnaissance and attack roles, remote sensing, commercial aerial surveillance, gas and mineral exploration and production, transport, scientific research and conservation. There are a wide variety of UAV shapes, sizes, configurations, and characteristics. But they are predominantly deployed for military applications.

2.1.1 UAV Types:

Target and decoy - providing ground and aerial gunnery a target that simulates an enemy aircraft or missile.
Reconnaissance - providing battlefield intelligence.
Combat - providing attack capability for high-risk missions (see Unmanned Combat Air Vehicle).
Research and development - used to further develop UAV technologies to be integrated into field deployed UAV aircraft.
Civil and Commercial UAVs - UAVs specifically designed for civil and commercial applications.

At first UAVs were called drones because UAVs were simple remotely piloted aircraft, this mean that a human pilot radio controls the aircraft from the ground at all times. But, since autonomous control is increasingly being employed there are more sophisticated versions of UAVs that may have built-in control and/or guidance systems with low level human pilot duties.

From this perspective, most early UAVs were not complete autonomous. In fact, the field of air vehicle autonomy is a recently emerging field, Because of this; autonomy has been and may continue to be the bottleneck for future UAV developments. According to this, these are the categories where the autonomy technology is becoming important:

Sensor fusion: Combining information from different sensors for use on board the vehicle

Communications: Handling communication and coordination between multiple agents in the presence of incomplete and imperfect information

Motion planning (also called Path planning): Determining an optimal path for vehicle to go while meeting certain objectives and constraints, such as obstacles

Trajectory Generation: Determining an optimal control maneuver to take to follow a given path or to go from one location to another

Task Allocation and Scheduling: Determining the optimal distribution of tasks amongst a group of agents, with time and equipment constraints

Cooperative Tactics: Formulating an optimal sequence and spatial distribution of activities between agents in order to maximize chance of success in any given mission scenario

Finally, in UAV context the autonomy is defined as the ability to make decisions without human intervention, this mean the ability of the machine to be "smart" and act like humans. From this perspective is commonly to associate the autonomy of the aircraft with the field of artificial intelligence .However, the mode of technological development in the field of autonomy is driven by the field of control science and not computer science, as one may think.

2.2 IMU

One of the most important categories in the autonomy technology is sensor fusion. Because the information that different sensors provides is required to make the control of the vehicle. With the control the aircraft is able to make the speed and flight path stabilization, and simple prescript navigation functions such as waypoint following, between many.

According to this, the aircraft need on boar an Integrated Inertial System. Because It contains the MEMS sensors (Micro-Electro-Mechanical Systems sensors) such as accelerometer and gyroscope, combined into full performance inertial navigation system (INS) aided by GPS receiver. The system outputs give the attitude and position data of the vehicle and transmit it to main board.

An electronic device that measures and reports the velocity, orientation, and gravitational forces of the aircraft is an inertial measurement unit, or IMU. The IMU is composed of accelerometers, gyroscopes, and sometimes also of magnetometers. Typically the IMUs are used to maneuver unmanned aerial vehicles (UAVs), spacecraft (satellites and landers), watercraft, and guided missiles among others.

Also the IMU is the main component of inertial navigation systems (INS). This is why the system outputs are in capacity of give the attitude and position data of the vehicle and transmits it to main board. The method in which the computer can track the craft's position allowed by the sensors is called dead reckoning.

Dead Reckoning is the process of estimating your position by advancing a known position using course, speed, time and distance to be traveled. In other words figuring out where you will be at a certain time if you hold the speed, time and course you plan to travel (1).

One of the most important developments of IMU is the production of IMU-enabled GPS devices. The device allows a GPS to work when GPS-signals are unavailable, this mean work in tunnels, inside buildings, or when electronic interference is present.

Is very common to associate the IMU with devices that only have three accelerometers, three gyroscopes, and, optionally, three magnetometers. Because the accelerometers are placed to measure inertial acceleration, which are known as G-forces. The gyroscopes are placed to measure angular velocity, in other words rotational position in reference to an arbitrarily coordinate system. And last, the magnetometers that allows better performance for dynamic orientation and calculation in attitude and heading in reference systems.

2.2.1   Disadvantages

There are a few disadvantages of using IMUs for navigation. The major disadvantage is that the IMU typically suffer from accumulated error, like Abbe error which "describes the magnification of angular error over distance." (2). These errors are because the dead reckoning method, in other words, because the guidance system is continually adding detected changes to its previously-calculated positions. Then any small errors in measurement is accumulated from point to point leading the aircraft to 'drift' or an increasing difference between where the system thinks it is located, and the actual location.

Because of the errors is why the IMUs are normally a navigation system component and others devices and systems are used to correct the errors that IMUs inevitably has. These devices could be a GPS, gravity sensors (for local vertical), external speed sensors (to compensate for velocity drift), a barometric system for attitude correction, and a magnetic compass.

2.3 SENSORS

In order to deal with all possible UAVs-on-board sensors is necessary to know something about type and classification of sensors. Next I will present some kind of sensors used in UAVs along with a brief explanation of them.

It should be noted that exist several criteria for classifying sensors. For the purpose of UAVs, the attitude determination would be the criteria that I will use. Therefore, here, sensors are distinguished between:

- Inertial sensors: Sensors capable of sensing movement variations without any communication link or field-of-view (3), like accelerometers and gyroscopes.

- Attitude sensors: Sensors capable of sensing movement variations with and without field-of-view. Sensors with field-of-view like the classical Sun and Earth sensors, star trackers and GPS (Global Positioning System). Sensors without field-of-view like magnetometers. It is important to say that some sensors are only for spatial use.

- Position sensors: Sensors which Accuracy limit by multipath beam and carrier tracking errors like GPS (Global Positioning System) and radio links (3).

2.3.1   Attitude sensors

2.3.1.1 Sun sensors

Solar radiation sensing devices are mounted on a large number of spacecraft because they can be use for attitude control and attitude determination. Also because of its luminosity and its small angular radius ($\rho s = 4.67\ mrad$).

In order to obtain a required output information is usually implemented a sun sensor system which basically consist in a combination of a number of individual sun sensors. Such systems must meet performance specifications, acceptable physical characteristics and environmental conditions.

 Sun sensors are usually employed for battery recharging and power supply, therefore typically they work during the sun acquisition phase. Moreover, sun sensors are employed for the initial attitude determination when there is a light source.
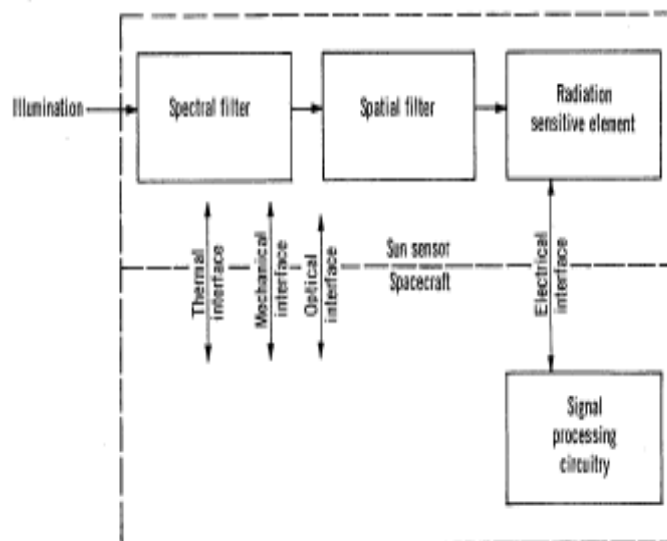
Figure1. Functional elements of sun sensors (4)

In the previous figure is present a very simple model of the functional elements of the sun sensors. These functional elements are the spectral filter, the spatial filter and the radiation sensitive element.

The spectral filters modify the incoming solar illumination and eliminate spectral bands where response from the radiation sensitive elements is not desired (3).

The spatial filter is the part of the sensor that is able to relate the radiation source with the system. Also known as the system of geometric relationship. It could be interpreted in two different ways. In one hand we have the digital sensor where the radiation arrives from a particular solid angle of space is compare with a preset threshold value. In the other hand we have the analogue sensor where the radiation arrived is compare with a select solid angle that comes from adjacent regions of view.

The radiation sensitive element is the part of the sensor that converts any radiant energy passing through the spatial and the spectral filters into electrical signals. This electrical signal is use as information in the spacecraft's attitude control system.

From this point of view, sun sensors can be classified in three different types: analogue sensors, detectors and digital sensors.

2.3.1.2 Horizon sensors

The horizon sensor is an optical instrument that detects light from a point away of Earth's atmosphere, a point that is at horizon. This horizon sensor provides orientation with respect to the Earth.

Earth is the second brightest object in the sky. Since the solid angle is large (3.9 steradian at 500km of altitude) the earth can be considered as an extended light source, and not as a point. The operation principle of the sensor requires specific observation and measuring concepts in order to retrieve the viewing direction of extended objects. For this purpose the horizon is defined as a geometric spot of points where the lines coming out from an observer in the space become tangent to the planet surface. But the horizon is uncertain and variable because of the reflected and the emitted radiation of the atmosphere and of surface irregularities.

Horizon sensors have four functional parts, which are:

1) A scanning mechanism,
2) An optical subsystem,
3) A detecting device,
4) An electronic unit.

There are 4 types of horizon sensors:

- Static horizon sensor: The field-of-view is larger than the entire Earth's edge (3). The static horizon sensor gives two angle orientations, the first is the roll angle around x-axis and the second is the pitch angle around y-axis. This two orientation's angles are with respect to local vertical z-axis. Typically an infrared detector is used.

- Body-mounted horizon sensors: They are used by spinning satellites and they are composed of an optical head with a narrow field-of-view (FOV) and of a detector in the visible or infrared spectral band. As we see in the figure2 the optical axis moves along a cone about the spin axis of the satellite (3). The sensor could or could not detect the Earth presence in the FOV. The spin axis attitude is kept constant by keeping the sensor cone aperture constant.
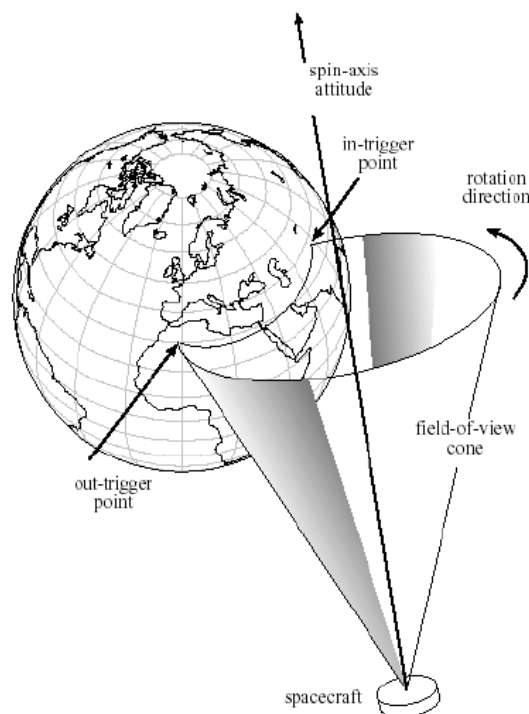
Figure2. Body-mounted horizon sensors

- Wheel-mounted horizon sensors: They are similar to body-mounted sensors, however to make the sensor rotate they are mounted on a wheel. The sensor is composed of two telescopes to make orthogonal scan.
- Non-spinning Earth sensors: only the optical head rotate to scan the Earth image.

2.3.1.3 Magnetometers

Magnetometers are instruments used to measure the magnitude and direction of magnetic field. This devises are reliable, consume low power, are free of moving parts and are able to operate in a wide temperature range. Unfortunately, due to the uncertainty on the planet magnetic field and the cross-coupling with on-board magnetic fields, the accuracy of the mechanism is greatly reduced - which is worse than 9 mrad; furthermore, the magnetic field of a planet decreases in magnitude with the altitude, in other words it is proportional to the inverse of the distance cube from the planet CoM. For the Earth there is a bound to the orbit altitude which is around 1500 to 200 km; commonly, magnetometers for higher elevations can be kept as ad-hoc applications. They are usually employed for damping the angular rate of Low-Earth-Orbit during the early stages of the mission. They include a sensible part (the magnetic sensor) and an electronic detector. Some physical principles are employed in their construction:

a) **Quantum** (Also known as proton precession) magnetometers employ important properties, like the nuclear magnetic resonance (NMR). Since these devises are heavy and expensive, they have very specific applications as scientific payloads.

b) **Inductive** magnetometers utilize magnetic induction (Faraday's law) and are constructed in two different ways: (i) search-coil and (ii) fluxgate. Due to their common use as attitude sensors; they will be fully treated in the present document.

2.3.1.4 Star trackers

These are the most accurate attitude sensors; in fact, modern versions directly provide the attitude measurements. This kind of magnetometer consists of three important items:

1. Optical subsystem.
2. Semiconductor detector and the relevant readout electronics.
3. Electronic unit.

The optical subsystem comprises a variable set of lenses (up to 7 and 8 lenses). The off-the-shelf sensors use a matrix of photo detectors (pixel) either Charged Coupled Devices (CCD) or Active Pixel Sensors (APS). The latter are more resistant to environment radiations, require less power and use a simpler proximity electronics (conversion electronics from analogue data to digital data), which conducts to a mass reduction. The assembly made by focal plane and proximity electronics is referred to as optical head.

The first star trackers were only capable of tracking star images in the focal plane. Therefore, they were entirely served to the control unit of the AOCS, which are able to provide the star coordinates in the focal plane. In the last ten years, autonomous star trackers have been capable of providing the sensor attitude; they

have developed progress in micro-electronics and are provided with memory and computing capabilities. Using star catalogues, autonomous star trackers allow attitude determination in a continuous and accurate way.

The optical subsystem FOV varies between 10°×10° and 40°×40°. Accuracy is determined by pixel size, FOV size and the algorithms. Usually the errors range between 5 and 50 rad for the optical axis attitude (two angles) and between 0.05 and 0.3 mrad for rotations about the optical axis. (No sé que cambiarle a esto, empezando porque… no entiendo nada)

The most modern devices include algorithms for the degraded performance in the case of higher angular rates, from 0.02 to 0.1 rad/s. In such cases attitude cannot be defined and only angular rates are stipulated.

Some of the limitations of start trackers are listed as follows:

1. Stray light: Sensitivity to angular separation from bright objects like Earth, Sun and Moon. Their light entering the FOV degrades performance may impede any measurements. The minimum angular separation from Earth and Moon is about 20 ° and from the Sun about 30°.
2. Radiation sensitivity.
3. Angular speed: Accuracy depends on the angular speed; the first attitude determination is usually guaranteed for angular speed less than 0.01 to 0.02 rad/s.
4. Complexity. Star tracker algorithms are rather complex and comparable to the algorithms of the overall ACS.

2.3.2 Inertial sensors

2.3.2.1 Accelerometer

Any instrument capable of measure accelerations is called accelerometer. However, this is not necessarily the same acceleration as the coordinate acceleration, which is the speed change in the space. Hence in the accelerometer the rate of acceleration is associated with the phenomenon of weight experienced by a proof mass that is in the reference frame device. To understand this point of view an example in which this type of acceleration are different is when the device is sitting on the ground and when the device is in free fall. The accelerometer measure a value when the device is sitting on the ground since the masses has a weight, although there is no change in speed. However, the accelerometer in free fall towards the center of the earth measure a value of zero because, although its speed is increasing, is in a frame of reference in which there is no weight.

Accelerometers are usually employed for measuring the non gravitational accelerations of UVA's. The essential implementation is that mentioned before of a small mass called proof-mass that is in the reference frame device. The proof-mass

is in a cage inside the spacecraft, as we can see in Figure3 this cage is only subject to gravity acceleration, but not to the forces $\bar{F} = m * \bar{d}$ acting on the device. This implies that if the proof-mass is unrestrained, it will drift in the cage and randomly bounce on the cage walls. Therefore an internal force $\overrightarrow{F_a}$ appears between cage and mass in order to keep a mass-to-cage fixed distance. Such distance will be proportional to the spacecraft acceleration that is not sensed by the proof-mass. (3)
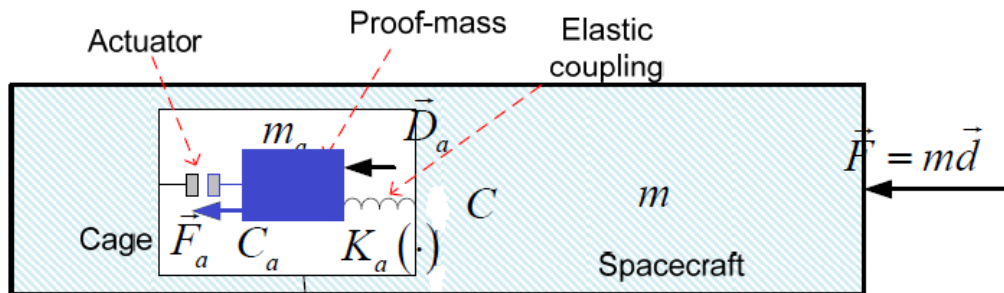
Figure3. The proof-mass within the spacecraft.

2.3.3 Angular rate sensors

2.3.3.1 Mechanical gyroscope

The gyroscope mechanical device composed essentially of a rotationally symmetrical body rotating around its axis of symmetry. When the gyro is subjected to a torque that tends to change the orientation of the axis of rotation of the device, it instead of change direction as a non rotate body would do, change of orientation in a direction perpendicular to the intuitive direction.

To understand better the functionality of the gyroscopes let's talk about the gimbals. Gimbals are a pivoted support that allows the rotation of an object about a single axis. A set of three gimbals, one mounted on the other with orthogonal pivot axes, may be used to allow an object mounted on the innermost gimbal to remain independent of the rotation of its support. (5).
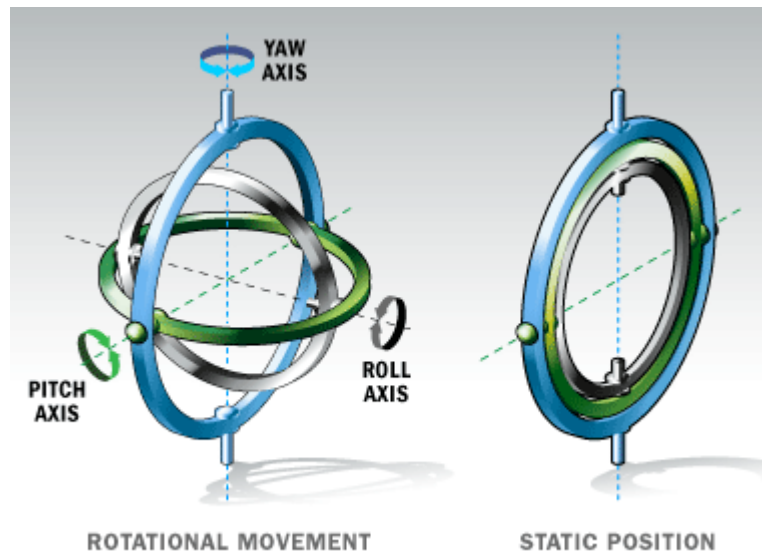
Figure4. How a gimbal works. (6)

A typically configuration of a gyroscope is the following:

1) There is an outer gimbal rotating around the inertial axis $\vec{\imath_3}$ of the angle φ (precession) and carrying around the first gimbal axis $\vec{g_1}$, and the intermediate axis$\vec{\imath_{21}}$. The first gimbal axis becomes the rotation axis of the inner gimbal.

2) The inner gimbal carries a spinning body around the third gimbal axis$\vec{g_3} = \vec{b_3}$, orthogonal to$\vec{g_1}$; the rotation angle of the inner gimbal about $\vec{g_1}$ is denoted by θ (nutation). The intermediate axis $\vec{\imath_{21}}$ when rotated by θ is denoted with $\vec{g_2}$: it is the second axis of the inner gimbal, and defines together with $\vec{g_1}$ the plane orthogonal to $\vec{g_3} = \vec{b_3}$, where the body axes $(\vec{b_1}, \vec{b_2})$ rotate by the angle φ (body spin).

3) The body centre of mass may be shifted by a length along the inner gimbal axis $\vec{g_3}$ to become a spinning top.
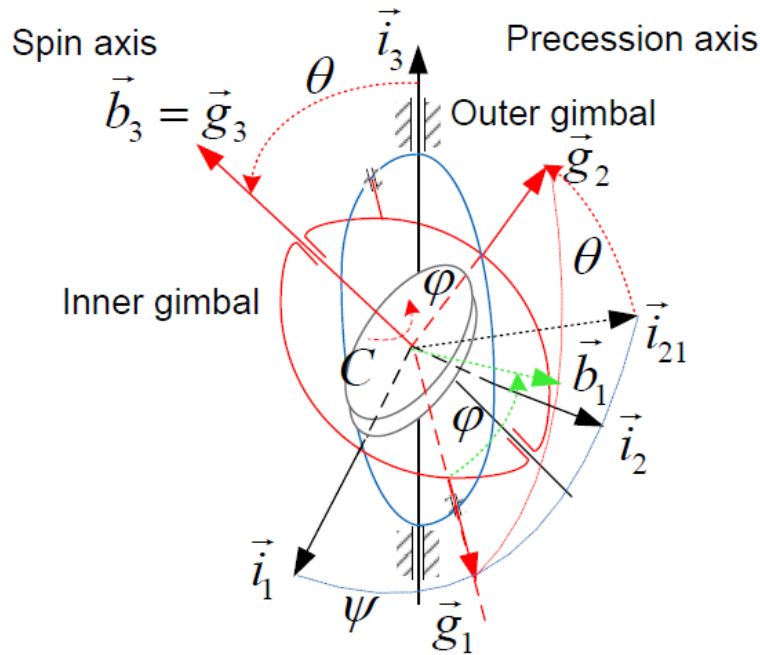
Figure5. Gyroscope geometry

2.3.4 Position sensors

2.3.4.1 The global navigation satellite system

Satellite navigation is a method that permits to accurate determine position and time anywhere on Earth through a satellite and ground network, designed and maintained as a Global Navigation Satellite System.

The NAVSTAR GPS (Navigation System with Time and Ranging Global Positioning System) is the only completely operative GNSS system, as of 2009. The GPS is a satellite-based radio navigation, positioning and time-transfer system; it was initiated in 1973 but it is fully operational since 1995. It consists of three segments:

1. The space segment consists of 24 spacecrafts orbiting in six orbit planes k = 0,...,5 with right ascension $\Omega_k = \Omega_o + k * \frac{\pi}{3}$ and equal inclination $i = 0.96$ rad (55 °) each orbit contains 4 satellites equally spaced; the orbit is close to be circular (e $\cong 0.003$) and the semimajor axis is about a $\cong 26560$ km , consistent to a flight altitude h_s = 20180 km and an orbit period of a semi-sidereal day (86164.091/2 s), about 2 minutes shorter than half standard solar day (86400/2 s).
2. The control segment consists of several ground stations.
3. Two user segments: the 'civil' Standard Positioning Service (SPS) provides positioning and timing information worldwide; while the Precise Positioning Service (PPS) provides data to authorized users.

There are two frequencies where the GPS satellites diffuse microwave carrier signals, these are L1 and L2. The L2 frequency permits to measure and correct the ionosphere signal delay. Three binary codes are modulated on the carriers.

1. The Coarse Acquisition (C/A) code is a short pseudorandom number (PRN) code of 1023 bits (1 ms duration) modulated on L1 carrier and specific of each satellite; it is the basis for the civil service. It is repeated equal 20 times, and corresponds to a single bit of the navigation message. Bit counter is called the clock epoch or fundamental time frame (FTF) and is counted from GPS time origin, reset each week.

2. The precise code (P) is a PRN code long about 6×10 bits, corresponding to one week. It modulates both L1 and L2 carrier phases and is the source for the authorized service. When Anti-Spoofing (AS) mode is active, the P code is encrypted (Y code).

3. The navigation data are transmitted in a 50 bits/s stream, added to C/A and P(Y) codes on L1 carrier. The message consists of 25 frames, each made of 5 sub frames, a sub-frame including 10 words of 30 bits each: in total 37500 bits each long 20 ms, repeated every 12.5 minutes. The message starts with the telemetry frame (TLM) of 32 bits (0.64 s) which allows recognizing the message onset. Then it contains low-accuracy (almanac data) and high-accuracy (broadcast ephemeris) satellite orbit data and clock corrections. (3)

2.4 RESULT'S ANALYSIS

2.4.1 NOISE AND RANDOM SIGNALS

The time course of a "noise" x (t) is typical of a random signal and it cannot be predicted by means of physical laws even knowing the initial conditions. The fundamental characteristic of a random signal is precisely related to its non-repeatability. For instance, if we repeat the same experiment to obtain the noise using the same experimental apparatus with the same elements, it will produce a noise x (t) with time course different. However, even if it is not possible to predict the time course of noise it is possible to characterize the behavior of the noise by introducing appropriate statistical parameters.

To determine the "expected value" of a statistical parameter there should be an average on all. For example, the "expected value" of x at time t, in other words the average of x (t), denoted as <x (t)>, will be obtained by averaging the values of x measured at time t in each of the items in the collection. Similarly, we can determine the root mean square value (equation 2-1) and the variance (equation 2-2). (7)

$$< x(t)^2 > \qquad\qquad\qquad \text{(2-1)}$$
$$\text{var}\{x(t)\} = < |x(t) - < x(t) >|^2 > \qquad\qquad \text{(2-2)}$$

2.4.2 POWER SPECTRAL DENSITY

For a stationary random signal, it is possible to define the function spectral density (power) as:

$$PSDx(w) = F\{C_{xx}(t)\} \tag{2-3}$$

Where F indicates the Fourier transform and C_{xx} indicates the autocorrelation function (equation 2-4).

$$C_{xx}(t_1, t_2) = < x^*(t_1)x(t_2) > \tag{2-4}$$

It is easily verify that:

$$< |x|^2 > = C_{xx}(0) = F^{-1}\{PSDx(w)\}_{t=0} = \int_{-\infty}^{\infty} PSDx(w)df \tag{2-5}$$

Where $< |x|^2 >$ can be interpreted as the average power dissipated by the signal x (t). Therefore the PSD precisely represents the frequency distribution of power associated with the signal x (t).

2.4.3 STANDARD DEVIATION

Another common statistical tool is the standard deviation. Once you know how to calculate the variance, the standard deviation is simply the square root of the variance and is denoted as "σ". (8)

The standard deviation shows how much variation or dispersion exists from the expected value. A low standard deviation indicates that the data points tend to be very close to the average; high standard deviation indicates that the data points are spread out over a large range of values.

2.5 BOREA

Borea is an aircraft without a human pilot on board (UAV) in quadricopter configuration. The project name "Borea" is development by The Space and Precision Automatics (S&PA) team of the Politecnico di Torino. Specifically the automatics and information department is in charge of the development of control algorithms for a soft landing demonstrator (WP 2.B – T2.B.3). In this case the demonstrator vehicle is a quadricopter.

The project born of the necessity of resolve the problem of on-ground testing guidance, navigation and control (GNC) algorithms for planetary accurate and safe landing. These problems can be approached through the flight of small quadricopters, approximately of mass smaller than 1kg, which are suitable for indoor and outdoor operations. At first this problem was planted by the STEPS project funded by Regione Piemonte, Italy, which is now under development.

The part of the project which I am interested is that under a short flight time, about 200s, the attitude, velocity and position can be obtained by gyroscope and accelerometer integration. Thus is essential the use of sensor devices namely IMU (accelerometers, gyros and something magnetometers).

The figure6 shows the structure of Borea. This prototype of quadricopter weighs less than 1Kg, however with the battery, the motors and all the boards the weigh is approximately 1.5Kg. All the components are presented in figure6 where is specify the type of connection. There are 5 different types of connection, differentiated from each other by the number of cables and the AWG type.

Figure6. Borea's structure

Type Cable	From	To	# Cables	AWG	
A	ESC	Motor	3	16	1.29mm
B	UBD4-PWM	ESC	2	22	0.64mm
C	UBD4-I2C	Magnetometer-I2C	4	22	0.64mm
D	UBD4-GPS	GPS	6	22	0.64mm
E	UBD4-IICSP	XBEE-ICSP	4	22	0.64mm
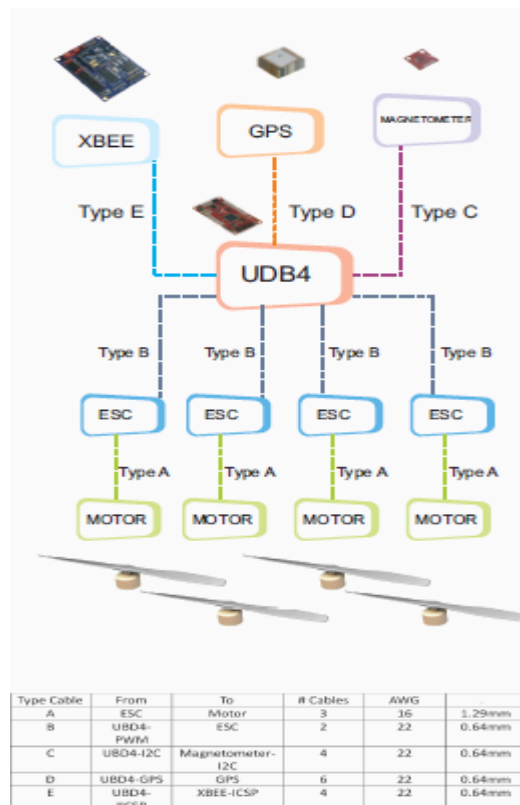
Figure7. Borea's Components.

Finally in figure8 presents the location and organization of every single component of the Borea. One can observe the different levels of the distribution. There is the main board level, the ESC level, the motor axis level, the battery level and the camera level.
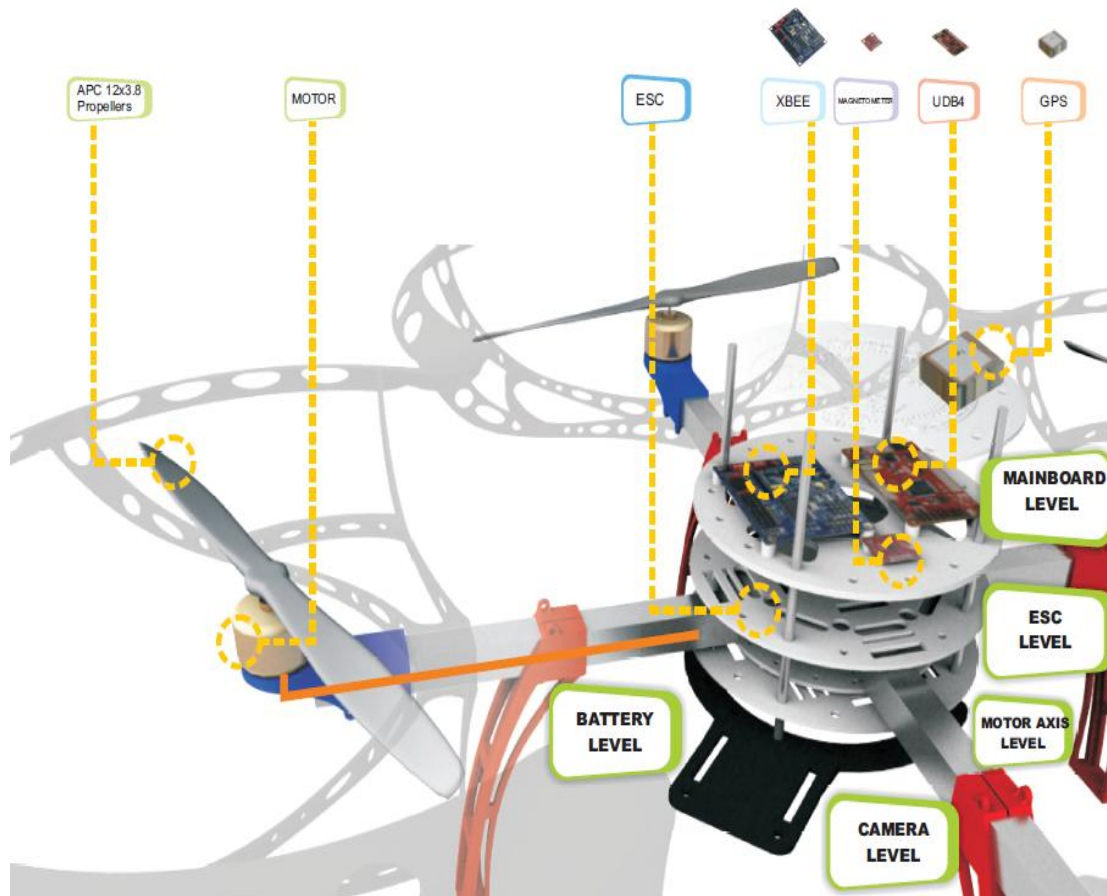
Figure8. Location and organization of Borea's components

3. HARDWARE

3.1 UBD4

This is the UAV Development Board in version 4. The UDB4 comes with a dsPIC33FJ256 CPU, an MMA7361 three axis accelerometer, a dual axis IDG500 gyroscope, and a single axis ISZ500 gyroscope. By itself, the board can be used to develop a three axis IMU controller. By addition of an EM406 or D2523T GPS receiver, it can be used to develop a UAV controller for an RC car, plane, helicopter, boat or quad rotor. Moreover it comes with self-testing firmware that can serve as a starting point for one to develop its own control and navigation firmware. Besides there is even fully functional, open source autopilot firmware available. (9) (10)

Features:

- compatible with 20-channel EM-406A SiRF III GPS
- compatible with 50-channel GS407 Helical GPS
- dsPIC33FJ256 Controller (with onboard 3.3V and 5V glue logic)
- dsPIC runs at 120MHz with 8MHz resonator and PLL
- MMA7361 three axis accelerometer
- IDG500 dual axis gyro and ISZ500 single axis gyro
- External 256Kbit EEPROM
- Up to 8 Input, 8 output PWM points
- 6-wire debug header or ICSP header
- 4 separate colored status LEDs
- On board 3.3V and 5V regulators (150mA max)
- Spare USART connection for debugging, flight logging, wireless telemetry, etc.
- 30 spare analog and digital I/O pins for debugging and interfacing to sensors
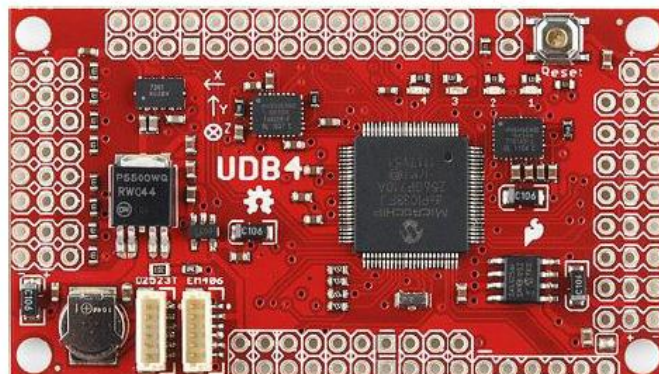
Figure9. UBD4

3.1.1 Regulator

This is a linear low drop voltage regulators provide up to 500 mA over an adjustable output range of 1.25 V to 5.0 V, or at a fixed output voltage of 1.5 V, 3.3 V or 5.0 V. it contains an internal PNP pass transistor that permits low dropout voltage and operation at full load current at the minimum input voltage. NCP5500 version includes an Enable/Shutdown function and is available in a DPAK 5 and SOIC 8 packages. This regulator family is ideal for applications that require a broad input voltage range, and low dropout performance up to 500 mA load using low cost ceramic capacitors.

Features
- Output Current up to 500 mA
- 2.9% Output Voltage Accuracy
- Low Dropout Voltage (230 mV at 500 mA)
- Enable Control Pin (NCP5500 / NCV5500)
- Reverse Bias Protection
- Short Circuit Protection
- Thermal Shutdown
- Wide Operating Temperature Range
- NCV5500 / NCV5501; −40⬚C to +125⬚C Ambient Temperature
- NCP5500 / NCP5501; −40⬚C to +85⬚C Ambient Temperature
- NCV Prefix for Applications that Require Site and Change Control
- Stable with Low Cost Ceramic Capacitors
- These are Pb−Free Devices

Figure10. Block diagram regulator (11)
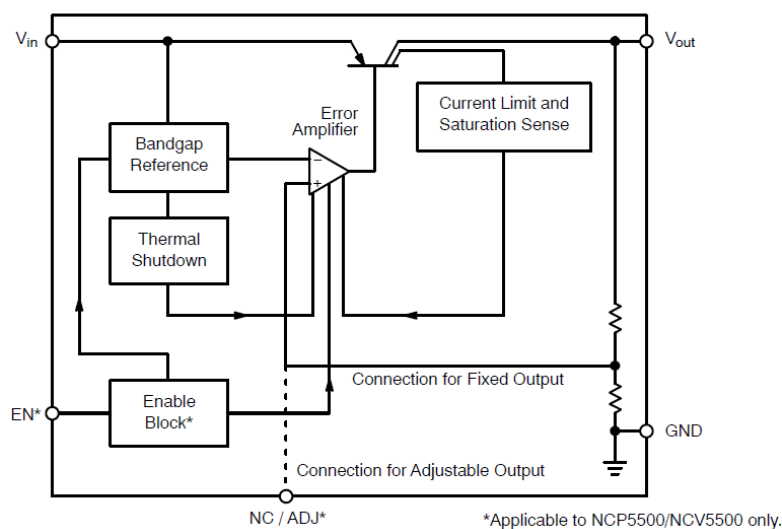
3.1.1.1 Circuit Description

28

The NCP5500 is integrated linear regulators with a DC load current capability of 500 mA. The output voltage is regulated by a PNP pass transistor controlled by an error amplifier and band gap reference. The choice of a PNP pass element provides the lowest possible dropout voltage, particularly at reduced load currents. Pass transistor base drive current is controlled to prevent oversaturation. The regulator is internally protected by both current limit and thermal shutdown as we can see in figure10. Thermal shutdown occurs when the junction temperature exceeds 150°C.

3.1.1.2 Regulator

The error amplifier compares the reference voltage to a sample of the output voltage (Vout) and drives the base of a PNP series pass transistor via a buffer. The reference is a band gap design for enhanced temperature stability. Saturation control of the PNP pass transistor is a function of the load current and input voltage. Oversaturation of the output power device is prevented, and quiescent current in the ground pin is minimized. (11)

3.1.2 Accelerometer

The MMA7361L is a low power, low profile capacitive micro machined accelerometer featuring signal conditioning, a 1-pole low pass filter, temperature compensation, self test, 0g-Detect which detects linear freefall, and g-Select which allows for the selection between 2 sensitivities ((±1.5g, ±6g) . Zero-g offset and sensitivity are factory set and require no external devices. The MMA7361L includes a Sleep Mode that makes it ideal for handheld battery powered electronics.

Features

- 3mm x 5mm x 1.0mm LGA-14 Package
- Low Current Consumption: 400 µA
- Sleep Mode: 3 µA
- Low Voltage Operation: 2.2 V – 3.6 V
- High Sensitivity (800 mV/g @ 1.5g)
- Selectable Sensitivity (±1.5g, ±6g)
- Fast Turn On Time (0.5 ms Enable Response Time)
- Self Test for Freefall Detect Diagnosis
- 0g-Detect for Freefall Protection
- Signal Conditioning with Low Pass Filter
- Robust Design, High Shocks Survivability
- RoHS Compliant
- Environmentally Preferred Product
- Low Cos
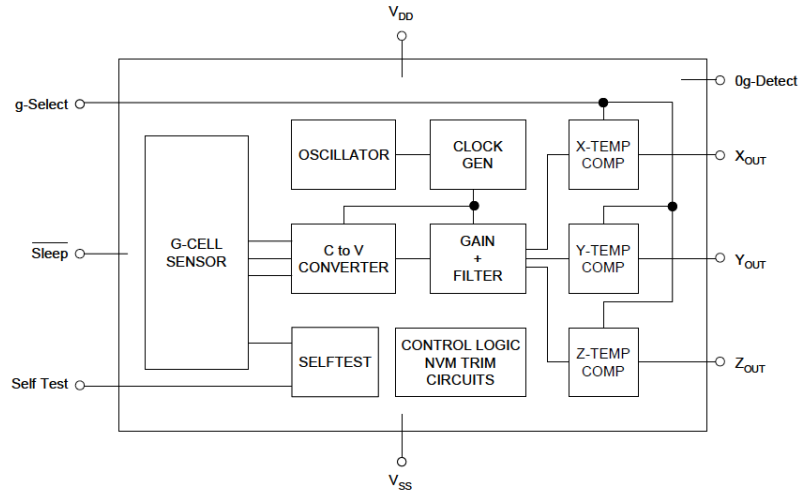
Figure11. Block diagram accelerometer (12)

The device consists of a surface micro machined, capacitive sensing cell (g-cell) and a signal conditioning ASIC contained in a single package. The g-cell is a mechanical structure formed from semiconductor materials (polysilicon) using semiconductor processes like masking and etching. The accelerometer can be modeled as a set of beams attached to a movable central mass that move between fixed beams, as shown in figure12 part left. The movable beams can be deflected from their rest position by subjecting the system to acceleration.

As the beams attached to the central mass move, the distance from them to the fixed beams on one side will increase by the same amount that the distance to the fixed beams on the other side decreases. The change in distance is a measure of acceleration.

The g-cell beams form two back-to-back capacitors (Figure12 part right). As the center beam moves with acceleration, the distance between the beams changes and each capacitor's value will change, according to the equation C = Aε/D. Where A is the area of the beam, ε is the dielectric constant, and D is the distance between the beams.

The ASIC uses switched capacitor techniques to measure the g-cell capacitors and extract the acceleration data from the difference between the two capacitors. Moreover the ASIC use signal conditions and filters with switched capacitor that provide a high level output voltage that is radiometric and proportional to acceleration. (12)
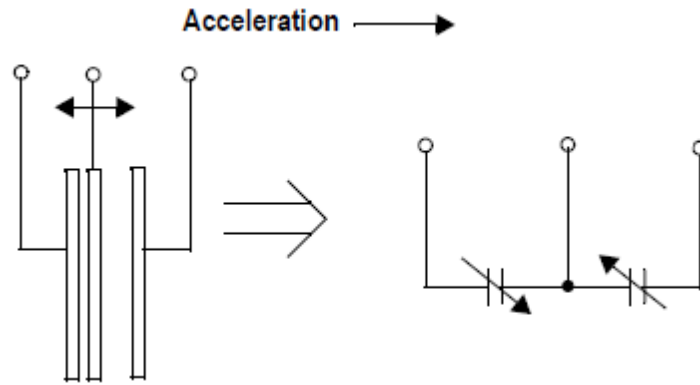
Figure12. Model of an accelerometer

3.1.3 Gyroscope

3.1.3.1 ISZ-500 Single-Axis Z-Gyro

The ISZ-500 is a single-axis Z-gyroscope designed specifically for complex motion sensing in 3D-input devices and gaming controllers. The ISZ-500 gyroscope utilizes MEMS fabrication with wafer-scale integration technology which combines completed MEMS wafers and completed CMOS electronic wafers together using a patented and proprietary wafer-scale bonding process that simultaneously provides electrical connections and hermetically sealed enclosures. Integration at the wafer-level minimizes parasitic capacitances, allowing for improved signal-to-noise over a discrete solution. With the addition of the new patent-pending Auto Zero feature for minimizing bias drift over temperature, the ISZ-500 offers unparalleled gyroscope performance in 3D-input and gaming applications.

Features

- Z-axis (yaw rate) gyro on a single chip
- Two separate analog outputs for standard and high sensitivity:

  - Z-Out Pin: 500°/s full scale range
    2.0mV/°/s sensitivity
  - Z4.5Out Pin: 110°/s full scale range
    9.1mV/°/s sensitivity

- Integrated amplifiers and low-pass filter
- Auto-Zero function
- On-chip temperature sensor
- High vibration rejection over a wide frequency range
- High cross-axis isolation by proprietary MEMS design
- 3V single-supply operation
- Hermetically sealed for temperature and humidity resistance
- 10,000 g shock tolerant

- Smallest single axis gyro package at 4 x 5 x 1.2mm
- RoHS and Green Compliant
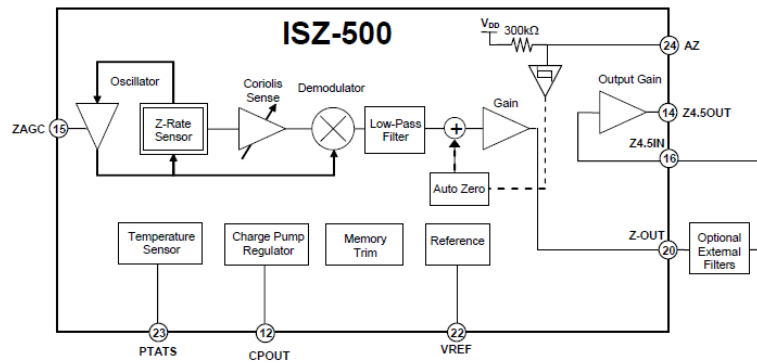
Figure13. Block diagram gyroscope (13)

3.1.3.2 Integrated Dual-Axis Gyro IDG-500

The IDG-500 is an integrated dual-axis angular rate sensor (gyroscope). It uses two sensor elements with novel vibrating dual-mass bulk silicon configurations that sense the rate of rotation about the X- and Y-axis (in-plane sensing). This results in a unique, integrated dual-axis gyro with guaranteed-by-design vibration rejection and high cross-axis isolation. It is specifically designed for demanding consumer applications requiring low cost, small size and high performance.

FEATURES

- Integrated X- and Y-axis gyros on a single chip
- Two separate outputs per axis for standard and high
- sensitivity:

  o X-/Y-Out Pins: 500°/s full scale range
     2.0mV/°/s sensitivity
  o X/Y4.5Out Pins: 110°/s full scale range
     9.1mV/°/s sensitivity

- Integrated amplifiers and low-pass filters
- Auto-Zero function
- On-chip temperature sensor
- High vibration rejection over a wide frequency range
- High cross-axis isolation by proprietary MEMS design
- 3V single-supply operation
- Hermetically sealed for temp and humidity resistance
- 10,000 g shock tolerant
- Smallest dual axis gyro package at 4 x 5 x 1.2mm

The IDG-500 gyro includes the integrated electronics necessary for application-ready functionality. It incorporates X- and Y-axis low-pass filters and an EEPROM for on-chip factory calibration of the sensor. Factory trimmed scale factors eliminate the need for external active components and end-user calibration.
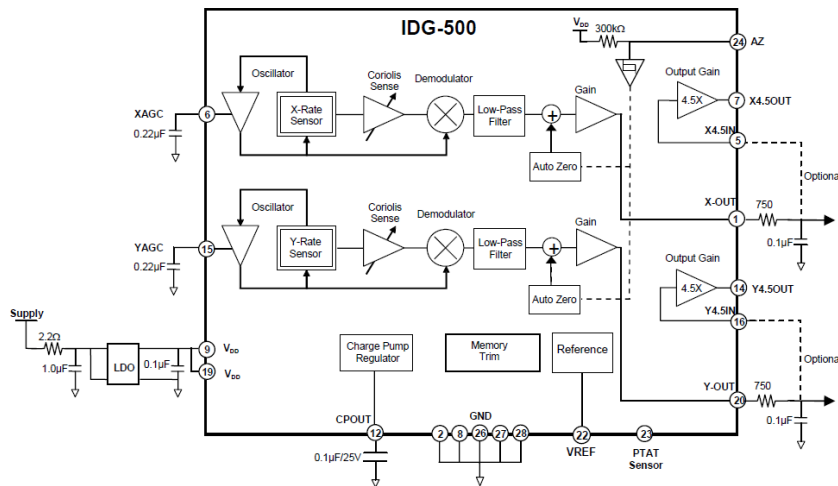
Figure14. Block diagram gyroscope (14)

The IDG-500 gyro is a dual-axis gyroscope consisting of two independent vibratory MEMS gyroscopes. One detects rotation about the X-axis; the other detects rotation about the Y-axis. The structures are covered and hermetically sealed at the wafer-level. The gyroscope's proof-masses are electrostatically oscillated at resonance. An internal automatic gain control circuit precisely sets the oscillation of the proof masses. When the sensor is rotated about the X- or Y-axis, the Coriolis Effect causes a vibration that can be detected by a capacitive pickoff. The resulting signal is amplified, demodulated, and filtered to produce an analog voltage that is proportional to the angular rate. (14)

The Coriolis Effect is a deflection of moving objects when they are viewed in a rotating reference frame. In a reference frame with clockwise rotation, the deflection is to the left of the motion of the object; in one with counter-clockwise rotation, the deflection is to the right. (15).

3.1.4 Magnetometer

The Honeywell HMC5883L is a surface-mount, multi-chip module designed for low-field magnetic sensing with a digital interface for applications such as low-cost compassing and magnetometry. The HMC5883L includes high-resolution HMC118X series magneto-resistive sensors plus an ASIC containing amplification, automatic degaussing strap drivers, offset cancellation, and a 12-bit ADC that enables 1° to 2° compass heading accuracy. The I^2C serial bus

allows for easy interface. The HMC5883L is a 3.0x3.0x0.9mm surface mount 16-pin leadless chip carrier (LCC). Applications for the HMC5883L include Mobile Phones, Netbooks, Consumer Electronics, Auto Navigation Systems, and Personal Navigation Devices.

FEATURES

- 3-Axis Magneto resistive Sensors and ASIC in a 3.0x3.0x0.9mm LCC Surface Mount Package.
- 12-Bit ADC Coupled with Low Noise AMR Sensors Achieves 2 milli-gauss Field Resolution in ±8 Gauss Fields
- Built-In Self Test
- Low Voltage Operations (2.16 to 3.6V) and Low Power Consumption (100 µA)
- Built-In Strap Drive Circuits
- I2C Digital Interface
- Lead Free Package Construction
- Wide Magnetic Field Range (+/-8 Oe)
- Software and Algorithm Support Available
- Fast 160 Hz Maximum Output Rate

The HMC5883L utilizes Honeywell's Anisotropic Magneto resistive (AMR) technology that provides advantages over other magnetic sensor technologies. These anisotropic, directional sensors feature precision in-axis sensitivity and linearity. These sensors' solid-state construction with very low cross-axis sensitivity is designed to measure both the direction and the magnitude of Earth's magnetic fields, from milli-gauss to 8 gauss.
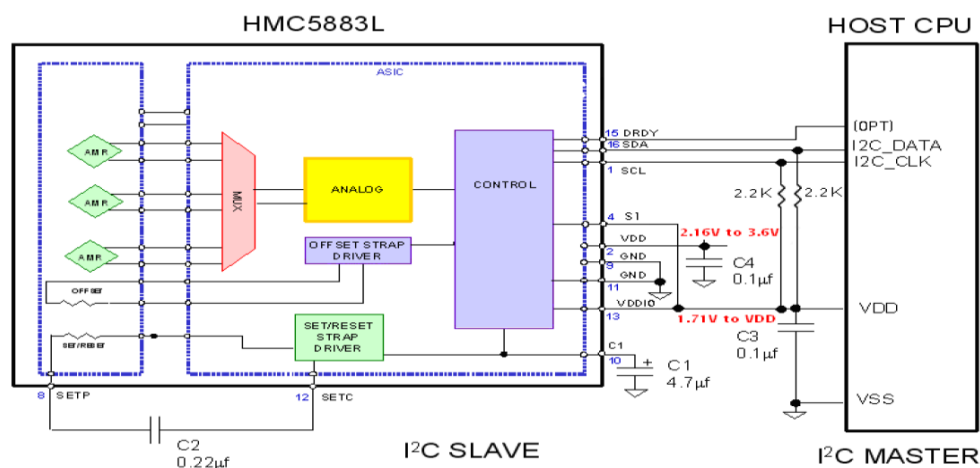

Figure15. Block diagram magnetometer

The Honeywell HMC5883L magneto resistive sensor circuit is a trio of sensors that measure magnetic fields. With power supply applied, the sensor converts any incident magnetic field in the sensitive axis directions to a differential voltage output. In the presence of a magnetic field, a change in the bridge

resistive elements causes a corresponding change in voltage across the bridge outputs. These resistive elements are aligned together to have a common sensitive axis that will provide positive voltage change with magnetic fields increasing in the sensitive direction. Because the output is only proportional to the magnetic field component along its axis, additional sensor bridges are placed at orthogonal directions to permit accurate measurement of magnetic field in any orientation. (16)

3.2 MICROCONTROLLER

PARAMETERS OF dsPIC33FJ256GP710A

Parameter Name	Value
Architecture	16-bit
CPU Speed (MIPS)	40
Memory Type	Flash
Program Memory (KB)	256
RAM Bytes	30,720
Temperature Range C	-40 to 150
Operating Voltage Range (V)	3 to 3.6
I/O Pins	85
Pin Count	100
System Management Features	PBOR
POR	Yes
WDT	Yes
Internal Oscillator	7.37 MHz, 512 kHz
nanoWatt Features	Fast Wake/Fast Control
Digital Communication Peripherals	2-UART 2-SPI 2-I2C
Codec Interface	Yes
Analog Peripherals	2-A/D 32x12-bit @ 500(ksps)
Op Amp	NO
CAN (#, type)	2 ECAN
Capture/Compare/PWM Peripherals	8/8
PWM Resolution bits	16
Timers	9 x 16-bit 4 x 32-bit
Parallel Port	GPIO
Hardware RTCC	No
DMA	8

XLP	NO

Table1. Parameters microcontroller

FEATURES

- ✓ DC – 40 MIPS (40 MIPS @ 3.0-3.6V, -40°C to +85°C)
- ✓ DC – 40 MIPS (40 MIPS @ 3.0-3.6V, -40°C to +125°C)
- ✓ Industrial temperature range (-40°C to +85°C)
- ✓ Extended temperature range (-40°C to +125°C)
- ✓ High temperature range (-40°C to +140°C)High-Performance DSC CPU
- ✓ Modified Harvard architecture
- ✓ C compiler optimized instruction set
- ✓ 16-bit wide data path
- ✓ 24-bit wide instructions
- ✓ Linear program memory addressing up to 4M instruction words
- ✓ Linear data memory addressing up to 64 Kbytes
- ✓ 83 base instructions: mostly 1 word/1 cycle
- ✓ Sixteen 16-bit General Purpose Registers
- ✓ Two 40-bit accumulators:- With rounding and saturation options
- ✓ Flexible and powerful addressing modes:- Indirect, Modulo and Bit-Reversed
- ✓ Software stack
- ✓ 16 x 16 fractional/integer multiply operations
- ✓ 32/16 and 16/16 divide operations
- ✓ Single-cycle multiply and accumulate:- Accumulator write back for DSP operations- Dual data fetch
- ✓ Up to ±16-bit shifts for up to 40-bit dataDirect Memory Access (DMA)
- ✓ 8-channel hardware DMA
- ✓ 2 Kbytes dual ported DMA buffer area (DMA RAM) to store data transferred via DMA:- Allows data transfer between RAM and a peripheral while CPU is executing code (no cycle stealing)
- ✓ Most peripherals support DMAInterrupt Controller
- ✓ 5-cycle latency
- ✓ 118 interrupt vectors
- ✓ Up to 67 available interrupt sources
- ✓ Up to 5 external interrupts
- ✓ 7 programmable priority levels
- ✓ 5 processor exceptionsDigital I/O:
- ✓ Wake-up/Interrupt-on-Change on up to 24 pins
- ✓ Output pins can drive from 3.0V to 3.6V
- ✓ All digital input pins are 5V tolerant
- ✓ 4 mA sink on all I/O pinsSys tem Management:
- ✓ Flexible clock options:- External, crystal, resonator, internal RC- Fully integrated PLL- Extremely low jitter PLL
- ✓ Oscillator Start-up Timer/Stabilizer
- ✓ Fail-Safe Clock Monitor
- ✓ Reset by multiple sourcesPower Management
- ✓ On-chip 2.5V voltage regulator
- ✓ Switch between clock sources in real time

- ✓ Timer/Counters, up to nine 16-bit timers:- Can pair up to make four 32-bit timers- 1 timer runs as Real-Time Clock with external 32.768 kHz oscillator- Programmable prescaler
- ✓ Input Capture (up to 8 channels):- Capture on up, down or both edges- 16-bit capture input functions- 4-deep FIFO on each capture
- ✓ Output Compare (up to 8 channels):- Single or Dual 16-Bit Compare mode- 16-bit Glitchless PWM modeCommunication Modules
- ✓ Data Converter Interface (DCI) module:- Codec interface- Supports I2S and AC'97 protocols- Up to 16-bit data words, up to 16 words per frame- 4-word deep TX and RX buffers
- ✓ Enhanced CAN (ECAN™ module) 2.0B active (up to 2 modules):- Up to 8 transmit and up to 32 receive buffers- 16 receive filters and 3 masks- Loopback, Listen Only and Listen All Messages modes for diagnostics and bus monitoring- Wake-up on CAN message- Automatic processing of Remote Transmission Requests- FIFO mode using DMA- DeviceNet™ addressing supportAnalog-to-Digital Converters (ADCs):
- ✓ Up to two ADC modules in a device
- ✓ 10-bit, 1.1 Msps or 12-bit, 500 Ksps conversion:- 2, 4 or 8 simultaneous samples- Up to 32 input channels with auto-scanning- Conversion start can be manual or synchronized with 1 of 4 trigger sources- Conversion possible in Sleep mode- ±2 LSb max integral nonlinearity- ±1 LSb max differential nonlinearityCMOS Flash Technology:
- ✓ Low-power, high-speed Flash technology
- ✓ Fully static design
- ✓ 3.3V (±10%) operating voltage
- ✓ Industrial temperature
- ✓ Extended temperature
- ✓ Low-power consumption

(17)

3.2.1 Oscillator

The dsPIC33F oscillator system includes the following characteristics:

• Four external and internal oscillator options
•On-chip Phase-Locked Loop (PLL) to boost internal operating frequency on select internal and external oscillator sources
• On-the-fly clock switching between various clock sources
• Doze mode for system power savings
•Fail-Safe Clock Monitor (FSCM) that detects clock failure and permits safe application recovery or shutdown
• Nonvolatile Configuration bits for clock source selection

A block diagram of the oscillator system is shown in Figure16.
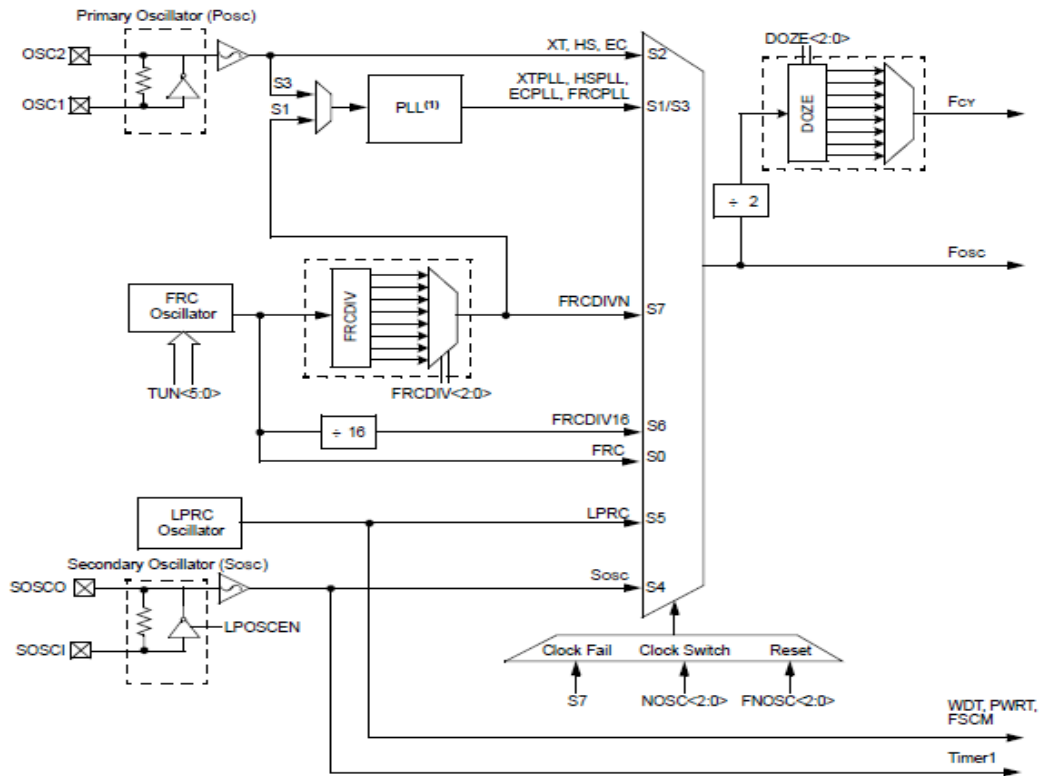
Figure16. Block diagram oscillator (18)

3.2.1.1 CPU CLOCKING

The system clock source, which is called FOSC, can be generated by one of the following oscillators:

• Primary Oscillator (POSC): position on the OSC1 and OSC2 pins.
• Secondary Oscillator (SOSC): position on the SOSCI and SOSCO pins.
• Internal Fast RC Oscillator (FRC) with optional clock divider.
• Internal Low-Power RC Oscillator (LPRC)
• Primary Oscillator with PLL
• Internal Fast RC Oscillator with PLL

The system clock source is divided by two to produce the internal instruction cycle clock, which is denoted by FCY. The FCY can be output on the OSC2 I/O pin if the Primary Oscillator mode or the HS mode is not selected as the clock source.

Figure17. Clock and Instruction Cycle Timing

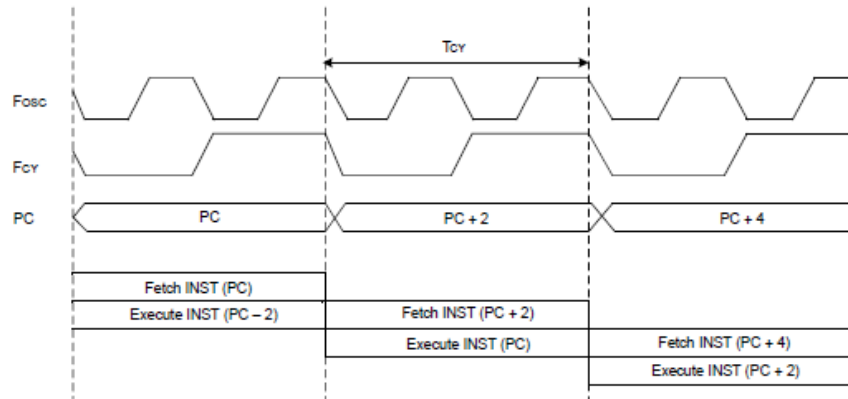The timing diagram in Figure17 shows the relationship between the system clock (FOSC), the instruction cycle clock (FCY) and the Program Counter (PC). It can be appreciate that the instruction cycle clock is the half of the system clock.

3.2.1.2 PRIMARY OSCILLATOR

The Primary Oscillator is possible to reach on the OSC1 and OSC2 pins of the microcontroller. In this connection an external crystal is enables to provide the clock to the device. However, it can be used with the internal PLL to impulse the system frequency (FOSC) to 80 MHz for 40 MIPS execution. The Primary Oscillator provides three modes of operation:

- **Medium Speed Oscillator (XT Mode)**

The XT mode is a medium gain, medium frequency mode used to work with crystal frequencies of 3 to 10 MHz.

- **High-Speed Oscillator (HS Mode)**

The HS mode is a high-gain, high-frequency mode used to work with crystal frequencies of 10 to 40 MHz.

- **External Clock Source Operation (EC Mode)**

If the on-chip oscillator is not used, the external clock mode allows the internal oscillator to be bypassed.

The crystal oscillator circuit diagram for the microcontroller is show on figure18 the optimum load capacitance CL for a given crystal is specified by the crystal manufacturer. However, load capacitance can be calculated as shown in Equation 3-1.
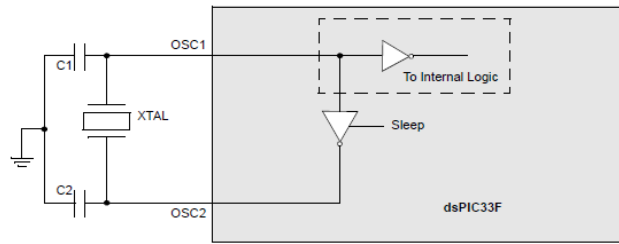
Figure18. Crystal oscillator circuit diagram.

$$C_L = C_S * \frac{C_1 * C_2}{C_1 + C_2} \qquad \text{(3-1)}$$

3.2.1.3 INTERNAL FAST RC (FRC) OSCILLATOR

The Internal Fast RC FRC Oscillator can provide a nominal 7.37 MHz clock without requiring an external crystal, which results in system cost savings for applications that do not require a precise clock reference. The principle difference between the primary oscillator and the internal fast oscillator is that the Internal FRC Oscillator starts up instantly, without delay. Unlike the primary oscillator that use a crystal oscillator, which can take several milliseconds to begin oscillation.

The application software can tune the frequency of the oscillator from -12% to +11.625% (30 kHz steps) of the nominal frequency value using the FRC Oscillator Tuning.

3.2.1.4 PHASE-LOCKED LOOP (PLL)

The Primary Oscillator and Internal FRC Oscillator sources can use a PLL to obtain higher operating speeds. Figure19 presents a block diagram of the PLL module.
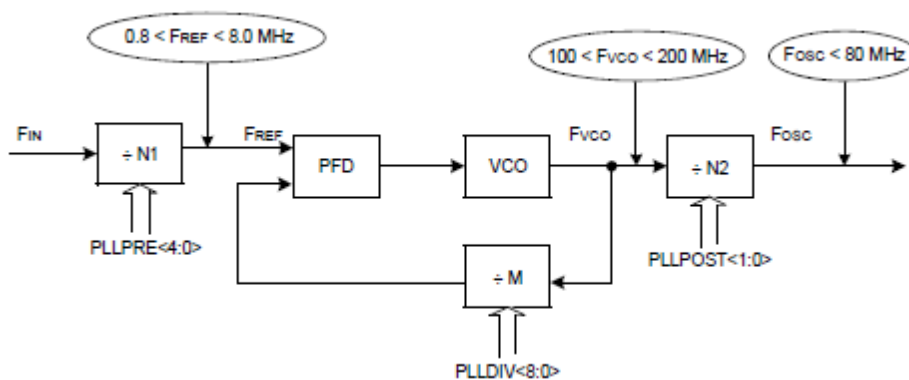

Figure19. PLL Block Diagram

In order to have an adequate PLL operation, the Phase Frequency Detector (PFD) input frequency and Voltage Controlled Oscillator (VCO) output frequency must meet the following requirements:

- The PFD input frequency (FREF) must be in the range of 0.8 to 8.0 MHz, as shown in figure18.
- The VCO output frequency (FVCO) must be in the range of 100 to 200 MHz, as shown in figure18.

The PLL Phase Detector Input Divider specify the input divider ratio (N1), which is used to scale down the input clock (FIN) to meet the PFD input frequency range of 0.8 MHz to 8 MHz. The PLL Feedback Divisor specifies the divider ratio (M), which scales down the VCO frequency (FVCO) for feedback to the PFD. The VCO frequency (FVCO) is 'M' times the input reference clock (FREF).

The PLL VCO Output Divider specifies the divider ratio (N2) to limit the system clock frequency (FOSC) to 80 MHz.

Equation 3-2 gives the relation between the input frequency (FIN) and the output frequency (FOSC).

$$F_{OSC} = F_{IN} * \left(\frac{M}{N1 * N2} \right) \qquad (3\text{-}2)$$

Where

$$N1 = PLLPRE + 2$$
$$N2 = 2 * (PLLPOST + 1)$$
$$M = PLLDIV + 2$$

The relation between the input frequency (FIN) and the VCO frequency (FVCO) is:

$$F_{vco} = F_{IN} * \left(\frac{M}{N1} \right) \qquad (3\text{-}3)$$

3.2.1.5 LOW-POWER SECONDARY OSCILLATOR (SOSC)

The Low-Power Secondary Oscillator uses a watch crystal at 32.768 kHz to be attached to the microcontroller as a secondary crystal clock source for low-power operation. It uses the SOSCI and SOSCO pins. The Low-Power Secondary Oscillator can also drive Timer1 for Real-Time Clock (RTC) applications.

There are two possibilities to enable the Low-Power Secondary Oscillator:

- The Initial Oscillator Source is appropriately set to select the Secondary Oscillator at a Power-on Reset.
- The user software initiates a clock switch to the Secondary Oscillator for low-power operation.

If the Low-Power Secondary Oscillator is disabled is to save power if it is not being used to provide the system clock, or if the device enters Sleep mode. When the Low-Power Secondary Oscillator is enabled, it takes a finite amount of time to start oscillating. However you can, optionally, leave the Secondary Oscillator running continuously. There are two reasons to leave the Low-Power Secondary Oscillator running. First, it is running to obtain a fast switch to the 32 kHz system clock for

lower power operation. Second, the oscillator should remain on at all times when Timer1 is being used as a Real-Time Clock. (18)

3.2.2 Timer

The microcontroller has several 16-bit Timer modules. They are classified into the following three types according to their functional differences:

• Type A timer (Timer1)
• Type B timer (Timer2, Timer4, Timer6 and Timer8)
• Type C timer (Timer3, Timer5, Timer7 and Timer9)

Each Timer module is a 16-bit timer/counter. However, the Type B and Type C timers can be combined to form a 32-bit timer. Moreover, each Timer module has these associated bits for interrupt control:

• Interrupt Enable Control bit
• Interrupt Flag Status bit
• Interrupt Priority Control bits

3.2.2.1 Type A Timer

The Type A timer has the following unique features over other types of timers:

• Can be operated from the low-power 32 kHz crystal oscillator available on the device
• Can be operated in Asynchronous Counter mode from an external clock source
• Optionally, the external clock input can be synchronized to the internal device and clock synchronization is performed after extern clock is divided by the prescaler.

However the unique and special feature of the Type A timer is that it can be used for Real-Time Clock (RTC) applications. Figure20 shows a block diagram of the Type A timer.
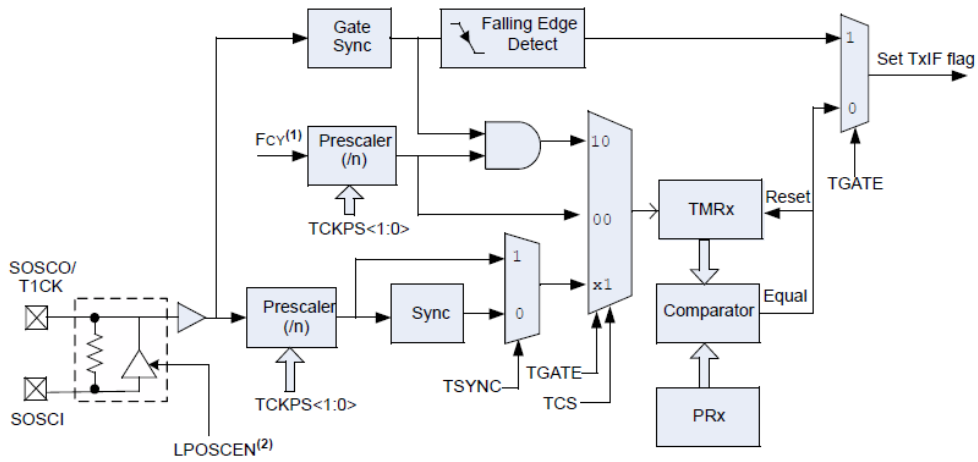
Figure20. Type A timer block diagram (19)

3.2.2.2 Type B Timer

A Type B timer consists of these features:

• It can be concatenated with a Type C timer to form a 32-bit timer
• The external clock input is always synchronized to the internal device clock and clock synchronization is performed after clock input is divided by the prescaler.

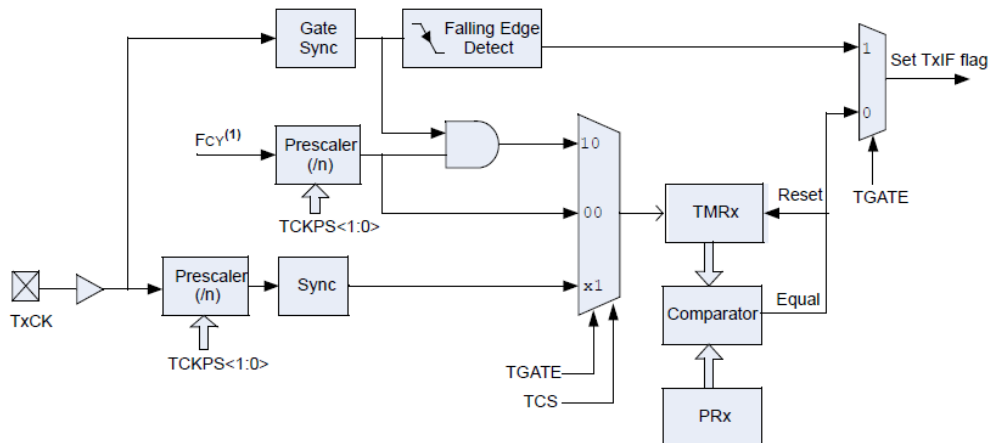In Figure21 is presented a block diagram of the Type B timer.

Figure21. Type B timer block diagram (19)

3.2.2.3 Type C Timer

A Type C timer consists of these specific features:

• It can be concatenated with a Type B timer to form a 32-bit timer

• At least one Type C timer has the ability to trigger an Analog-to-Digital (A/D) conversion
• The external clock input is always synchronized to the internal device clock. The clock synchronization is performed using external clock input, after which this synchronized clock is divided by the prescaler

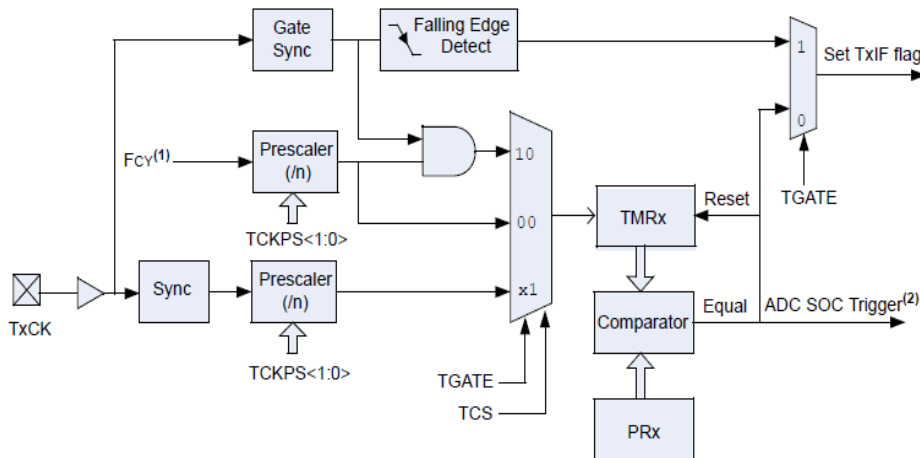Figure22 shows a block diagram of the Type C timer.

Figure22. Type C timer block diagram (19)

3.2.2.4 MODES OF OPERATION

There are four different modes in which the Timer module can operate:

• Timer mode
• Gated Timer mode
• Synchronous Counter mode
• Asynchronous Counter mode (Type A timer only)

In Timer and Gated Timer modes, the input clock is derived from the internal instruction cycle clock (FCY). In Synchronous and Asynchronous Counter modes, the input clock is derived from the external clock input at the TxCK pin. Also, the input to all 16-bit timers has prescaler options of 1:1, 1:8, 1:64, and 1:256.

3.2.2.4.1   Timer Mode

In Timer mode, as mentioned, the input clock to the timer is derived from the internal clock (FCY) and it is divided by a programmable prescaler. When the timer is enabled, it increments by one on every rising edge of the input clock and generates an interrupt on a period match.

3.2.2.4.2   Synchronous Counter Mode

In Synchronous Counter mode, as mentioned, the input clock to the timer is derived from the external clock input and is divided by a programmable prescaler. when this mode is enabled, the external clock input is synchronized with the internal device clock. Although here the timer also increments by one on every rising edge of the input clock and generates an interrupt on a period match. This mode does not operate in Sleep mode because the synchronization circuit is shut off during Sleep mode.

For proper synchronization of Type C timers, it is necessary for the external clock input period to be high for at least 0.5 TCY and an additional input buffer delay of 20 ns, and low for at least 0.5 TCY and an additional input buffer delay of 20 ns. But, for a Type A and Type B timer, the external clock input period must be at least 0.5 TCY divided by the prescaler value and an additional input buffer delay of 20 ns. However, the high and low time of the external clock input must not violate the minimum pulse width requirement of 10 ns nominal or 50 MHz nominal frequency.

3.2.2.4.3   Asynchronous Counter Mode (Type A Timer only)

Only Type A timer has the ability to operate in an Asynchronous Counting mode. In Asynchronous Counter mode, the input clock to the timer is derived from the external clock input divided by a programmable prescaler. However in this mode the external clock input is not synchronized with the internal device clock. But when it is enabled, the timer also increments by one on every rising edge of the input clock and generates an interrupt on a period match.

Special features in Asynchronous Counter mode:

• The timer can be clocked from the low-power 32 kHz secondary crystal oscillator for Real-Time Clock (RTC) applications by setting the Secondary Oscillator Enable.
• The timer can operate during Sleep mode, if the external clock input is active or the secondary oscillator is enabled. The timer can generate an interrupt on a period register match to wake-up the processor from Sleep mode.

Moreover in Asynchronous Counter mode, the external clock input high and low time must not violate the minimum pulse width requirement of 10 ns nominal or 50 MHz nominal frequency. (19)

3.2.3   I/O port

All the microcontroller device pins, except VDD, VSS, MCLR, and OSC1/CLKI, are used by the peripherals and the general purpose of Input/output (I/O) ports. This general purpose of I/O ports allows the microcontroller to monitor and control other devices. That's why the I/O pins are multiplexed with alternate function. The multiplexing will depend on the peripheral features on the device. In general, when a peripheral is functioning, that pin may not be used as a general purpose I/O pin.

A block diagram of a typical I/O port is shown in figur23. It's important to say that this block diagram does not take into account peripheral functions that may be multiplexed onto the I/O pin.
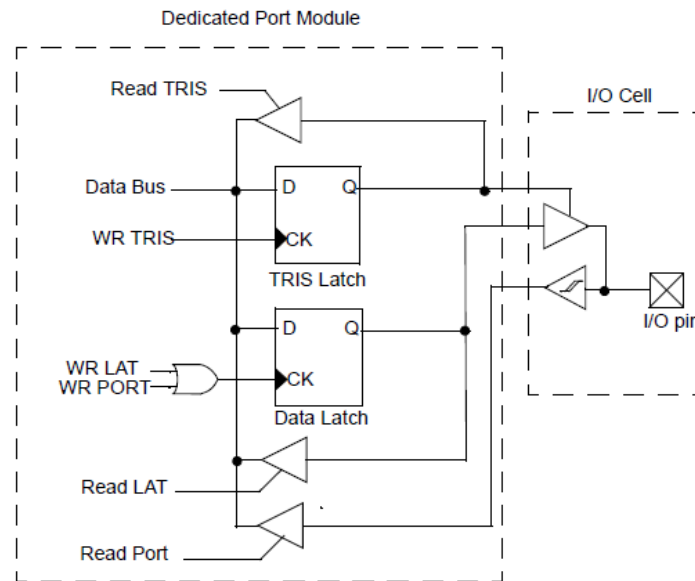

Figure23. Dedicated Port Structure Block Diagram (20)

There are four registers directly associated with the operation of the port which all I/O ports have:

• TRISx: Data Direction register
• PORTx: I/O Port register
• LATx: I/O Latch register

where 'x' is a letter that denotes the particular I/O port and each I/O pin on the device has an associated bit in the TRIS, PORT, and LAT registers.

3.2.3.1 TRIS Registers

The TRIS register control bits determine whether each pin associated with the I/O port is an input or an output. If the TRIS bit is a '1' the pin is an input. And if the TRIS bit is a '0' the pin is configured for an output. However all port pins are defined as inputs after a Reset.

3.2.3.2 PORT Registers

The data on an I/O pin can be reached by a PORT register. When one read the PORT register, one reads the value of the I/O pin, while when one writes to the PORT register, one writes the value to the port data latch. Therefore, a write to a port implies that the port pins are read; this value is modified, and is written to the port data latch. This is called a read-modify-write operation. There are many read-modify-write operations like instructions such as BSET and BCLR instructions.

When one uses read-modify-write commands should take care when I/O pins associated with the port are configured as inputs because If an I/O pin configured as an input is changed to an output at some later time, an unexpected value may be output on the I/O pin. This effect occurs because the read-modify-write instruction reads the instantaneous value on the input pin and loads that value into the port data latch. In addition, if read-modify-write instructions are used on the PORT registers while I/O pins are configured as output, unintended I/O behavior may occur based on the device speed and I/O capacitive loading.

3.2.3.3 LAT Registers

The LAT register associated with an I/O pin eliminates the problems that can occur with read-modify-write instructions. This mean that a read of the LAT register returns the values held in the port output latches instead of the values on the I/O pins. Also, a read-modify-write operation on the LAT register associated with an I/O port avoids the possibility of writing the input pin values into the port latches. However, a write to the LAT register has the same effect as a write to the PORT register. (20)

3.2.4 A/D converter

The microcontroller has up to 32 A/D input channels. Also it has up to two ADC modules, each with its own set of Special Function Registers (SFRs). Each of the ADC modules has the 10-bit or 12-bit Operation Mode that can be configured by the user. There are two possibilities a 10-bit, 4 Sample/Hold (S/H) ADC or a 12-bit, 1 Sample/Hold ADC.

The 10-bit ADC configuration has the following key features:

• Successive Approximation (SAR) conversion
• Conversion speeds of up to 1.1 Msps
• Up to 32 analog input pins
• External voltage reference input pins
• Simultaneous sampling of up to four analog input pins
• Automatic Channel Scan mode
• Selectable conversion trigger source
• Selectable Buffer Fill modes
• DMA support, including Peripheral Indirect Addressing
• Four result alignment options (signed/unsigned, fractional/integer)
• Operation during CPU Sleep and Idle modes

In addition of 32 A/D input channels there are two analog input pins for external voltage reference connections. These voltage reference inputs can be shared with other analog input pins.

The analog inputs are multiplexed to four Sample/Hold amplifiers, designated CH0-CH3. Where one, two, or four of the Sample/Hold amplifiers can be enabled for acquiring input data. The analog input multiplexers can be switched between

two sets of analog inputs during conversions. It is possible make unipolar differential conversions. Moreover, it is possible to make an Analog Input Scan mode for the CH0 Sample/Hold Amplifier where the user specifies which analog input channels are included in the scanning sequence.

The ADC is connected to a single-word result buffer. Each conversion result is converted to one of four 16-bit output formats when it is read from the buffer. However, multiple conversion results can be stored in a DMA RAM buffer with no CPU overhead.

The 12-bit ADC configuration supports all the 10-bit ADC features, except:

• In the 12-bit configuration, conversion speeds of up to 500 ksps are supported
• There is only one Sample/Hold amplifier in the 12-bit configuration, so simultaneous sampling of multiple channels is not supported.
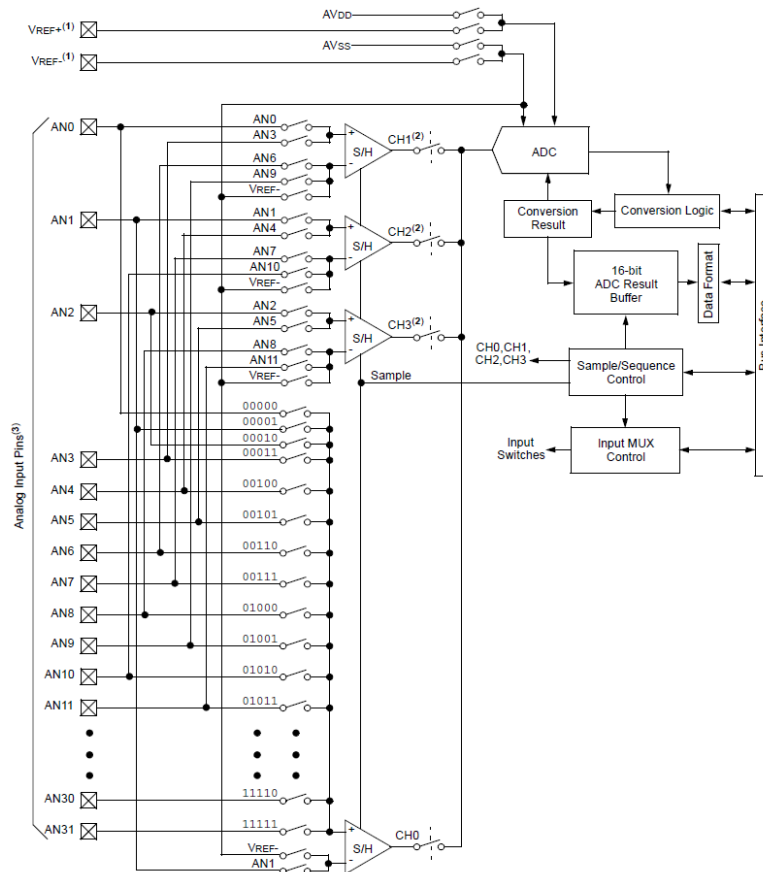

Figure24.ADC block diagram (21)

3.2.4.1 A/D CONVERSION SEQUENCE

A basic conversion sequence is presented in figure25. As we know the sampling of the analog input pin voltage is performed by Sample/Hold amplifiers. The Sample/Hold channels are connected to the analog input pins via the analog input multiplexer. There are two sets of multiplexer control bits in the ADC channel

select registers that function identically. These two sets of control bits allow two different analog input multiplexer configurations to be programmed called MUX A and MUX B. The ADC can optionally switch between the MUX A and MUX B configurations between conversions. In addition the ADC can also optionally scan through a series of analog inputs.

The sample time is the time that the ADC module's Sample/Hold Amplifier is connected to the analog input pin. The sample time can be started manually or started automatically by the ADC hardware. In the same way, it is ended manually by clearing the SAMP control bit in the user software or automatically by a conversion trigger source.

The conversion time is the time required for the ADC to convert the voltage held by the Sample/Hold Amplifier. In this part the ADC is disconnected from the analog input pin. The ADC requires one A/D clock cycle (TAD) to convert each bit of the result plus two additional clock cycles. Therefore a total of 12 TAD cycles are required to perform the complete conversion in 10-bit mode. On the other hand a total of 14 TAD cycles are required to perform the complete conversion in 12-bit mode. When the conversion time is complete, the result is loaded into the ADCxBUF0 register, the Sample/ Hold Amplifier can be reconnected to the input pin and a CPU interrupt can be generated.

It is important to take into account that there is a minimum sample time to ensure that the Sample/Hold Amplifier provides the desired accuracy for the A/D conversion. Furthermore, there are multiple input clock options for the ADC, so be sure that do not violet the minimum TAD.

Moreover, the ADC allows many options for specifying the sample/convert sequence. The sample/convert sequence can be using only one Sample/Hold amplifier, or multiple conversions using more than one Sample/Hold amplifier. The 10-bit ADC configuration can use two Sample/Hold amplifiers to perform two conversions in a sample/convert sequence or four Sample/Hold amplifiers with four conversions.
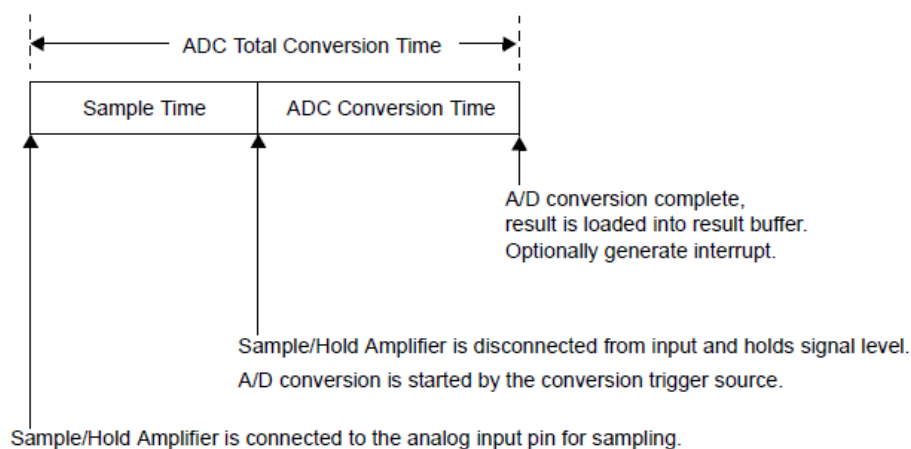

Figure25. ADC sample/conversion sequence

A sample/convert sequence that uses multiple Sample/Hold channels can be simultaneously sampled or sequentially sampled. Where, simultaneously sampling multiple signals ensures that the snapshot of the analog inputs occurs at precisely the same time for all inputs, and sequential sampling takes a snapshot of each analog input just before conversion starts on that input. (21)

3.2.5 I^2C communication

I^2C stands for inter-Integrated Circuit module. This module is a serial interface very useful for communicating with others peripherals like serial EEPROMs, display drivers, A/D converters or microcontroller devices.

There are three different systems in which the I^2C module can operate:

• As a slave device
• As a master device in a single-master system (slave may also be active)
•As a master/slave device in a multi-master system (bus collision detection and arbitration available).

The I^2C module contains two independent logics, the I2C master logic and I2C slave logic. Each logic is able to generate interrupts based on their events. Nevertheless, in multi-master systems, the software is divided into master controller and slave controller.

When the I^2C master logic is enabled, the slave logic also remains active. The salve detects the state of the bus and is able to receive messages from itself in a single-master system or from other masters in a multi-master system. Therefore, no messages are lost during multi-master bus arbitration.

In a multi-master system, bus collision conflicts with other masters in the system can occur, however the module is able to provide a method to terminate the operation and then restart the message.

The I^2C module contains a Baud Rate Generator. The Baud rate is the number of signal units per second; this means that a baud may contain several bits. A very important fact is that the I^2C Baud Rate Generator does not consume other timer resources in the microcontroller.

 Features of the I^2C module are:

• Independent master and slave logic
• Multi-master support which prevents message losses in arbitration
• Detects 7-bit and 10-bit device addresses with configurable address masking in Slave mode
• Detects general call addresses as defined in the I2C protocol
•Bus Repeater mode, allowing the module to accept all messages as a slave regardless of the address

•Automatic SCLx clock stretching provides delays for the processor to respond to a slave data request
• Supports 100 kHz and 400 kHz bus specifications
• Supports the Intelligent Platform Management Interface (IPMI) standard

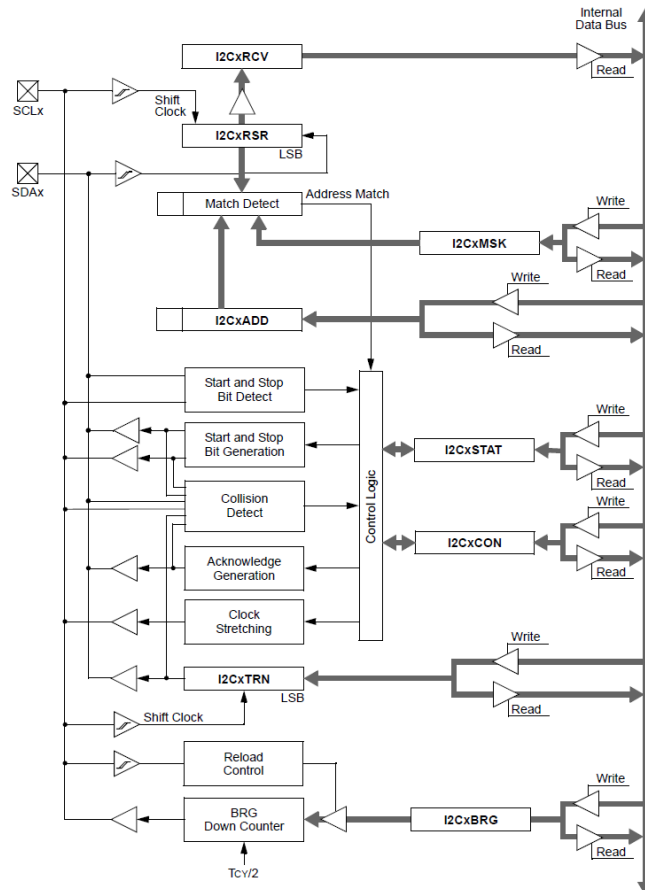The block diagram of the I^2C module is presented in figure26.

Figure26. Block diagram I^2C module. (22)

3.2.5.1 I^2C -BUS CHARACTERISTICS

The I^2C -bus is composed of two-wire serial interface. There is the SDA wire, in which the data is transmitted, and the SCL, in which the clock is transmitted. The interface uses an exhaustive protocol to ensure reliable transmission and reception of data.

The device acting as a master initiates transfer on the bus and also generates the clock signals to permit that transfer. The device acting as slave just responses to the transfer. Therefore, the clock line (SCLx) is an output from the master and an input to the slave, although occasionally the slave drives the SCLx line. However, The data line (SDAx) can be output and input from both the master and slave.

Is important to notice that the output stages of the devices driving the SDAx and SCLx lines must have an open drain in order to perform the wired AND function of the bus. Therefore the SDAx and SCLx lines are bidirectional. Moreover there are

external pull-up resistors to ensure a high level when no device is pulling the line down.

In the I^2C interface protocol, each device has an address. Then, when a master wishes to initiate a data transfer, it first transmits the address of the device that it wants to transfer to. All devices receive the request to see if this is their address. Within this address the last bit indicates whether the master wants to read from or write to the slave device. The master and slave can operate in either of the following two relations:

• Master-Transmitter and Slave-Receiver
• Slave-Transmitter and Master-Receiver

Very important, in either case, the master originates the SCLx clock signal.

3.2.5.2 Bus Protocol

The I2C-bus protocol is defined as:

• Data transfer may be initiated only when the bus is not busy.
•During data transfer, the data line must remain stable whenever the SCLx clock line is high. Changes in the data line while the SCLx clock line is high will be interpreted as a Start or Stop condition.

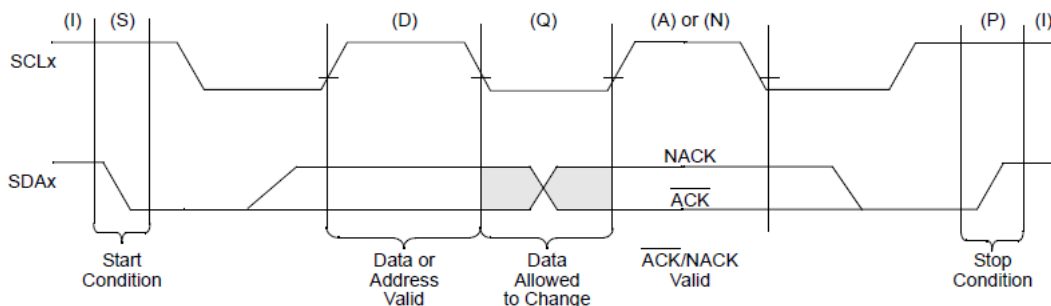According to this, the bus conditions are shown in Figure27.

Figure27. Bus conditions (22)

3.2.5.2.1   START DATA TRANSFER (S)

After a bus Idle state, a high-to-low transition of the SDAx line while the clock (SCLx) is high determines a Start condition. All data transfers must be preceded by a Start condition.

3.2.5.2.2   STOP DATA TRANSFER (P)

A low-to-high transition of the SDAx line while the clock (SCLx) is high determines a Stop condition. All data transfers must end with a Stop condition.

3.2.5.2.3   REPEATED START (R)

After a wait state, a high-to-low transition of the SDAx line while the clock (SCLx) is high determines a Repeated Start condition. Repeated Starts allow a master to change bus direction or addressed slave device without relinquishing control of the bus.

3.2.5.2.4   DATA VALID (D)

The state of the SDAx line represents valid data when, after a Start condition, the SDAx line is stable for the duration of the high period of the clock signal. There is one bit of data per SCLx clock.

3.2.5.2.5   ACKNOWLEDGE (A) OR NOT ACKNOWLEDGE (N)

All data byte transmissions must be Acknowledged (ACK) or Not Acknowledged (NACK) by the receiver. The receiver will pull the SDAx line low for an ACK or release the SDAx line for a NACK. The Acknowledge is a 1-bit period using one SCLx clock.

3.2.5.2.6   WAIT/DATA INVALID (Q)

The data on the line must be changed during the low period of the clock signal. Devices may also stretch the clock low time by asserting a low on the SCLx line, causing a wait on the bus.

3.2.5.2.7   BUS IDLE (I)

Both data and clock lines remain high at those times after a Stop condition and before a Start condition.

3.2.5.3 Message Protocol

The message protocol is defined as: the data as driven by the master device and the data as driven by the slave device, taking into account that the combined SDAx line is a wired AND of the master and slave data. The master device controls and sequences the protocol. The slave device will only drive the bus at specifically determined times.

3.2.5.3.1   START MESSAGE

Each message is initiated with a "Start" condition and terminated with a "Stop" condition. The number of data bytes transferred between the Start and Stop conditions is determined by the master device. As defined by the system protocol, the bytes of the message may have special meaning, such as "device address byte" or "data byte".

3.2.5.3.2   ADDRESS SLAVE

the first byte must be the device address byte. It contains a device address and an R/W status bit. Note that R/W = 0 indicates that the master will be a transmitter and the slave will be a receiver and R/W = 1 is vice versa.

3.2.5.3.3   SLAVE ACKNOWLEDGE

The receiving device has to generate an Acknowledge signal, "ACK", after the reception of each byte, because the master device must generate an extra SCLx clock, which is associated with this Acknowledge bit.

3.2.5.3.4   MASTER TRANSMIT

The next two bytes, sent by the master to the slave, are data bytes containing the location of the requested data byte. The slave must Acknowledge each of the data bytes.

3.2.5.3.5   REPEATED START

When the slave has the address information necessary to return the requested data byte to the master, the bus must be turned in the read direction for the slave to send data to the master. To perform this function without ending the message, the master sends a "Repeated Start". The Repeated Start is followed with a device address byte containing the same device address as before and with the R/W = 1 to indicate slave transmission and master reception.

3.2.5.3.6   SLAVE REPLY

The slave transmits the data byte by driving the SDAx line, while the master continues to originate clocks but releases its SDAx drive.

3.2.5.3.7   MASTER ACKNOWLEDGE

During reads, a master must terminate data requests to the slave by Not Acknowledging Which is generating a "NACK" on the last byte of the message.

3.2.5.3.8   STOP MESSAGE

The master sends a Stop to terminate the message and return the bus to an Idle state.

3.2.5.4 ENABLING I2C OPERATION

The I^2C module fully implements all master and slave functions. When the module is enabled, the master and slave functions are active simultaneously and will respond according to the software or bus events. Moreover the module will release the SDAx and SCLx pins, putting the bus into the Idle state. There are two actions that initiate a master event: first set the SEN control bit and second load the data into the I2CxTRN register.

As mentioned before, when the master logic is active, the slave logic also remains active. Therefore, the slave functions will begin to monitor the bus. Then, if the slave logic detects a Start event and a valid address on the bus, the slave logic will begin a slave transaction.

There are two pins used for bus operation: the SCLx pin, which is the clock, and the SDAx pin, which is the data. When the module is enabled, assuming no other module with higher priority has control, it will assume control of the SDAx and SCLx pins. In addition, the module software does not has to be concerned of the state of the port I/O pins because it overrides the port state and direction. However, at initialization, the pins are tri-stated (released).

The I^2C module is able to generate two interrupts. One interrupt is assigned to master events; the other interrupt is assigned to slave events.

The master interrupt can be generated with the following master message events:

• Start condition
• Stop condition
• Data transfer byte transmitted/received
• Acknowledge transmit
• Repeated Start
• Detection of a bus collision event

On the other hand the slave interrupt is generated the following slave message events:

• Detection of a valid device address (including general call)
• Request to transmit data (ACK) or to stop data transmission (NACK)
• Reception of data

3.2.5.4.1 Setting Baud Rate When Operating as a Bus Master

When operating as I^2C master, the module must generate the system SCLx clock. I^2C system clocks are specified to be one of these: 100 kHz, 400 kHz or 1 MHz. The system clock rate is specified as the minimum SCLx low time and the minimum SCLx high time.

The reload value for the Baud Rate Generator (BRG) is the I2CxBRG register. It is calculated as shown in equation 3-4. When the Baud Rate Generator is loaded with this calculated value, the generator begins to count down to 0 and stops until another reload has taken place. It is important to say that the generator count is decremented twice per instruction cycle (TCY). The Baud Rate Generator is reloaded automatically on baud rate restart. (22)

$$I2CBRG = \left(\frac{Fcy}{Fscl} - \frac{Fcy}{10,000,000}\right) - 1 \qquad (3\text{-}4)$$

4. DEVELOPMENT SOFTWARE

In this section I will introduce the configurations of every device on the UDB4 and every module in the microcontroller, along with the explication of why is configure in that way. In addition I will present all the flowcharts of every code.

3.1 CONFIGURATION MICROCONTROLLER

4.1.1 Oscillator

It is widely known that the microcontroller needs, to function, some sort of external oscillator. This is because the hardware in the controller is based on sequential logic. In other words, without an oscillator the microcontroller would not execute instructions consistently, and as a result, the outputs will become unpredictable in terms of timing and value.

I configure the oscillator to operate as fast as it possible could go in order to obtain a high frequency operation of instructions. To this aim, the internal FRC is selected, which operates with a 7.37 MHz crystal. At this point, I enable the clock switching and select the primary oscillator in XT mode; as a result the main oscillator will run the processor on the microcontroller at 40 MIPS (80 MHz). However, as mentioned before, the clock frequency is half of oscillator's frequency therefore the Fcy will be 40MHz.

In addition to this configuration, I have to use the PLL, because PLL is the one that makes things go faster. To achieve 40 MHz, the PLL prescaler, PLL postscaler and PLL divisor have to be settled down. As we see in section 2.2.1.4 there are equations that give us these parameters. Figure28 remain us the PLL block diagram. After all, I obtain M=43 (PLL divisor), N1=2 (PLL prescaler) and N2=2 (PLL postscaler).

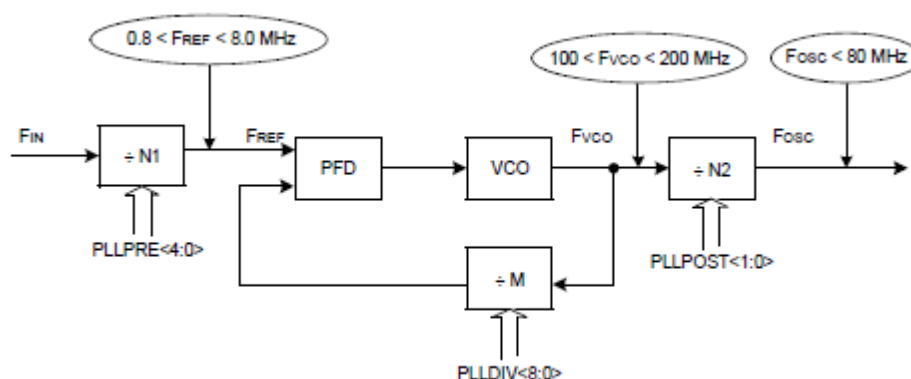Figure28. PLL block diagram

4.1.2 Timer

At first, one may thing that timers are exactly what they sound like. Something that keeps track of time and sends back a signal when the time is up. However, one may thing twice because microcontrollers do not keep track of absolute time. Microcontrollers are able to keep track of relative time with the use of a clock signal, whether it is externally generated or created internally. Consequently, the interpretation of a timer isn't counting clock, but more of a counter of clock cycles. Nevertheless, the simplest way to imagine the timer is as a counter where one set a value to count and it starts to count down the clock cycles. Once it has reached the value, sends a signal to make the microcontroller know.

As a matter of fact I use two timers type A in a counter mode. the first timer is use to generate an interruption every 1ms. In brief the interruption is the signal that the timer sends when the time is up. The second timer is use to generate an interruption every 20ms. The first timer is use to run the instruction where all data output of the ADC is save. In the other hand, the second timer is use to run the instruction where all the data output of the magnetometer is save.

In table2 is present the frequencies and times that a timer type A could possible has. The time can change because of the prescaler. The count is loaded into the register TMR. The value that has to be calculated is the PR1 value. This value corresponds to the count of clock frequency necessary to obtain the desired interruption value.

VARIABLE	VALUE	UNITS	NOTE
Clock frequency Fcy	40M	Hz	The maximum frequency is 80MHz but Fcy=Fosc/2
PR1	65536		Maximum value of the counter TMR (2^16)
Frequency-Prescaler 256	156250	Hz	Fcy=Fcy/256
Period-Prescaler 256-bit	6,4u	s	1/Fcy
Total-Period-prescaler 256	0.41	s	P=PR1*(1/Fcy)
Frequency-Prescaler 64	625000	Hz	Fcy=Fcy/64
Period-Prescaler 64-bit	1.6u	s	1/Fcy
Total-Period-prescaler 64	104,8m	s	P=PR1*(1/Fcy)
Frequency-Prescaler 8	5M	Hz	Fcy=Fcy/8
Period-Prescaler	200n	s	1/Fcy

8-bit			
Total-Period-prescaler 8	13.10m	s	P=PR1*(1/Fcy)
Frequency-Prescaler 1	40M	Hz	Fcy=Fcy
Period-Prescaler 1-bit	25n	s	1/Fcy
Total-Period-prescaler 1	1.63m	s	P=PR1*(1/Fcy)

Table2. Timer values.

4.1.3 I/O port

Before configuring the pins as an input or output, one must first be able to identify the pins that can be or want to be configured. In the figure below taken directly from UDB4's datasheet, there are several important things to notice.
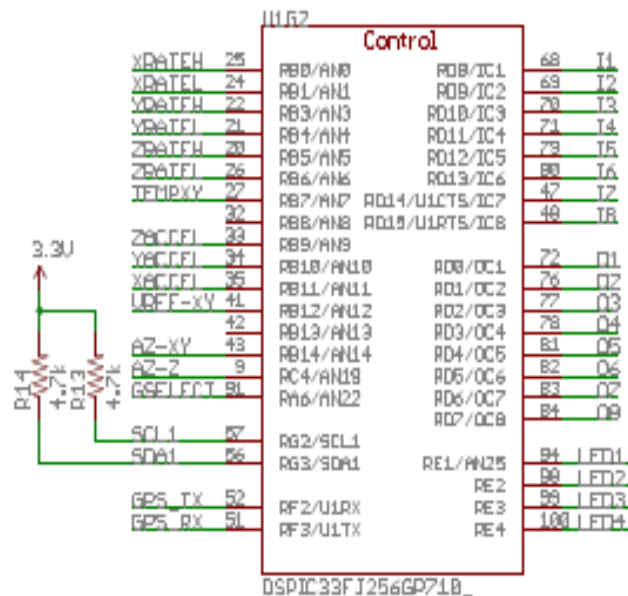
Figure29. Microcontroller diagram

1. The analog/digital pins have the prefix AN (ex. AN0, AN1 … AN22).
2. Pins with levels RB (ex. RA0, RA1 …) and RD (ex. RB0, RB1 …) are its input and output banks.
3. On the low part, pins with RE are specially for leds.

Basically I am concerned in the analog pins which correspond to the output of the sensors (accelerometer and gyroscopes). As we can see in figure28 these analog pins are all in port B, therefore I configured all port B as an input to the microcontroller.

4.1.4 A/D converter

The A/D conversion is very useful when one has to obtain data from the sensors. There are two sensors with an analog output. Moreover, each sensor has 3 different axes to read. After all, there are 9 analog channels to read from the sensors. The following steps explain the configuration of the module to perform an A/D conversion:

1. I Select 12-bit mode to obtain conversion speed up to 500 ksps. Faster than the 10-bit mode.

2. I Select voltage reference source to be the internal AVDD and AVSS voltage rails to match expected range on analog inputs.

3. I select the analog conversion clock to match desired data rate with processor clock. The conversion clock is known as TAD. The A/D conversion requires 14 clock periods (14 TAD) in the 12-bit mode. The A/D conversion clock is derived from the device instruction clock. The period of the A/D conversion clock is software selected using a 6-bit counter therefore there are 256 possible options for TAD. However, For correct A/D conversions, the A/D conversion clock (TAD) must be selected to ensure a minimum TAD time of 75 nsec. In order to obtain the fastest conversion time I configure TAD to be 75 ns.

4. I select every port pin, where the outputs of the sensors are, as analog inputs. This analog input is connected to the sample and hold channel internally.

5. As I have selected to work in 12-bit mode, I can only use one Sample/Hold channels. Consequently I have to change manually the conversion channel between the 9 input channels.

6. I select Manual Sampling mode instead of auto sampling mode. As mentioned before, I will select manually the channel for conversion, then I star the sampling manually.

7. I select auto conversion trigger in order to have the conversion trigger under A/D clock control. This trigger option provides the fastest conversion rates. Finally, The Auto Sample Time selects the number of TAD clock cycles between the start of sampling and the start of conversion. The auto sample time is 14*TAD.

8. I select to store the conversion results in the buffer as an integer.

9. Finally I turn on ADC module.

In figure30 is showed the flowchart of the ADC module. One should notice that the selection of channel is manual and the conversion of each channel is auto. All in all, in table3 there are all the ADC times' values.
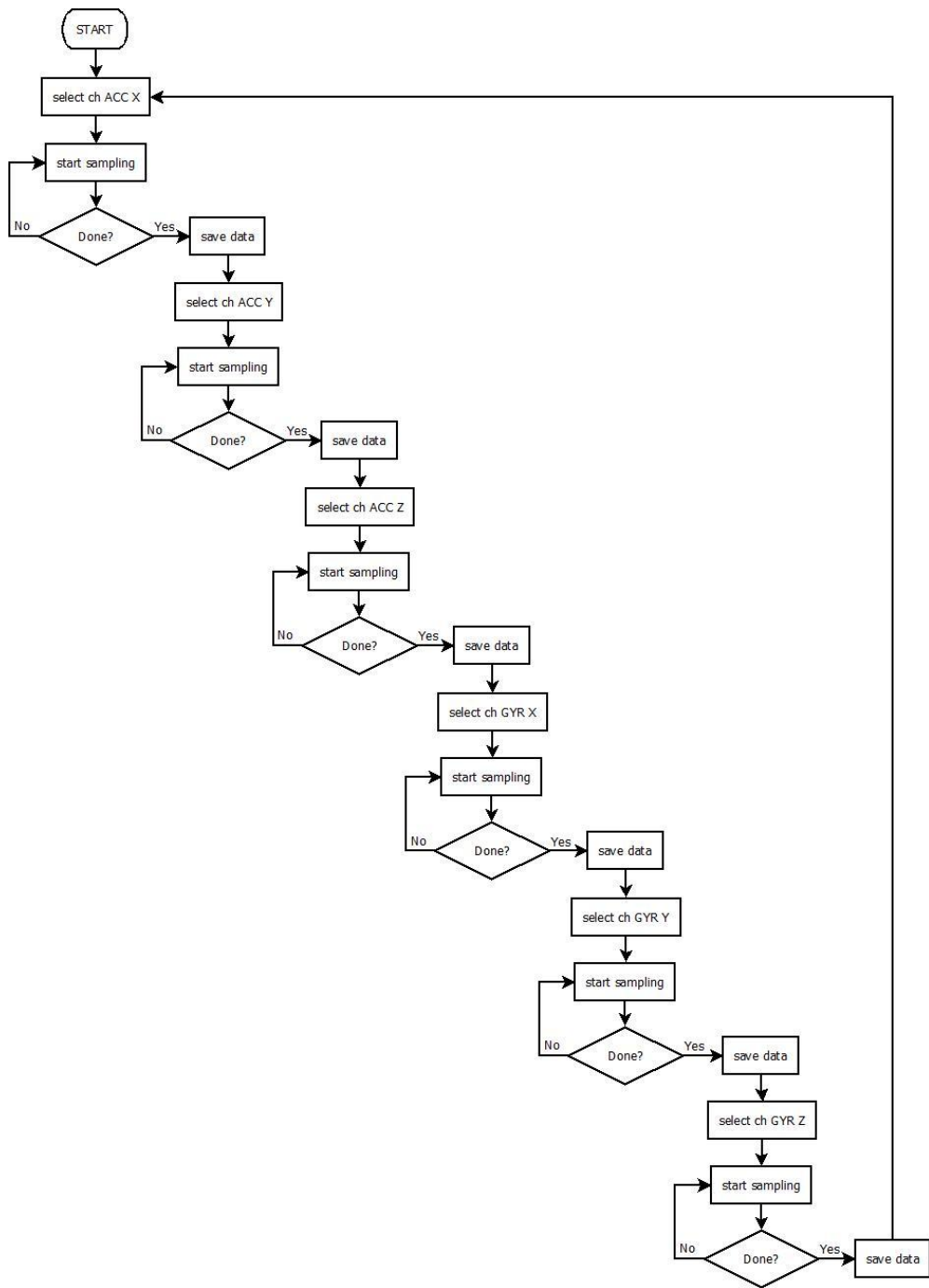
Figure30. ADC flowchart.

VARIABLE	VALUE	UNITS	NOTE
Frequency oscillation Fcy	40M	Hz	The maximum frequency is 80MHz but Fcy=Fosc/2
PR1	65536		Maximum value of the counter TMR (2^16)
Tad	75n	s	Bit Acquisition time
Number of Channels	9	[]	3*Acc 3*Gyro
Sample single channel	75n*14=1.05μ	s	Sample single channel time
Sample measure period	1.05 μ*9=9.45 μ	s	Sample single channel time* Number of Channels
Sample measure Frequency	105.82k	Hz	1/ Sample measure period
Control period	20m	s	
Control Frequency	50	Hz	

Table3. ADC values.

4.1.5 I^2C Communication

The I^2C module is use to communicate the microcontroller, as a master, with the magnetometer, as a slave. In this communication there are two main types of operations, the write command, and the read command. In general, a packet sent by the master to the slave for a write command is like this:
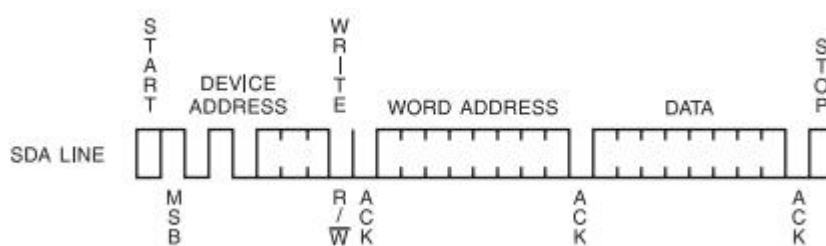
Figure31. Write command [taken from the datasheet of the AT24C02B EEPROM chip from Amtel.]

There are three bytes sent from the master device to the slave device. The first byte is the slave address, in figure30 is the "DEVICE ADDRESS", along with the read or write indicator bit. In this first byte the first 7 bits are the slave device address, usually this value is indicated in the data sheet of the slave device. In order for the I2C bus to allow for multiple slaves, the master must indicate which device the message is intended. The last (8th) bit of the first byte is the read or write indicator, as mentioned before, if the bit is a 0, the master wants to write and

if it is a 1, the master intends to read. Next, the master waits for an acknowledge bit from the slave. The slave device send the acknowledge bit if the address sent by the master corresponds to the slave address. If the ACK bit is 1, which means a non-acknowledge, the master thinks there is no slave device, and then the master terminates the packet with a STOP bit. The second byte is the slave's internal address; in figure30 is the "WORD ADDRESS". After the second byte, the slave device must acknowledge that the specified address exists as one of the slave device's internal addresses. Lastly, the third byte is where the master device sends the data it intends to write. This is usually referred to as the data byte. Here also after the third byte, the slave device acknowledges the received byte, and the communications is terminated by a stop bit.

The second command is the read command. Sometimes it is called a random read because the command has the ability to read any address at will, instead of sequential read, where everything must be read until the desired data is located. A read command is like this:
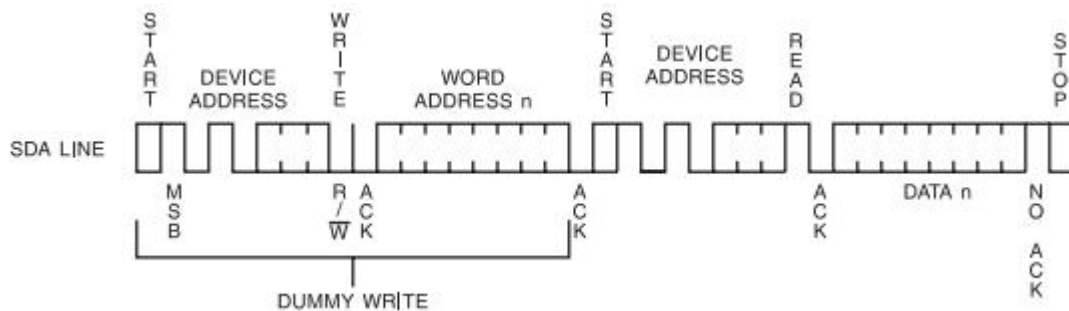
Figure32. Read command [taken from the datasheet of the AT24C02B EEPROM chip from Amtel.]

First of all, to make a random read the master device must first act like it intends to do a write by sending the slave device address with a write command bit, this mean sending the first byte of a write command. Then the master sends the internal address, the second byte of a write command. The slave device has to send ACK bit of both bytes to indicate to the master device of its presence and correct internal address. However, the intention is to read and not to write, for this, the master device don't send the third byte of the write command, instead it presents a start bit. In other words, in the 3rd byte the master device resends the slave address, but this time the last (8th) bit, which is the read or write indicator, is set in 1, to indicate a read. At this point, after the slave address sends an ACK bit back to the master, the master device is still in control of the SDA line, but the slave device takes over the SDA line starts transmitting the byte located at the internal address, and then waits for ACKs from the master device. After the transmission of data, the master device must indicate a NACK, the inverse of the ACK bit to tell the slave device to stop sending data. Finally the master ends the transmission with a stop bit.

In the magnetometer there are 3 register to write the desired configuration. This configuration will be explained in the **section 3.2.3.** However, the procedure to

write these register is the same explained above. In addition to the explication, in figure33 is presented the flowchart of the write command.
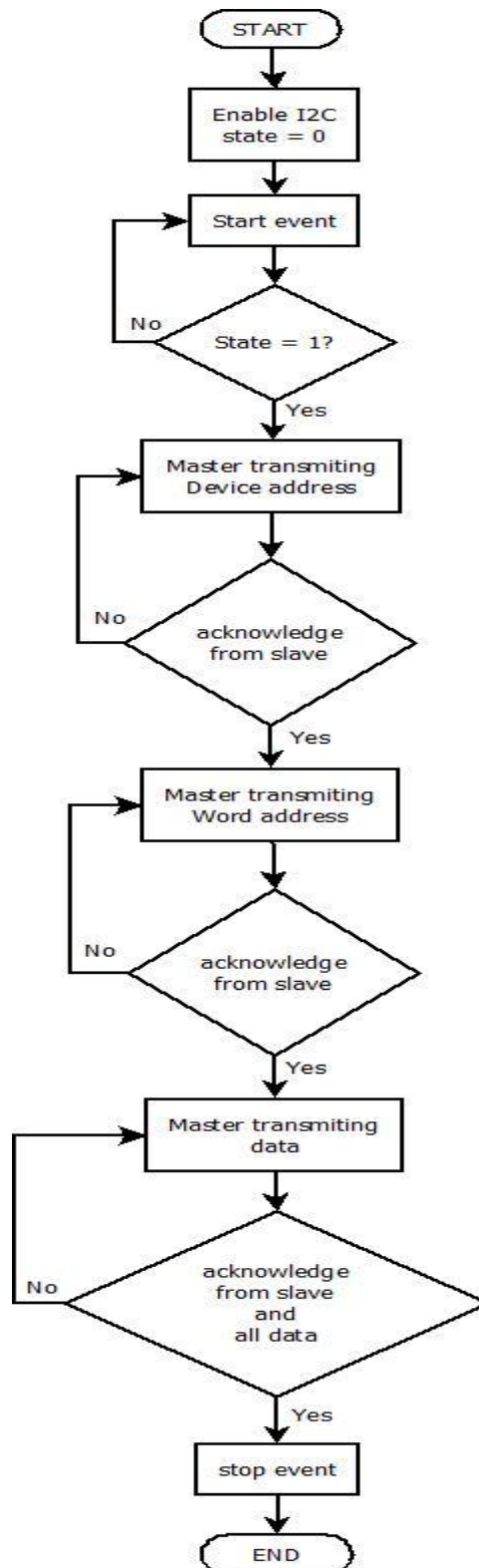

Figure33. Flowchart I^2C write command

There are 13 registers to read in the magnetometer. However, just six registers contains the data output that interests me, which is the data output of each axes. There are two registers for each one. Eventually to read these registers I use the procedure explain above. . In addition to the explication, in figure34 is presented the flowchart of the read command.
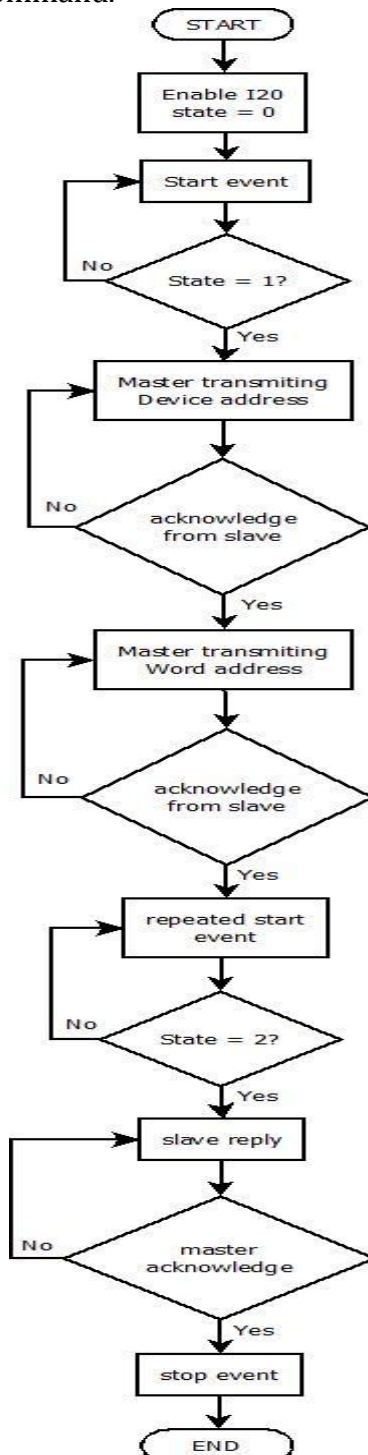
Figure34. Flowchart I^2C read command

4.2 Configuration UBD4

4.2.1 Accelerometer

As mentioned before, the accelerometer has X-axis, Y-axis and Z-axis. These 3 axes are analog inputs to the microcontroller. For this reason they are controlled by the ADC. To sum up, table4 shows parameters and configuration for the accelerometer.

Number	Variable	Symbol	Unit	Value	Comment	Equation
1	Zero-g	g	V	1.65	Output without acceleration	
2	Sensitivity value	S	mV*s^2/m	81.549	The value of the sensitivity	
3	Max-Output-Voltage	V_{outmax}	V	2.85		Vout=Vzero-g+ Sensitivity*1.5g
4	Min-Output-Voltage	V_{outmin}	V	0.45		Vout=Vzero-g- Sensitivity*1.5g
6	Max-Digital word-ADC	D_{max}		4096		12-bit then 2^12
7	Max-Digital word-ACC	D_{max}		3537		Round(2.85 *4096/3.3)
8	Min-Digital word-ACC	D_{min}		559		Round(0.45 *4096/3.3)
9	Range-Digital word-ACC	ΔD_{acc}		2978		
10	Rho voltage	Rho	V	805.664 μ		3.3/2^12
11	Rho Acceleration	Rho	m/s^2	9.87m		(3.3/2^12)/ 81.549m
12	Max-acceleration-1.5g	a_{max}	m/s^2	14.715		g=9.81 m/s^2
13	Min-acceleration-1.5g	a_{min}	m/s^2	-14.715		g=9.81 m/s^2

Tabla4. Configuration Accelerometer.

4.2.2 Gyroscope

As mentioned before, there are two gyroscopes. The first one has X-axis and Y-axis, and the second one has Z-axis. These 3 axes has 2 outputs, one with an amplifier to make it more sensible, and one without amplifier. These 6 outputs are analog inputs to the microcontroller. For this reason they are controlled by the ADC. To sum up, table5 shows parameters and configuration for the gyroscope.

Number	Variable	Symbol	Units	Value	Notes	Equation
1	ZERO-RATE OUTPUT	V_{ZERO}	V	1.35	Output without any gyro	
2	Full-Scale Range X-OUT		rad/s	±8.72	Range for the sensitivity	
3	Sensitivity value X-OUT	S	mV/(rad/s)	114.6	The value of the sensitivity	
4	Max-X-Output-Voltage	V_{outmax}	V	2.35		$V_{outmax}=V_{ZERO}+S*\omega_{qmax}$
5	Min- X -Output-Voltage	V_{outmin}	V	0.35		$V_{outmin}=V_{ZERO}+S*\omega_{qmin}$
6	Max-Digital word-ADC	D_{maxADC}		4096	12-bit then 2^12	
7	Max-Digital word-GYRO	D_{max}		2917		$(V_{outmax}*D_{maxADC})/3.3$
8	Min-Digital word-GYRO	D_{min}		434		$(V_{outmin}*D_{maxADC})/3.3$
9	Range-Digital word	ΔD_{gyr}		2483	12-bit	
10	Full-Scale Range X4.5-OUT		rad/s	±1.91	Range for the sensitivity	
11	Sensitivity value X4.5-OUT	S	V/(rad/s)	0.52	The value of the sensitivity	
12	Max-X4.5-Output-	V_{outmax}	V	2.351		$V_{outmax}=V_{ZERO}+S*$

	Voltage				ω_{qmax}
13	Min- X4.5 - Output- Voltage	$\boldsymbol{V_{outmin}}$	V	0.349	$\boldsymbol{V_{outmin}} = \boldsymbol{V_{ZERO}} + \mathbf{S}^* \, \boldsymbol{\omega_{qmin}}$
14	Max- Digital word- GYRO4.5	$\boldsymbol{D_{max}}$		2918	$(\boldsymbol{V_{outmax}} * \boldsymbol{D_{maxADC}}) / \mathbf{3.3}$
15	Min-Digital word- GYRO4.5	$\boldsymbol{D_{min}}$		433	$(\boldsymbol{V_{outmin}} * \boldsymbol{D_{maxADC}}) / \mathbf{3.3}$
16	Range- Digital word	$\boldsymbol{\Delta D_{gyr}}$		2485	12-bit
17	Rho voltage	**Rho**	V	805.664 µ	3.3/2^12
18	Rho Angular acceleration WITHOUT AMPLIFIER	**Rho**	rad/s	7.030m	(3.3/2^12) / 114.6m
	Rho Angular acceleration WITH 4.5 AMPLIFIER	**Rho**	rad/s	1.54m	(3.3/2^12) / 520m
19	Max- angular velocity	$\boldsymbol{\omega_{qmax}}$	rad/s	8.72	1rad---57.3°
20	Min- angular velocity	$\boldsymbol{\omega_{qmin}}$	rad/s	-8.72	1rad---57.3°

Tabla5. Configuration Gyroscope.

4.2.3 Magnetometer

As mentioned before, the magnetometer has 3 register in charge of the configuration of itself. To configure these 3 registers it is necessary use the I^2C module, as mentioned in **section 3.1.5**. all in all, these 3 registers are configured in such way to obtain: 8 samples averaged, 75Hz rate output data, normal measurement configuration and the most sensitive gain (72.99 nT). In table6 are presented all the parameters and values of the magnetometer's configuration.

Number	Variable	Symbol	Unit	Value	Comment	Equation
1	Field Range		uT	±800		
2	Dynamic Range		uT	±88		
3	Sensitivity	S	nT/Lsb	72.99	In another unit is 1370Lsb/gauss	
4	Noise floor		uT	0.2		
6	Measurement Period	T	ms	6	Time from receiving command to data ready	
7	Turn on time	Ton	us	200	Time to be ready for I2C commands	
8	I2C read address	Radd	hex	0x3D		
9	I2C write address	Wadd	hex	0x3C		
10	Output Rate In time	ODR	ms	13.3	For continuous measurement mode	1/75
11	Output Rate	ODR	Hz	75	For continuous measurement mode	
12	I2C Rate		Hz	400	Baud rate used by the Master	

Tabla6. Configuration Magnetometer.

5. RESULTS

5.1 DESCRIPTION OF TEST

In order to obtain a reliable data from the accelerometer, gyroscopes and magnetometer, they were subjected to a test. The test consists in measure the data output of every sensor in an uncontrolled environment and then make the same measures on a controlled environment. At the end of the test is expected to obtain the Bias, the standard deviation and the noise of every sensor.

One should take into account that every sensor has its own method to be measure. The accelerometer has three axes, and then every single axis has to be subjected to positive gravity and negative gravity. The magnetometer has its own self test, where a current is forced to pass in positive and negative way. Therefore there will be a known electromagnetic field for positive and negative way. And finally, the gyroscope is measure without any gyro or disturbance just to see the noise.

5.1.1 EQUIPMENT REQUIERED

NUMBER	INSTRUMENT	CHARACTERISTIC	COMMENT
1.	Voltage supply	0 – 12 V and 0 – 1 A	We are working with 7 V
2.	Digital voltmeter	NA	To measure 7 V in the input
3.	Cables		To connect the DVM with the voltage supply

Tabla7. Equipment required.

5.1.2 MEASUREMENTS

After settle down the timer, the oscillator and the ADC with all the channels that are connected to every single exit of the gyroscope and accelerometer, I was able to obtain the data from the sensors. Now I want to analyze the data. For this aim I set the timer to interrupt every 100 us and save the data from the one channels of the sensors (every channel is connected to a X, Y and Z axes of the sensors).This mean that I will sample the data value from the ADC every 100 us, this is in frequency every 10 kHz. I choose to sample 10000 times to obtain the result of 1 seconds (100 us * 10000).

Also I applied one filter to reduce the noise at the output. At first I was sampling the output data from the ADC every 100 us and save the value. Then to make the filter I take 10 values and calculate the average value of them. This mean that I will

take one average value every 1ms, which is equivalent to 10 values times 100 us. So if the time of the measurement is 1s I am able to calculate 1000 averages values. At the end the output data that I will be save is the average value that I can get every 1ms, in frequency 1 kHz. The filter is implemented due to the acquisition velocity is very high while the control command runs at 20ms therefore it is no necessary take samples at 10kHz, but doing this allow us to make a free measure of the noise at 1KHz.

Then the results are passed to matlab where I can do my analysis. Basically in matlab the results of every single axe of the sensors are plotted and from it I get the bias, the variance, the standard deviation and the power spectral density.

5.1.3   LIST OF MEASUREMENTS

In table8 are present all the measures that I made in order to analyze the data output of all sensors. As one can see, every axis is subjected to a test.

NUMBER	PROGRAM	MEASURE	TEST	SAMPLES	FREQUENCY	COMMENTS
1.	sensorsTimerfiltro - 10000 - acc channel X	Channel X without filter	Bottom view	10000	10KHz	There are 10000 values. sample every 100us
2.	sensorsTimerfiltro - 10000 - acc channel X	Channel X with filter	Bottom view	1000	1KHz	There are 1000 values. sample every 1ms
3.	sensorsTimerfiltro - 10000 - acc channel X	Channel X without filter	Side view	10000	10KHz	There are 10000 values. sample every 100us
4.	sensorsTimerfiltro - 10000 - acc channel X	Channel X with filter	Side view	1000	1KHz	There are 1000 values. sample every 1ms
5.	sensorsTimerfiltro - 10000 - acc channel X	Channel X without filter	Front inclination	10000	10KHz	There are 10000 values. sample

						every 100us
6.	sensorsTimerfiltro - 10000 - acc channel X	Channel X with filter	Front inclination	1000	1KHz	There are 1000 values. sample every 1ms
7.	sensorsTimerfiltro - 10000 - acc channel X	Channel X without filter	Back inclination	10000	10KHz	There are 10000 values. sample every 100us
8.	sensorsTimerfiltro - 10000 - acc channel X	Channel X with filter	Back inclination	1000	1KHz	There are 1000 values. sample every 1ms
9.	sensorsTimerfiltro - 10000 - acc channel X	Channel X without filter	Right inclination	10000	10KHz	There are 10000 values. sample every 100us
10.	sensorsTimerfiltro - 10000 - acc channel X	Channel X with filter	Right inclination	1000	1KHz	There are 1000 values. sample every 1ms
11.	sensorsTimerfiltro - 10000 - acc channel X	Channel X without filter	Left inclination	10000	10KHz	There are 10000 values. sample every 100us
12.	sensorsTimerfiltro - 10000 - acc channel X	Channel X with filter	Left inclination	1000	1KHz	There are 1000 values. sample every 1ms
13.	sensorsTimerfiltro - 10000 - acc channel Y	Channel Y without filter	Bottom view	10000	10KHz	There are 10000 values. sample

						every 100us
14	sensorsTimerfiltro - 10000 - acc channel Y	Channel Y with filter	Bottom view	1000	1KHz	There are 1000 values. sample every 1ms
15.	sensorsTimerfiltro - 10000 - acc channel Y	Channel Y without filter	Side view	10000	10KHz	There are 10000 values. sample every 100us
16.	sensorsTimerfiltro - 10000 - acc channel Y	Channel Y with filter	Side view	1000	1KHz	There are 1000 values. sample every 1ms
17.	sensorsTimerfiltro - 10000 - acc channel Y	Channel Y without filter	Front inclination	10000	10KHz	There are 10000 values. sample every 100us
18.	sensorsTimerfiltro - 10000 - acc channel Y	Channel Y with filter	Front inclination	1000	1KHz	There are 1000 values. sample every 1ms
19.	sensorsTimerfiltro - 10000 - acc channel Y	Channel Y without filter	Back inclination	10000	10KHz	There are 10000 values. sample every 100us
20.	sensorsTimerfiltro - 10000 - acc channel Y	Channel Y with filter	Back inclination	1000	1KHz	There are 1000 values. sample every 1ms
21.	sensorsTimerfiltro - 10000 - acc channel Y	Channel Y without filter	Right inclination	10000	10KHz	There are 10000 values. sample

						every 100us
22.	sensorsTimerfiltro - 10000 - acc channel Y	Channel Y with filter	Right inclination	1000	1KHz	There are 1000 values. sample every 1ms
23.	sensorsTimerfiltro - 10000 - acc channel Y	Channel Y without filter	Left inclination	10000	10KHz	There are 10000 values. sample every 100us
24.	sensorsTimerfiltro - 10000 - acc channel Y	Channel Y with filter	Left inclination	1000	1KHz	There are 1000 values. sample every 1ms
25.	sensorsTimerfiltro - 10000 - acc channel Z	Channel Z without filter	Bottom view	10000	10KHz	There are 10000 values. sample every 100us
26.	sensorsTimerfiltro - 10000 - acc channel Z	Channel Z with filter	Bottom view	1000	1KHz	There are 1000 values. sample every 1ms
27.	sensorsTimerfiltro - 10000 - acc channel Z	Channel Z without filter	Side view	10000	10KHz	There are 10000 values. sample every 100us
28.	sensorsTimerfiltro - 10000 - acc channel Z	Channel Z with filter	Side view	1000	1KHz	There are 1000 values. sample every 1ms
29.	sensorsTimerfiltro - 10000 - acc channel Z	Channel Z without filter	Front inclination	10000	10KHz	There are 10000 values. sample

						every 100us
30.	sensorsTimerfiltro - 10000 - acc channel Z	Channel Z with filter	Front inclination	1000	1KHz	There are 1000 values. sample every 1ms
31.	sensorsTimerfiltro - 10000 - acc channel Z	Channel Z without filter	Back inclination	10000	10KHz	There are 10000 values .sample every 100us
32.	sensorsTimerfiltro - 10000 - acc channel Z	Channel Z with filter	Back inclination	1000	1KHz	There are 1000 values. sample every 1ms
33.	sensorsTimerfiltro - 10000 - acc channel Z	Channel Z without filter	Right inclination	10000	10KHz	There are 10000 values. sample every 100us
34.	sensorsTimerfiltro - 10000 - acc channel Z	Channel Z with filter	Right inclination	1000	1KHz	There are 1000 values. sample every 1ms
35.	sensorsTimerfiltro - 10000 - acc channel Z	Channel Z without filter	Left inclination	10000	10KHz	There are 10000 values .sample every 100us
36.	sensorsTimerfiltro - 10000 - acc channel Z	Channel Z with filter	Left inclination	1000	1KHz	There are 1000 values. sample every 1ms
37.	sensorsTimerfiltro - 10000 – gyroscope X	Channel X without amplifie		1000	1KHz	There are 1000 values. sampled

				1000	1KHz	every 1ms
		r				
38.	sensorsTimerfiltro - 10000 – gyroscope X	Channel X with amplifier 4.5		1000	1KHz	There are 1000 values every 1ms
39.	sensorsTimerfiltro - 10000 – gyroscope Y	Channel Y without amplifier		1000	1KHz	There are 1000 values every 1ms
40.	sensorsTimerfiltro - 10000 – gyroscope Y	Channel Ywith amplifier 4.5		1000	1KHz	There are 1000 values every 1ms
41.	sensorsTimerfiltro - 10000 – gyroscope Z	Channel Z without amplifier		1000	1KHz	There are 1000 values every 1ms
42.	sensorsTimerfiltro - 10000 – gyroscope Z	Channel Z with amplifier 4.5		1000	1KHz	There are 1000 values every 1ms
43.	MAGNETOMETER	All three channels	Positive Bias	1000	50Hz	There are 1000 values. Sample every 20ms
44.	MAGNETOMETER	All three channels	Negative Bias	1000	50Hz	There are 1000 values. Sample every 20ms

Table8. List of measurements.

5.2 UNCONTROLLED ENVIRONMENT

5.2.1 ACCELEROMETER

As we see before, the accelerometer measures the acceleration that has every axis with respect to gravity. But the output data of the ADC is a digital word of 12bit, then, is necessary to converts this digital word into acceleration. If I multiply the

digital word by the quantization error of the ADC, I obtain the voltage. This voltage divide by the sensitivity of the accelerometer gives me the acceleration. To obtain the Bias I make the difference between the voltage at zero gravity from the datasheet and the mean value of the results I got from the ADC.

Finally I obtain the power spectral density of every channel. This basically is the power of the noise that will help me in the future when I make the control.

To test the accelerometer there are six different positions of the board, where every single axes is putted against the gravity. Next we will see the result and plots of the 6 different tests, everyone with the Bias, standard deviation and the power spectral density of each channel.

5.2.1.1 CHANNEL X

5.2.1.1.1   SIDE VIEW

In blue we can see 10000 samples at 10kHz; in red we can see the filter which is 1000 samples at 1kHz.

POWER SPECTRAL DENSITY Channel X
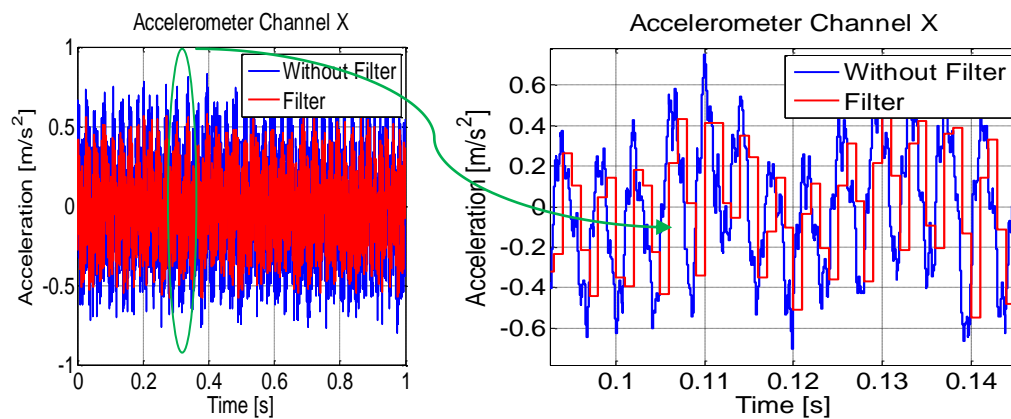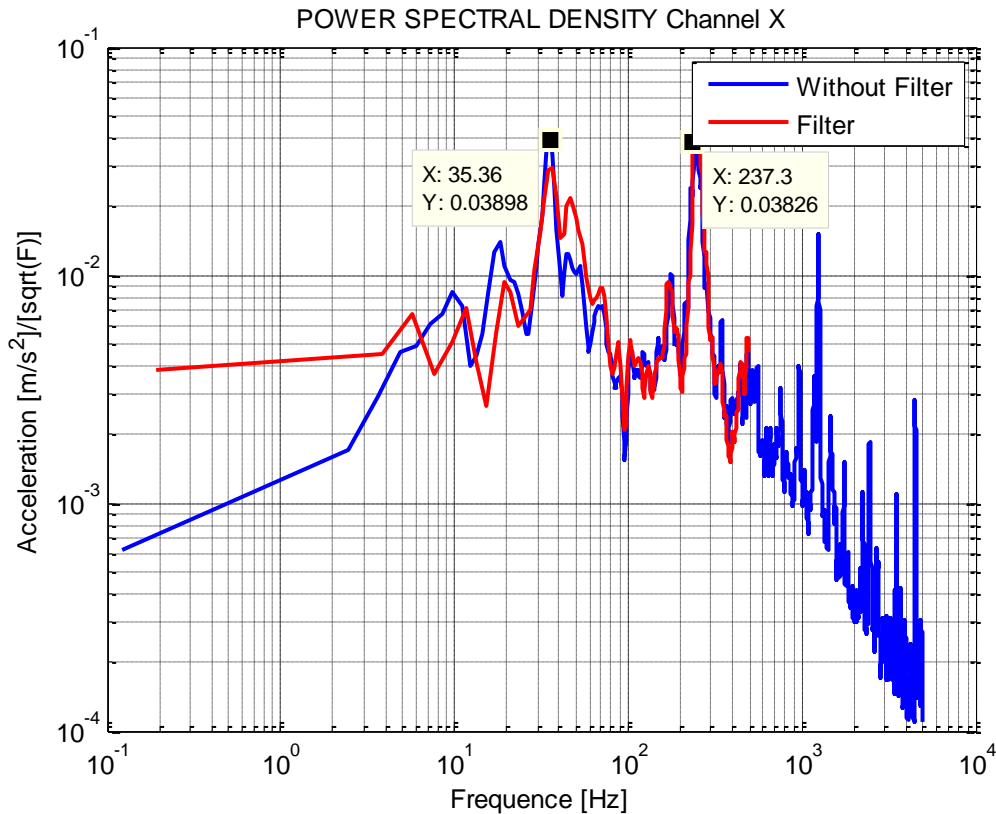
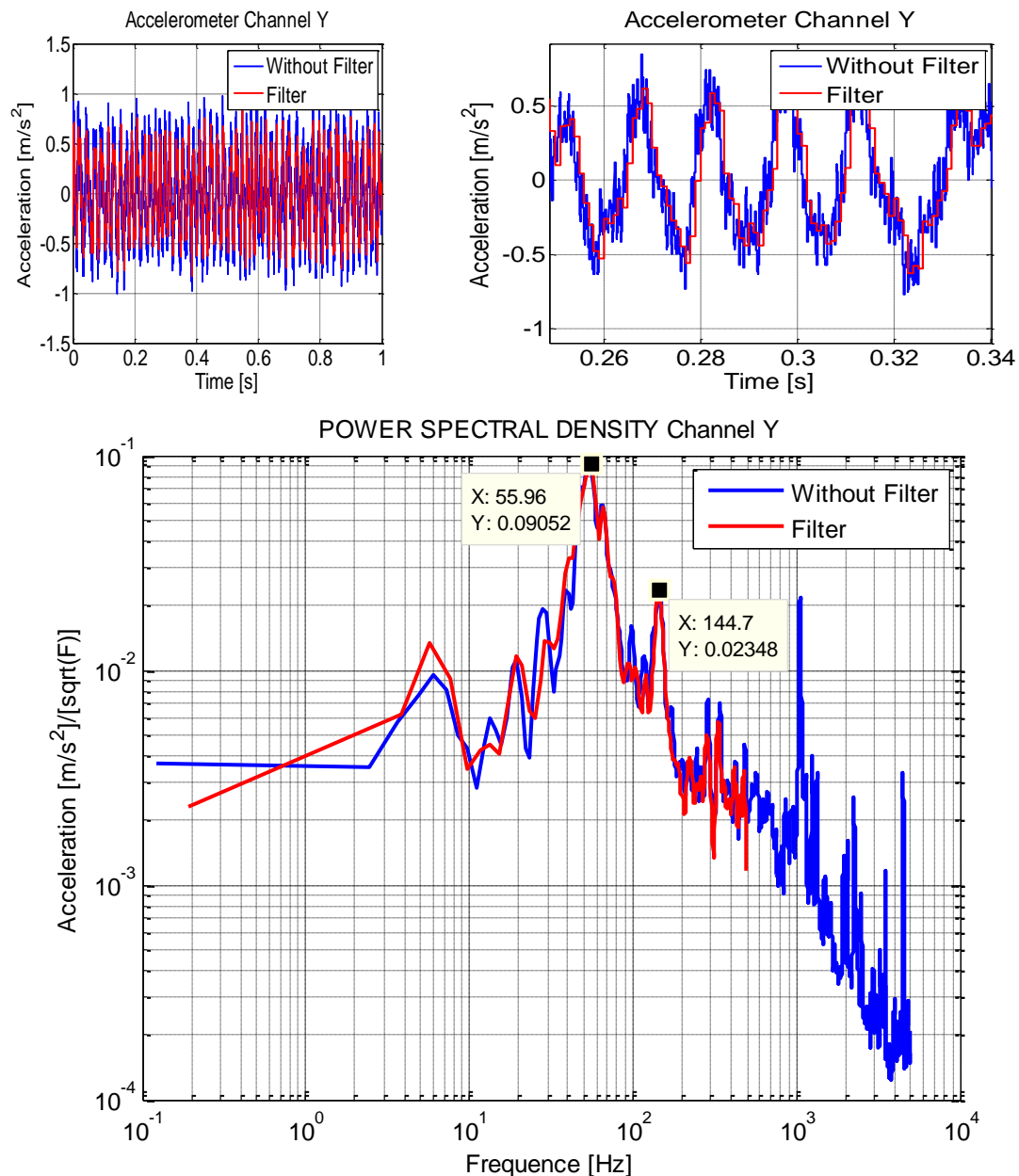| TEST	CHANNEL	ZERO [V]	ZERO[M/S^2]	STANDARD DEVIATION[M/S^2]	AVERAGE[M/S^2]
Side view	X	0.2417	2.9640	0.3222	17.2692

From the figure above, we can see the output data in time and its power spectral density. We should notice that the sensor with the filter has less noise and, also has a quantization error similar with the theoretical (9.87m [m/s^2]). Moreover there are some frequencies that the sensor sense with and without the filter. These frequencies could be due to aliasing or could be due to vibration on the building or vibrations on the table where the sensor was.

However, in side view the X-axis does not measure the gravity, but it present a big standard deviation compared with the datasheet's value, which is 0.108 [M/S^2].

5.2.1.1.2   BOTTOM VIEW

In blue we can see 10000 samples at 10kHz; in red we can see the filter which is 1000 samples at 1kHz.
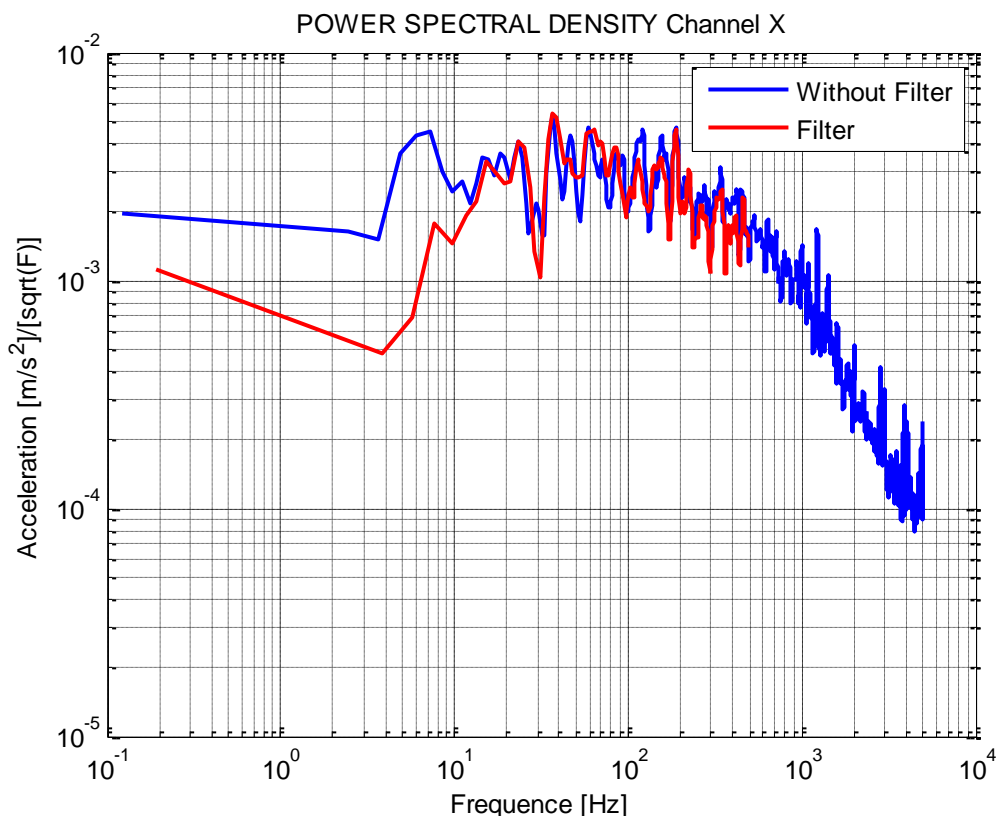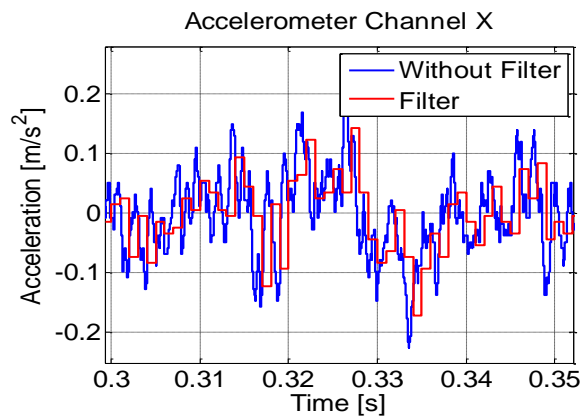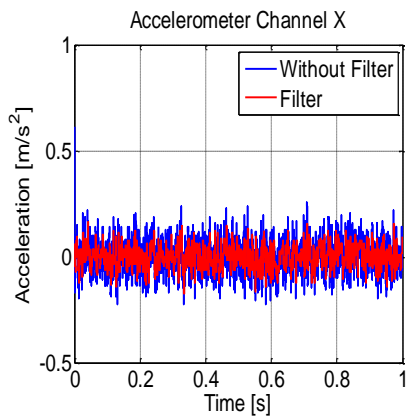
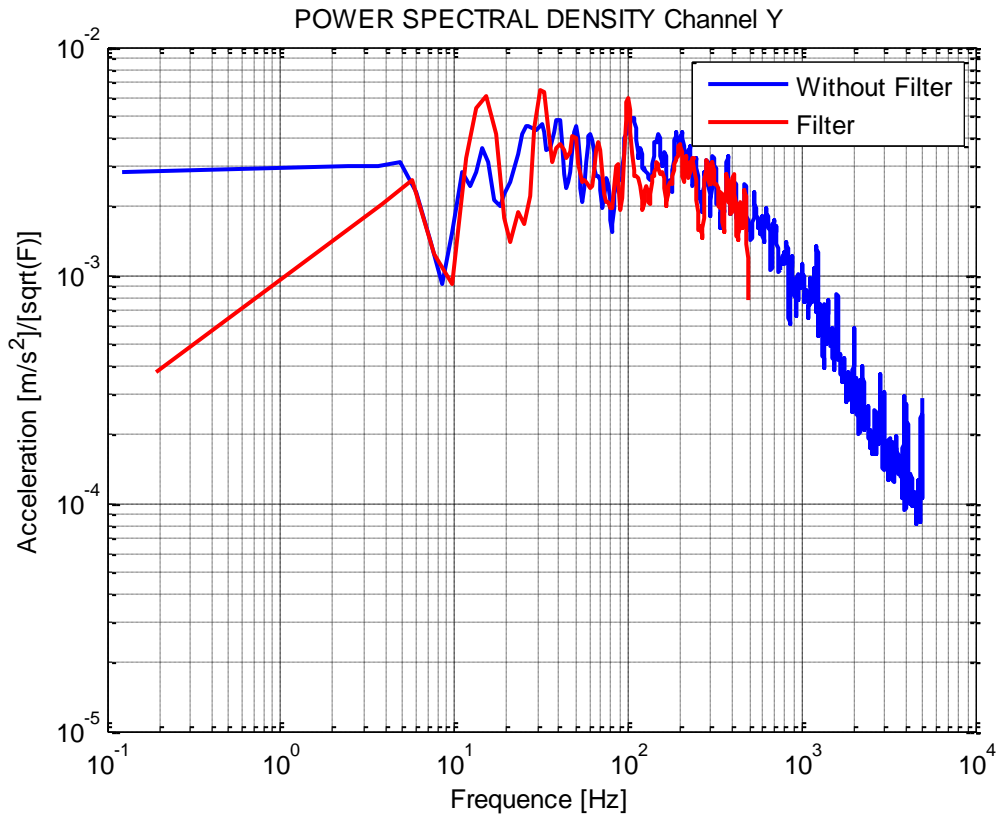| TEST	CHANNEL	ZERO [V]	ZERO[M/S^2]	STANDARD DEVIATION[M/S^2]	AVERAGE[M/S^2]
Bottom view	X	0.2990	3.6661	0.0695	16.5671

From the figure above, we can see the output data in time and its power spectral density. We should notice that the sensor with the filter has less noise and, also has a quantization error similar with the theoretical (9.87m [m/s^2]). Moreover, here there are not some strong frequencies, like the side view. Nevertheless there are small frequencies that could be due to aliasing or could be due to vibration on the building or vibrations on the table where the sensor was.

However, in bottom view the X-axis does not measure the gravity, but it present a similar standard deviation compared with the datasheet's value, which is 0.108 [M/S^2].

5.2.1.1.3 FRONT INCLINATION

In blue we can see 10000 samples at 10kHz; in red we can see the filter which is 1000 samples at 1kHz.

POWER SPECTRAL DENSITY Channel X
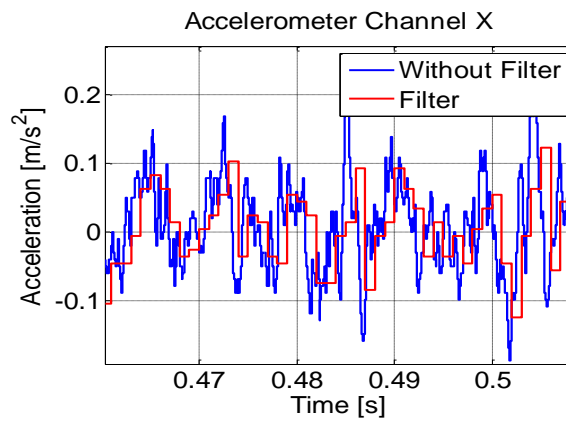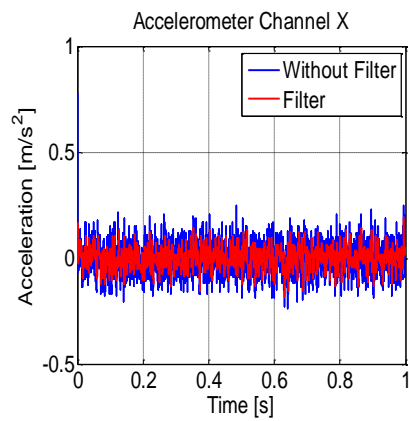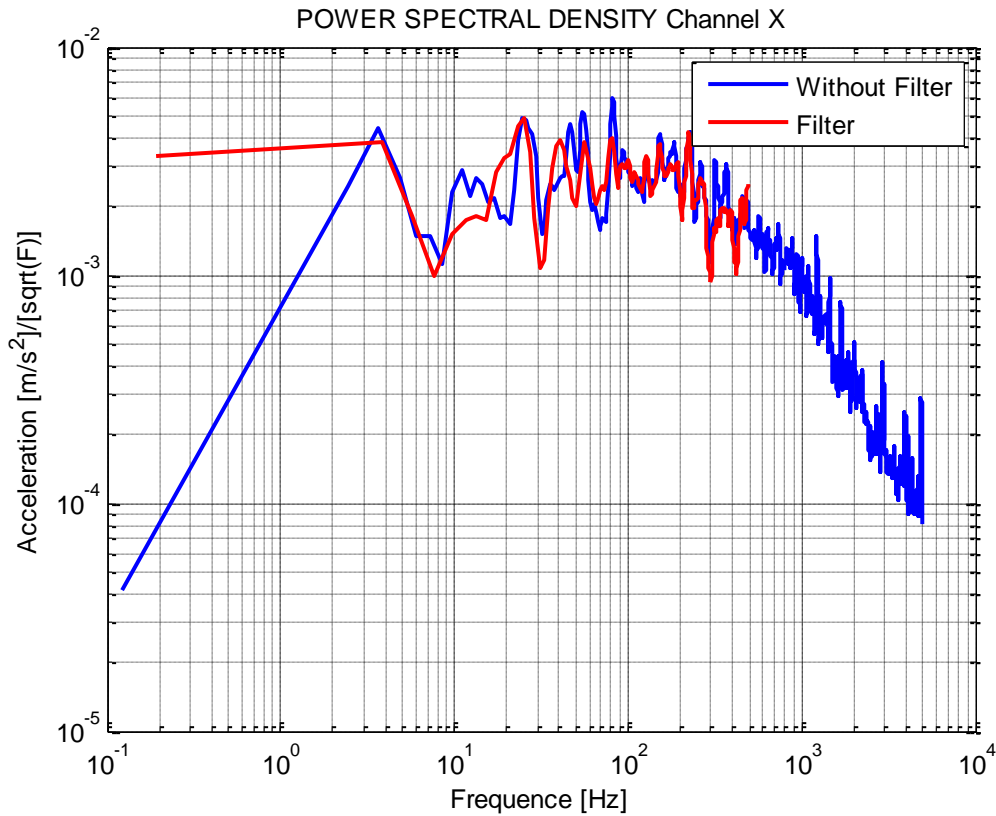
TEST	CHANNEL	ZERO [V]	ZERO[M/S^2]	STANDARD DEVIATION[M/S^2]	AVERAGE[M/S^2]
Front inclination	X	0.3416	4.1889	0.0692	16.0443

From the figure above, we can see the output data in time and its power spectral density. We should notice that the sensor with the filter has less noise and, also has a quantization error similar with the theoretical (9.87m [m/s^2]). Moreover, here there are not some strong frequencies, like the side view. Nevertheless there are small frequencies that could be due to aliasing or could be due to vibration on the building or vibrations on the table where the sensor was.

However, in front view the X-axis does not measure the gravity, but it present a similar standard deviation compared with the datasheet's value, which is 0.108 [M/S^2].

5.2.1.1.4   BACK INCLINATION

In blue we can see 10000 samples at 10kHz; in red we can see the filter which is 1000 samples at 1kHz.
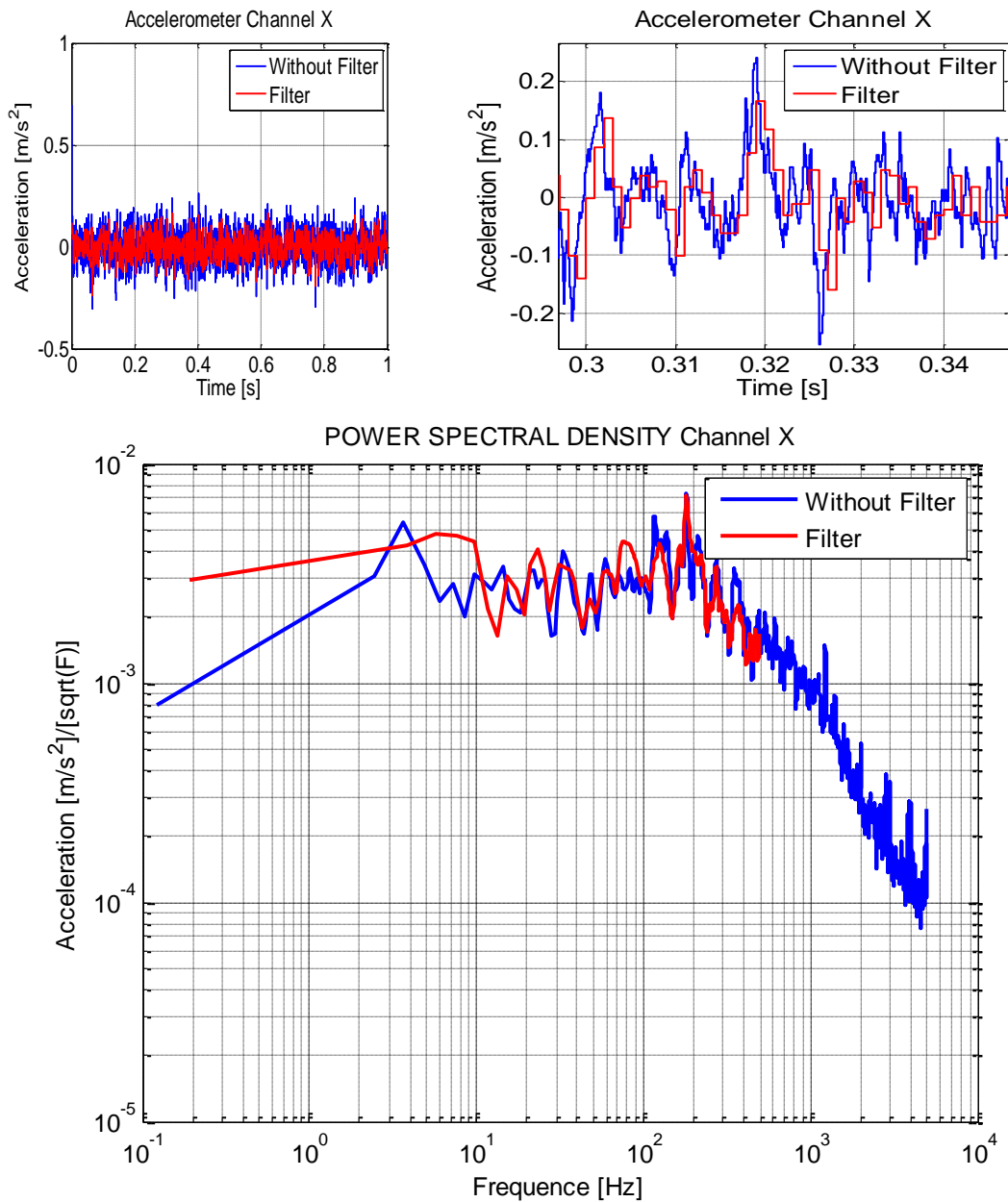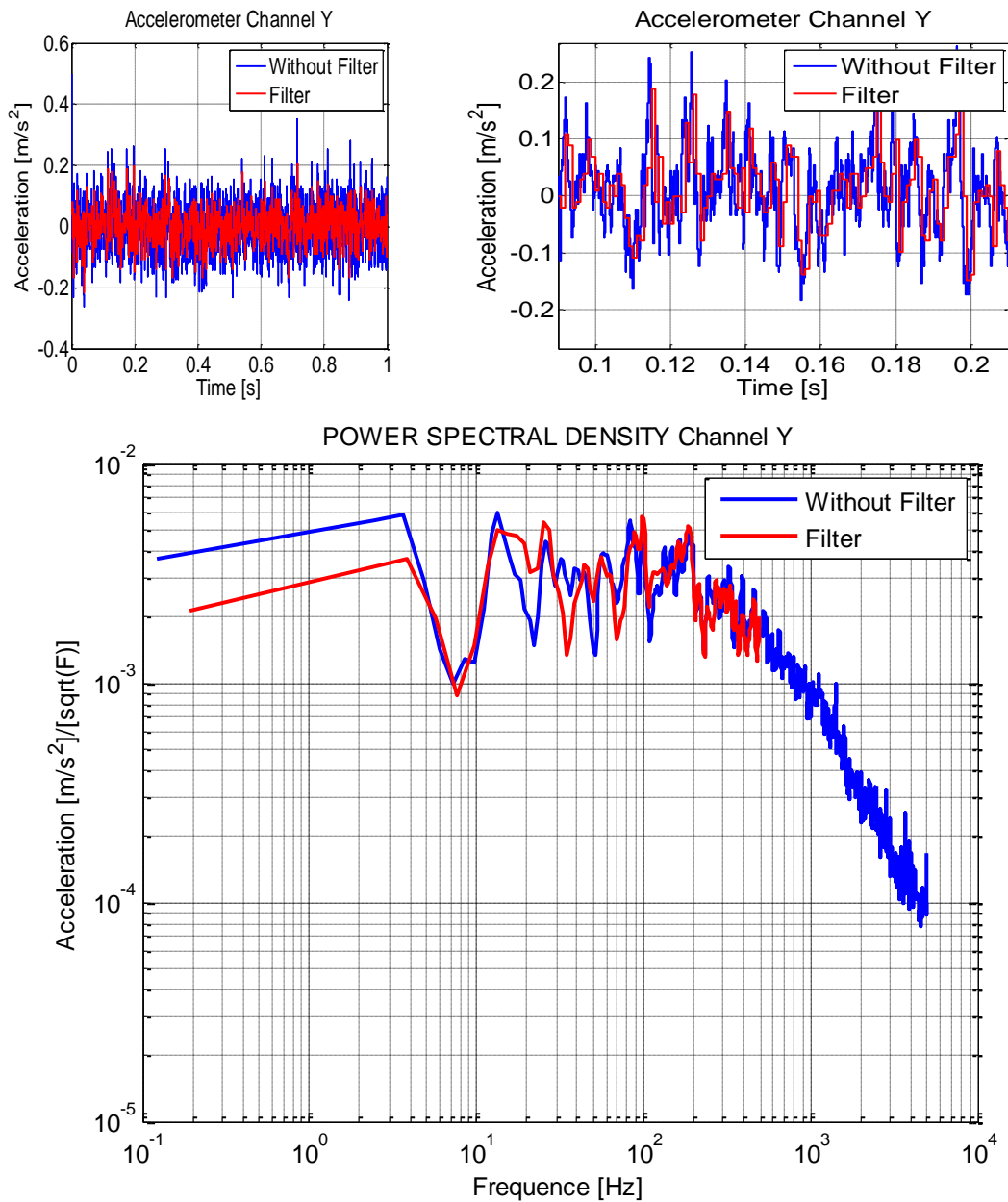
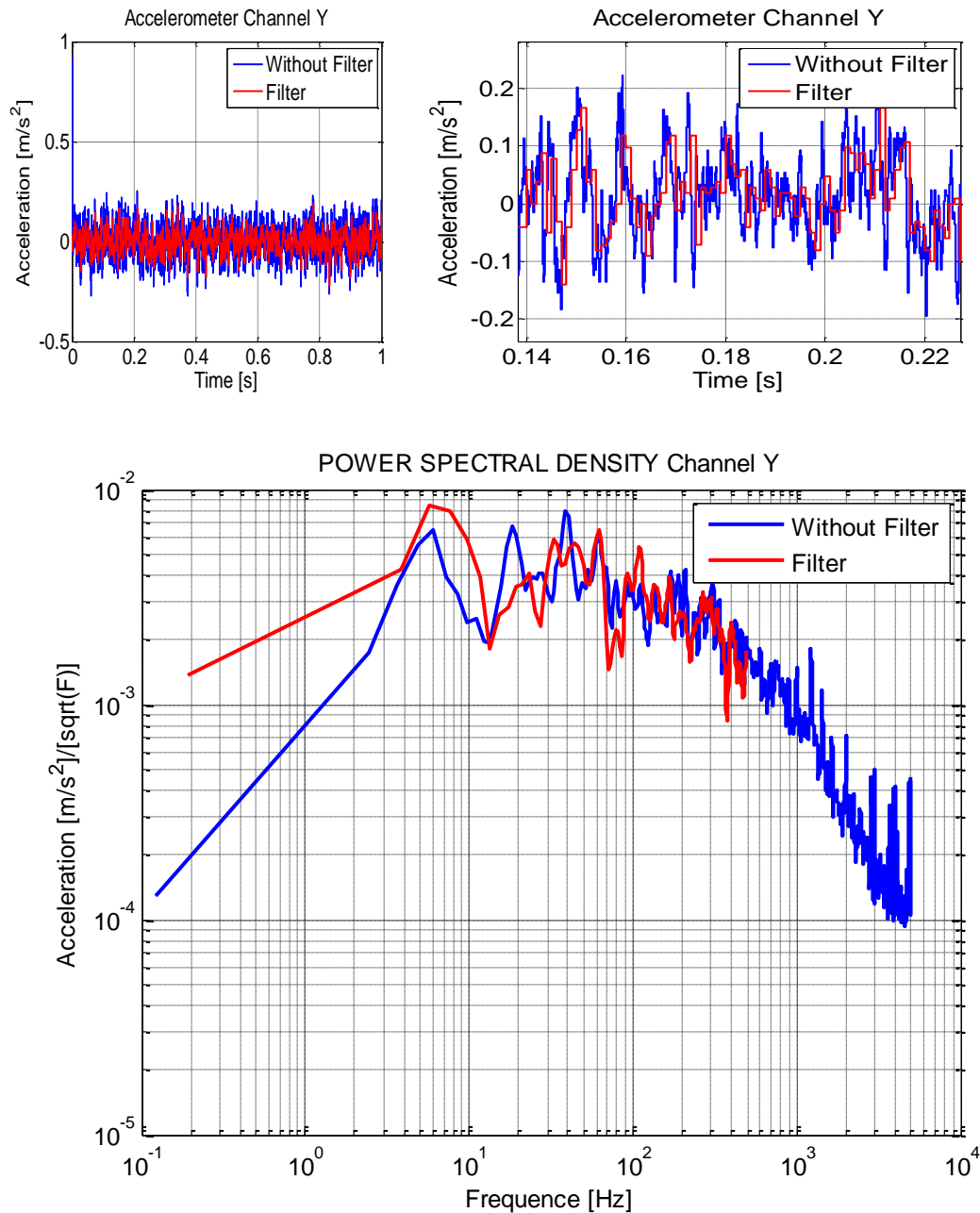| TEST	CHANNEL	ZERO [V]	ZERO[M/S^2]	STANDARD DEVIATION[M/S^2]	AVERAGE[M/S^2]
Back inclination	X	0.3249	3.9846	0.0721	16.2486

From the figure above, we can see the output data in time and its power spectral density. We should notice that the sensor with the filter has less noise and, also has a quantization error similar with the theoretical (9.87m [m/s^2]). Moreover, here there are not some strong frequencies, like the side view. Nevertheless there are small frequencies that could be due to aliasing or could be due to vibration on the building or vibrations on the table where the sensor was.

However, in front view the X-axis does not measure the gravity, but it present a similar standard deviation compared with the datasheet's value, which is 0.108 [M/S^2].

5.2.1.1.5 RIGHT INCLINATION

In blue we can see 10000 samples at 10kHz; in red we can see the filter which is 1000 samples at 1kHz.
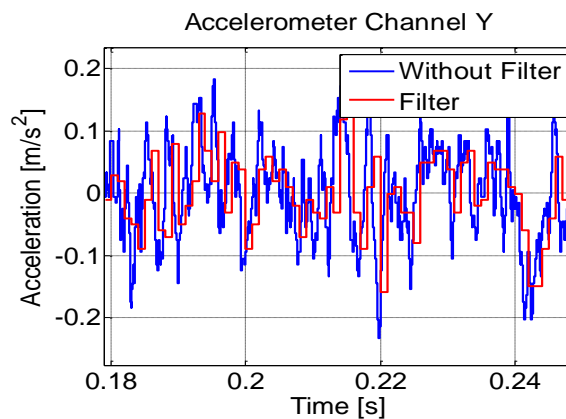
POWER SPECTRAL DENSITY Channel X
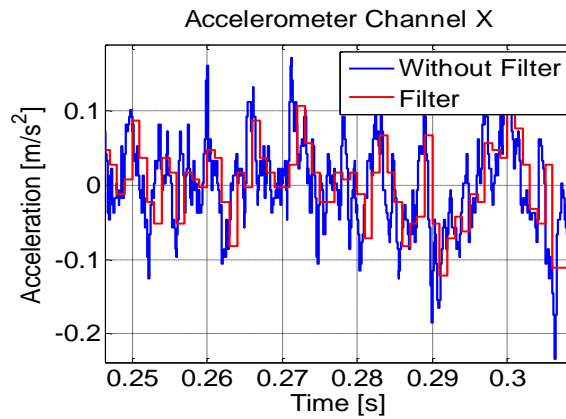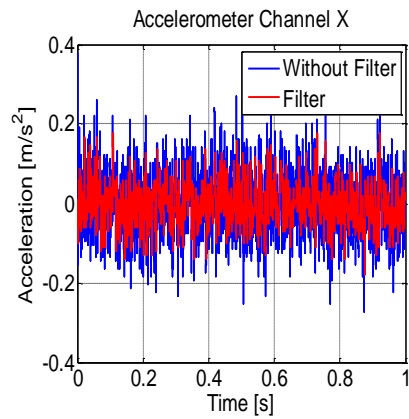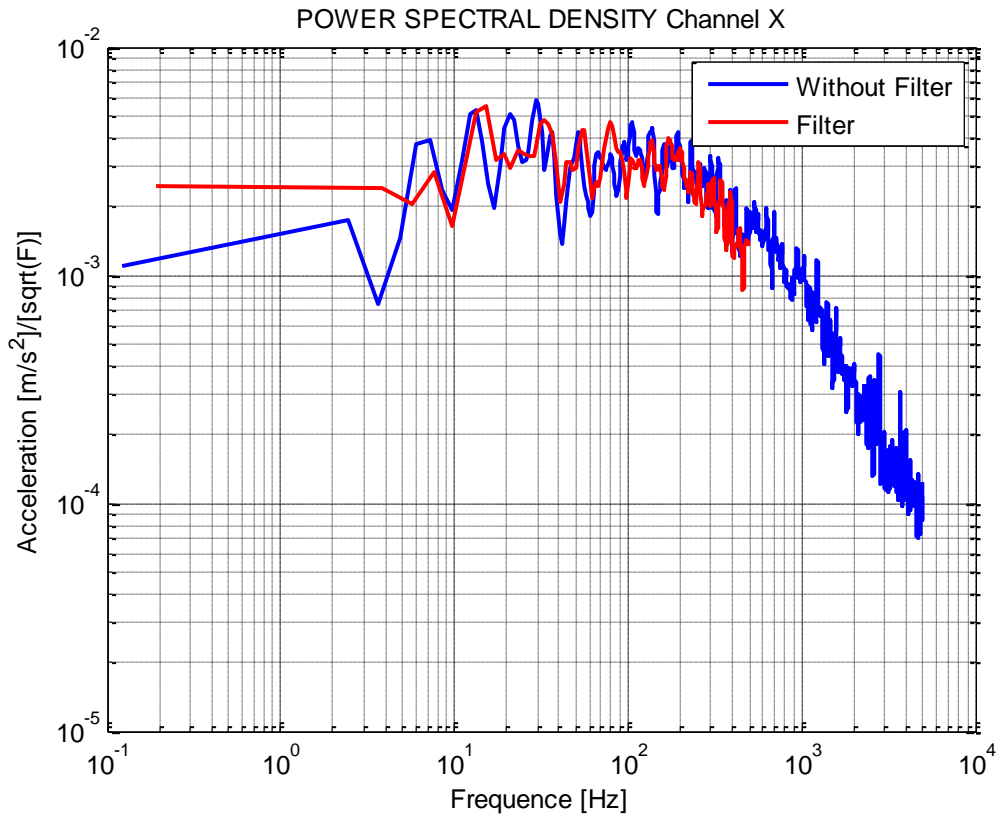
TEST	CHANNEL	ZERO [V]	ZERO[M/S^2]	STANDARD DEVIATION[M/S^2]	AVERAGE[M/S^2]
Right inclination	X	0.1920	2.3545	0.0704	8.0687

From the figure above, we can see the output data in time and its power spectral density. We should notice that the sensor with the filter has less noise and, also has a quantization error similar with the theoretical (9.87m [m/s^2]). Moreover, here there are not some strong frequencies, like the side view. Nevertheless there are small frequencies that could be due to aliasing or could be due to vibration on the building or vibrations on the table where the sensor was.

In right view the X-axis does measure the gravity, this is the reason that the average value is 8.0687 m/s^2, which is smaller than the expect value. But it present a similar standard deviation compared with the datasheet's value, which is 0.108 [M/S^2].

5.2.1.1.6   LEFT INCLINATION

In blue we can see 10000 samples at 10kHz; in red we can see the filter which is 1000 samples at 1kHz.
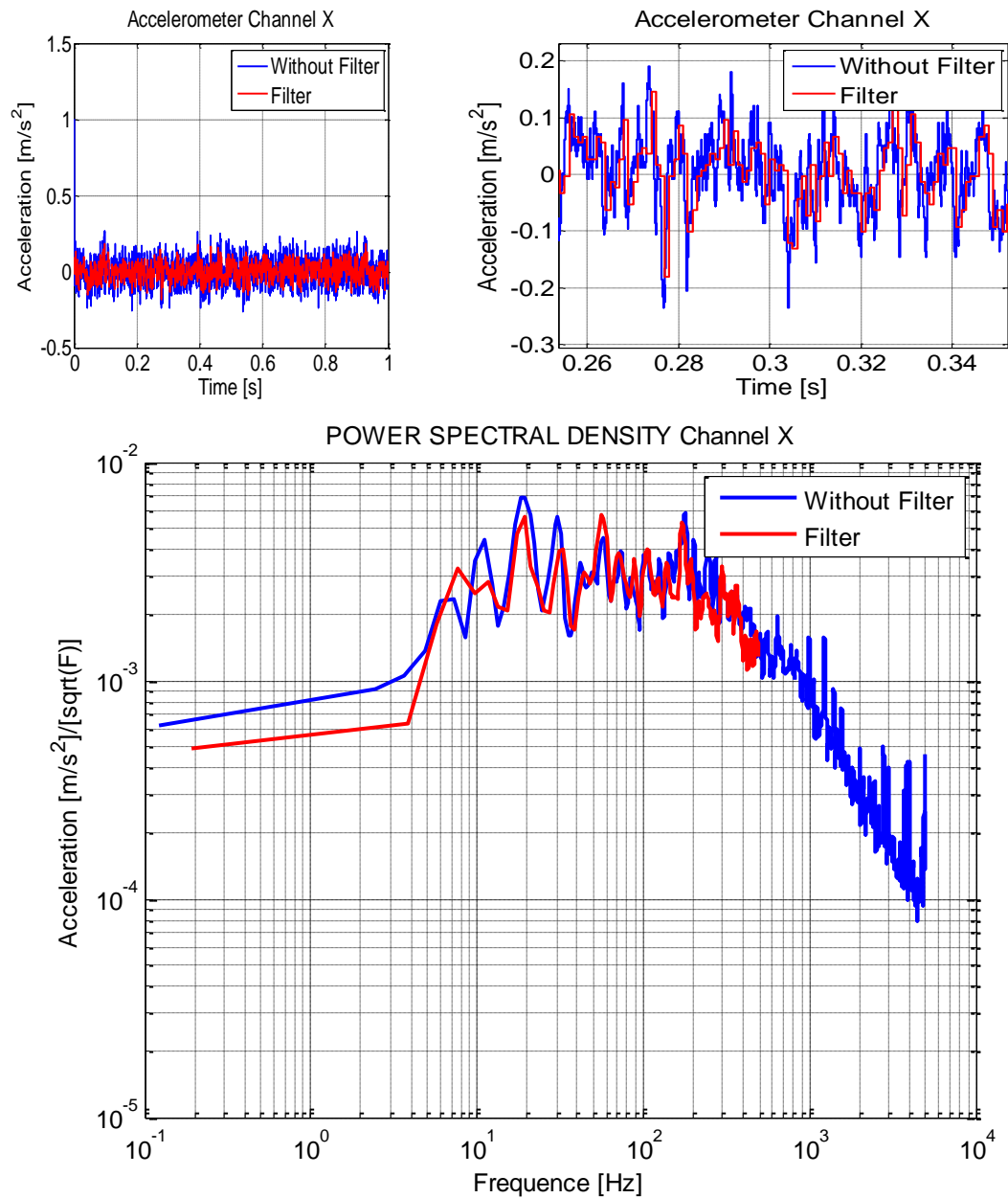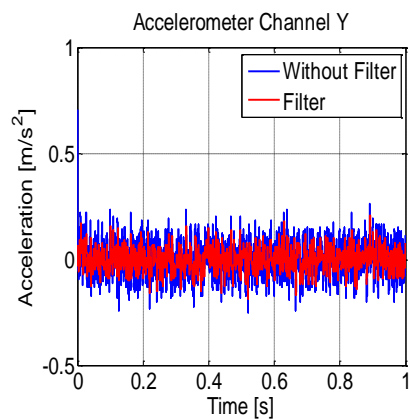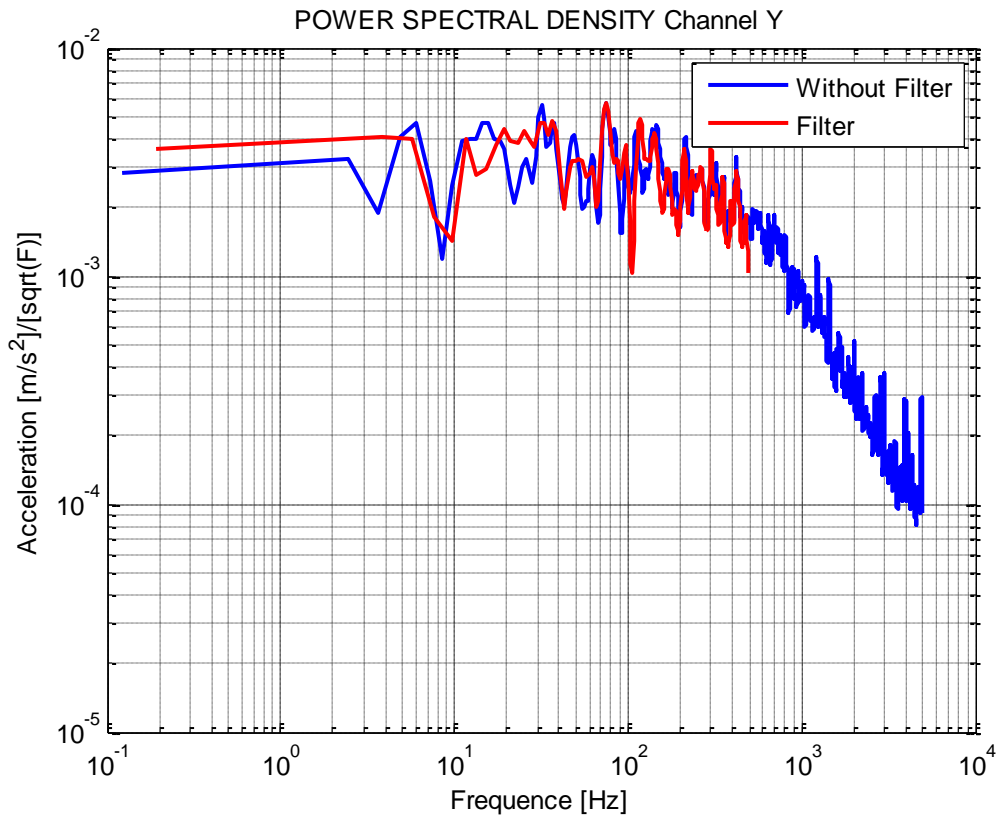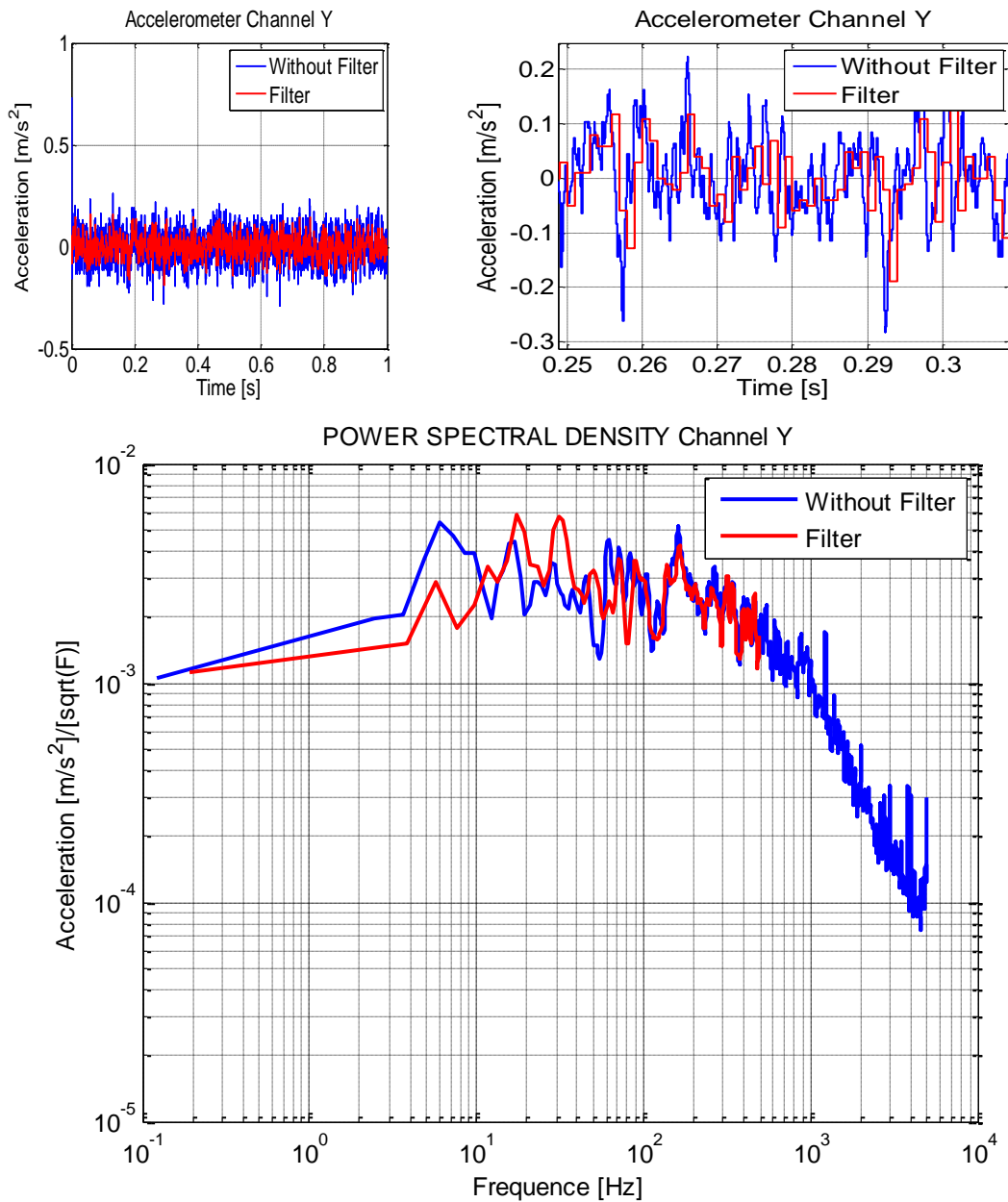

TEST	CHANNEL	ZERO [V]	ZERO[M/S^2]	STANDARD DESVIATION[M/S^2]	AVERAGE[M/S^2]
Left inclination	X	0.4820	5.9101	0.0731	24.1332

From the figure above, we can see the output data in time and its power spectral density. We should notice that the sensor with the filter has less noise and, also has a quantization error similar with the theoretical (9.87m [m/s^2]). Moreover, here there are not some strong frequencies, like the side view. Nevertheless there are small frequencies that could be due to aliasing or could be due to vibration on the building or vibrations on the table where the sensor was.

In left view the X-axis does measure the gravity, this is the reason that the average value is 24.133 m/s^2, which is bigger than the expect value. But it present a similar standard deviation compared with the datasheet's value, which is 0.108 [M/S^2].

5.2.2 CHANNEL Y

5.2.2.1.1 SIDE VIEW

In blue we can see 10000 samples at 10kHz; in red we can see the filter which is 1000 samples at 1kHz.

TEST	CHANNEL	ZERO [V]	ZERO[M/S^2]	STANDARD DEVIATION[M/S^2]	AVERAGE[M/S^2]

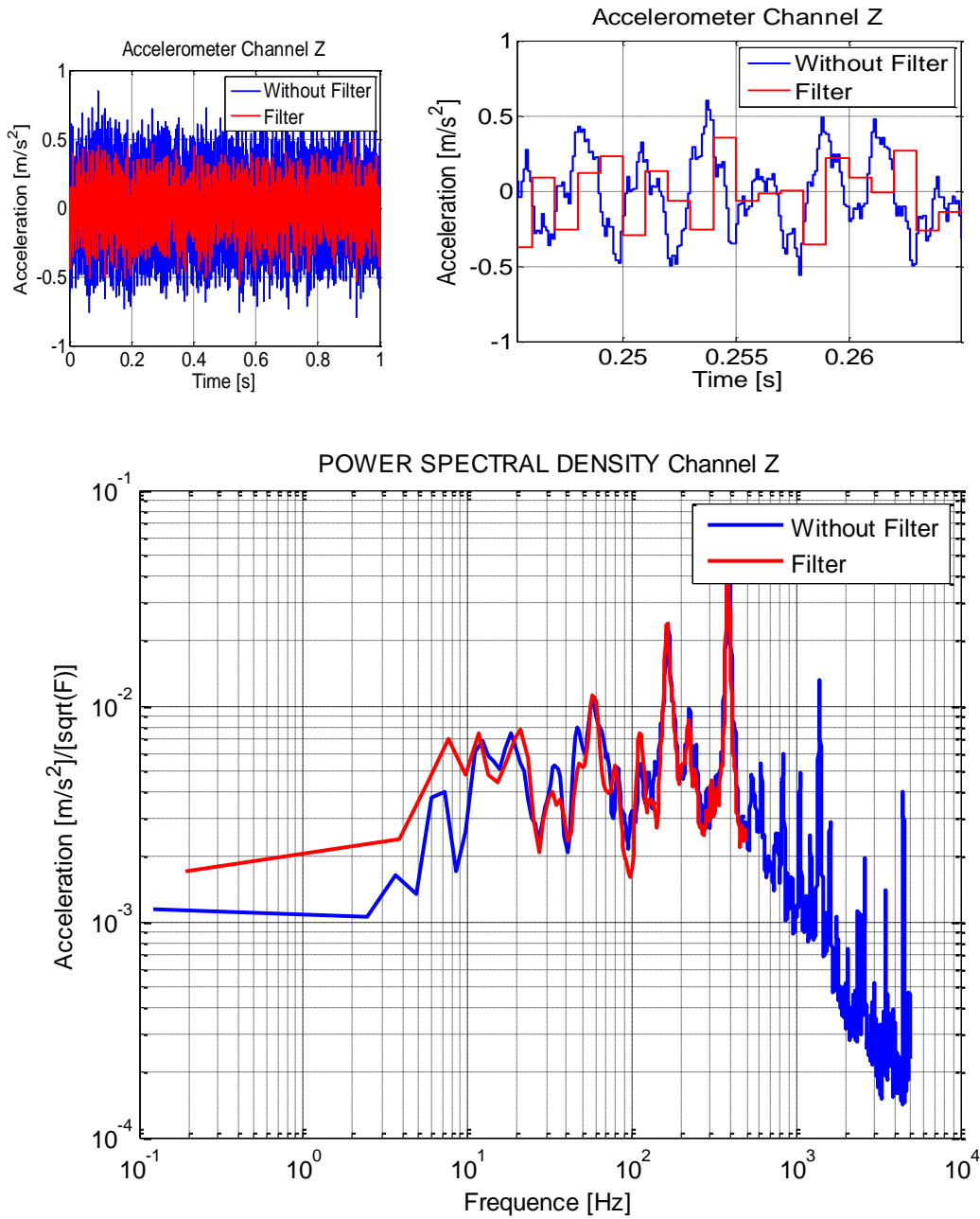|					
Side view	Y	0.0057	0.0702	0.4064	20.1630

From the figure above, we can see the output data in time and its power spectral density. We should notice that the sensor with the filter has less noise and, also has a quantization error similar with the theoretical (9.87m [m/s^2]). Moreover there are some frequencies that the sensor sense with and without the filter. These frequencies could be due to aliasing or could be due to vibration on the building or vibrations on the table where the sensor was.

However, in side view the Y-axis does not measure the gravity, but it present a big standard deviation compared with the datasheet's value, which is 0.108 [M/S^2].

5.2.2.1.2   BOTTOM VIEW

In blue we can see 10000 samples at 10kHz; in red we can see the filter which is 1000 samples at 1kHz.

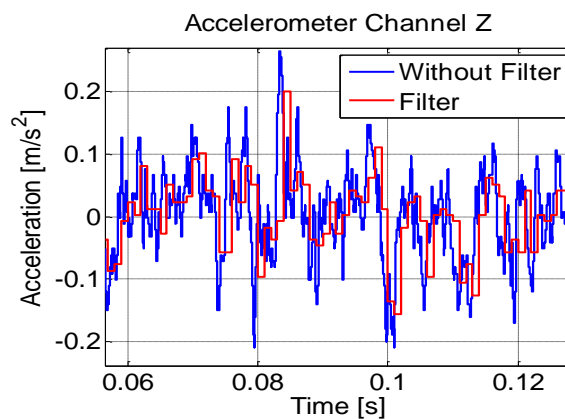POWER SPECTRAL DENSITY Channel Y
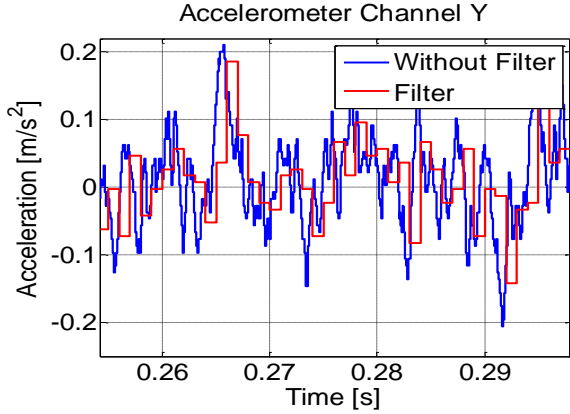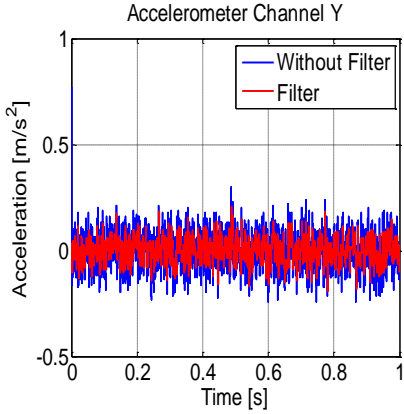
TEST	CHANNEL	ZERO [V]	ZERO[M/S^2]	STANDARD DESVIATION[M/S^2]	AVERAGE[M/S^2]
Bottom view	Y	0.1363	1.6717	0.0753	18.5615

From the figure above, we can see the output data in time and its power spectral density. We should notice that the sensor with the filter has less noise and, also has a quantization error similar with the theoretical (9.87m [m/s^2]). Moreover, here there are not some strong frequencies, like the side view. Nevertheless there are small frequencies that could be due to aliasing or could be due to vibration on the building or vibrations on the table where the sensor was.

However, in bottom view the Y-axis does not measure the gravity, but it present a similar standard deviation compared with the datasheet's value, which is 0.108 [M/S^2].

5.2.2.1.3 FRONT INCLINATION

In blue we can see 10000 samples at 10kHz; in red we can see the filter which is 1000 samples at 1kHz.

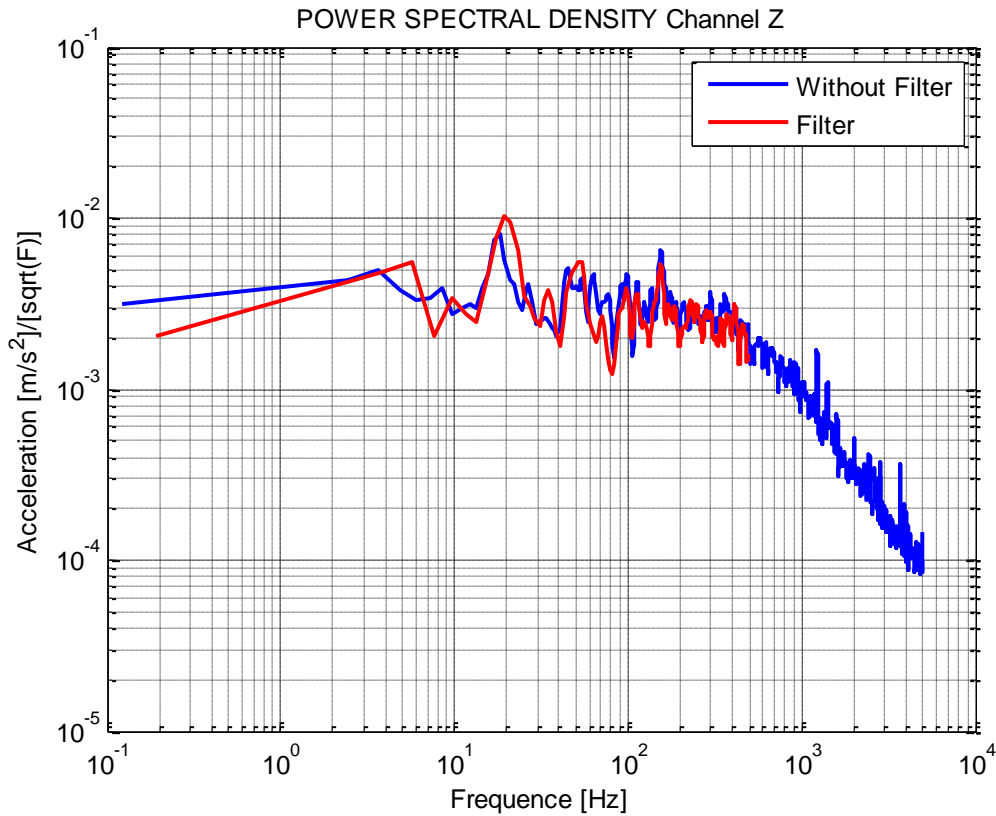| TEST	CHANNEL	ZERO [V]	ZERO[M/S^2]	STANDARD DEVIATION[M/S^2]	AVERAGE[M/S^2]
Front inclination	Y	-0.0076	-0.0936	0.0726	10.5168

From the figure above, we can see the output data in time and its power spectral density. We should notice that the sensor with the filter has less noise and, also has a quantization error similar with the theoretical (9.87m [m/s^2]). Moreover, here there are not some strong frequencies, like the side view. Nevertheless there are small frequencies that could be due to aliasing or could be due to vibration on the building or vibrations on the table where the sensor was.

In front inclination the Y-axis does measure the gravity, this is the reason that the average value is 10.51 m/s^2, which is smaller than the expect value. But it

present a similar standard deviation compared with the datasheet's value, which is 0.108 [M/S^2].

5.2.2.1.4 BACK INCLINATION

In blue we can see 10000 samples at 10kHz; in red we can see the filter which is 1000 samples at 1kHz.
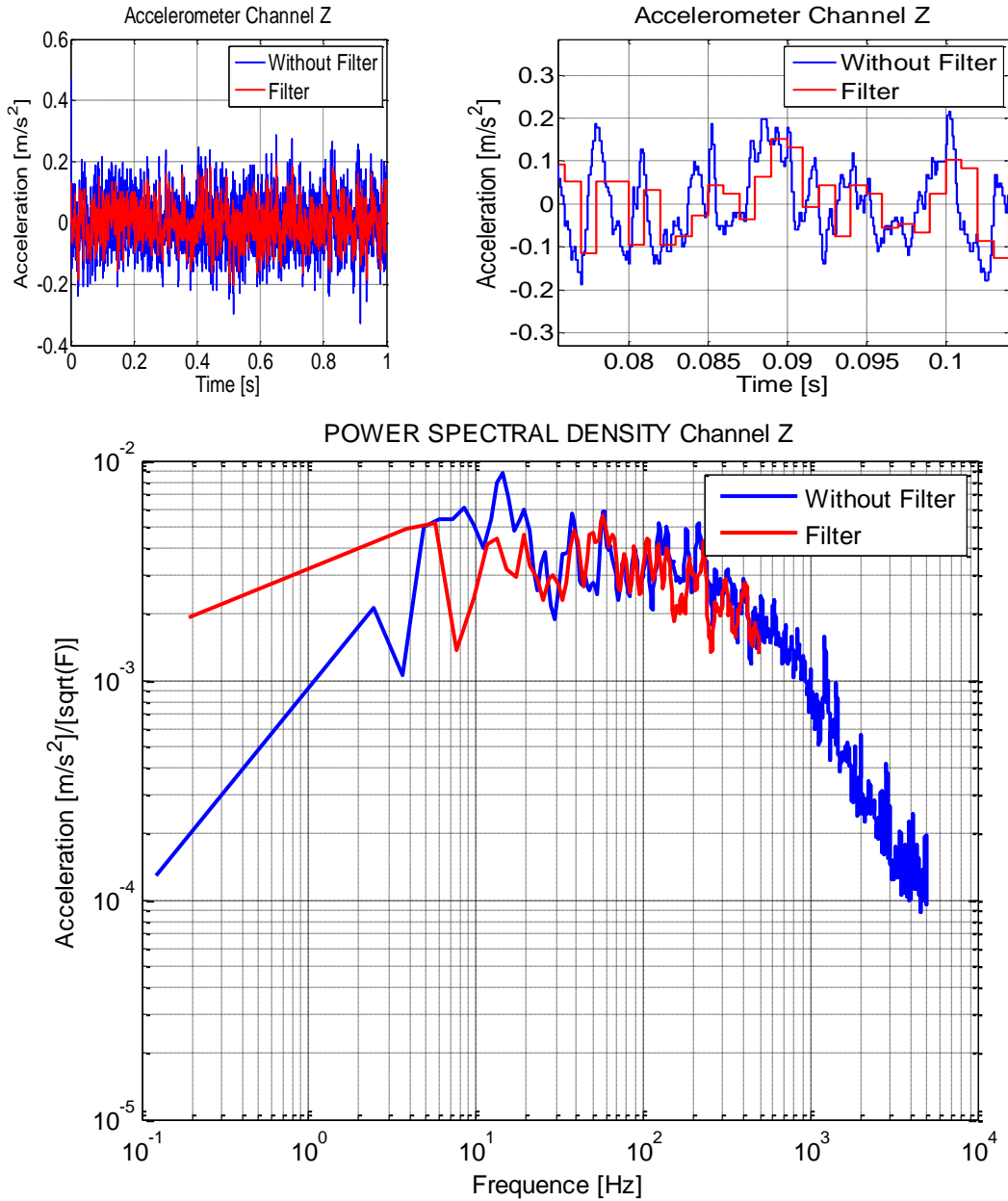

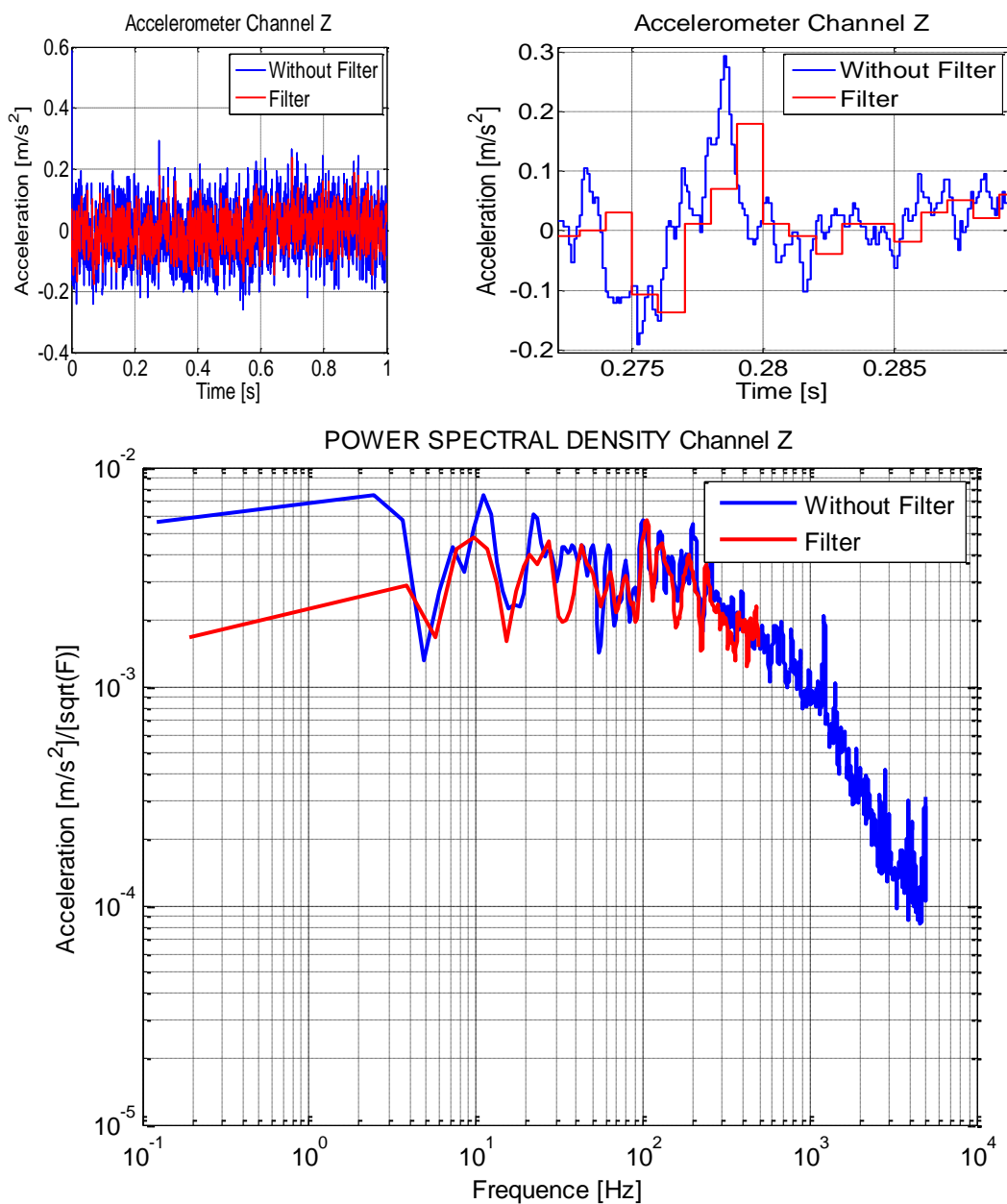| TEST	CHANNEL	ZERO [V]	ZERO[M/S^2]	STANDARD DEVIATION[M/S^2]	AVERAGE[M/S^2]
Back inclination	Y	0.2549	3.1255	0.0745	26.9178

From the figure above, we can see the output data in time and its power spectral density. We should notice that the sensor with the filter has less noise and, also has a quantization error similar with the theoretical (9.87m [m/s^2]). Moreover, here there are not some strong frequencies, like the side view. Nevertheless there are small frequencies that could be due to aliasing or could be due to vibration on the building or vibrations on the table where the sensor was.

In back inclination the Y-axis does measure the gravity, this is the reason that the average value is 26.91 m/s^2, which is bigger than the expect value. But it present a similar standard deviation compared with the datasheet's value, which is 0.108 [M/S^2].

5.2.2.1.5   RIGHT INCLINATION

In blue we can see 10000 samples at 10kHz; in red we can see the filter which is 1000 samples at 1kHz.

POWER SPECTRAL DENSITY Channel Y

TEST	CHANNEL	ZERO [V]	ZERO[M/S^2]	STANDARD DEVIATION[M/S^2]	AVERAGE[M/S^2]
Right inclination	Y	0.1228	1.5061	0.0714	18.7271

From the figure above, we can see the output data in time and its power spectral density. We should notice that the sensor with the filter has less noise and, also has a quantization error similar with the theoretical (9.87m [m/s^2]). Moreover, here there are not some strong frequencies, like the side view. Nevertheless there are small frequencies that could be due to aliasing or could be due to vibration on the building or vibrations on the table where the sensor was.

However, in right inclination the Y-axis does not measure the gravity, but it present a similar standard deviation compared with the datasheet's value, which is 0.108 [M/S^2].

5.2.2.1.6   LEFT INCLINATION

In blue we can see 10000 samples at 10kHz; in red we can see the filter which is 1000 samples at 1kHz.

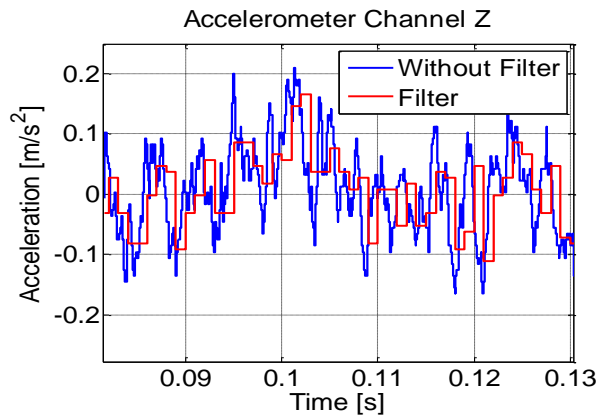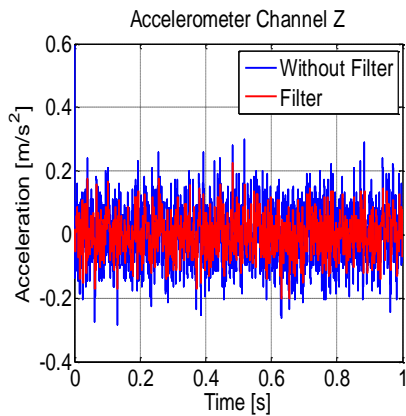POWER SPECTRAL DENSITY Channel Y

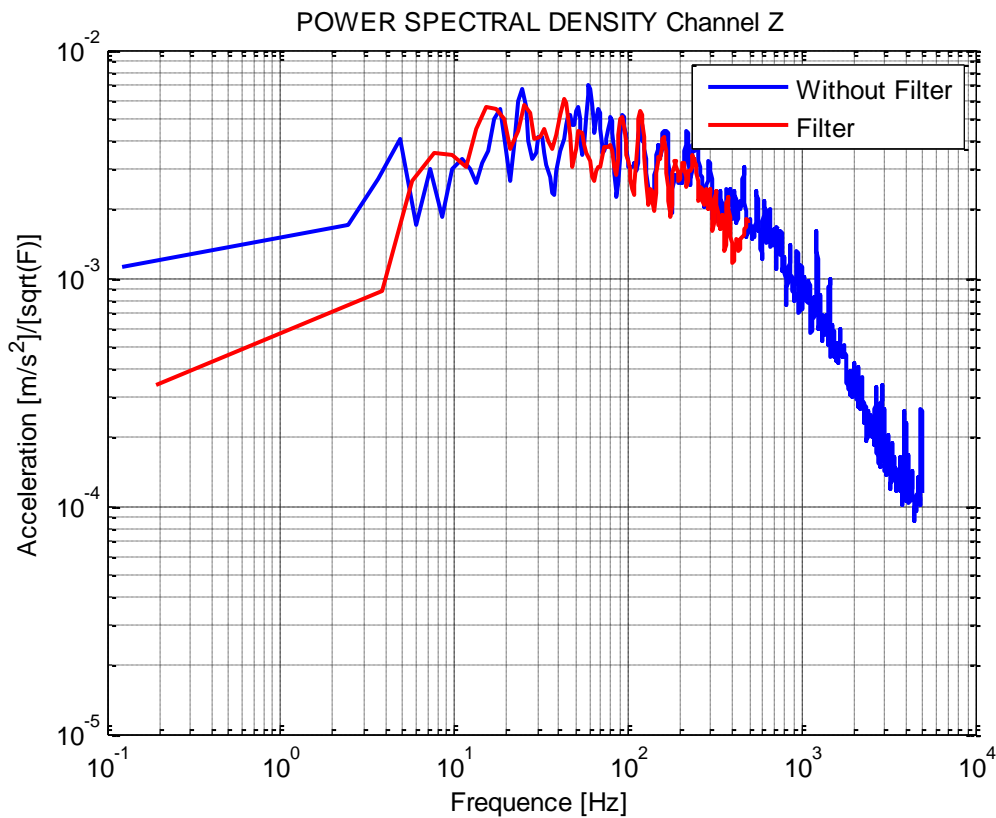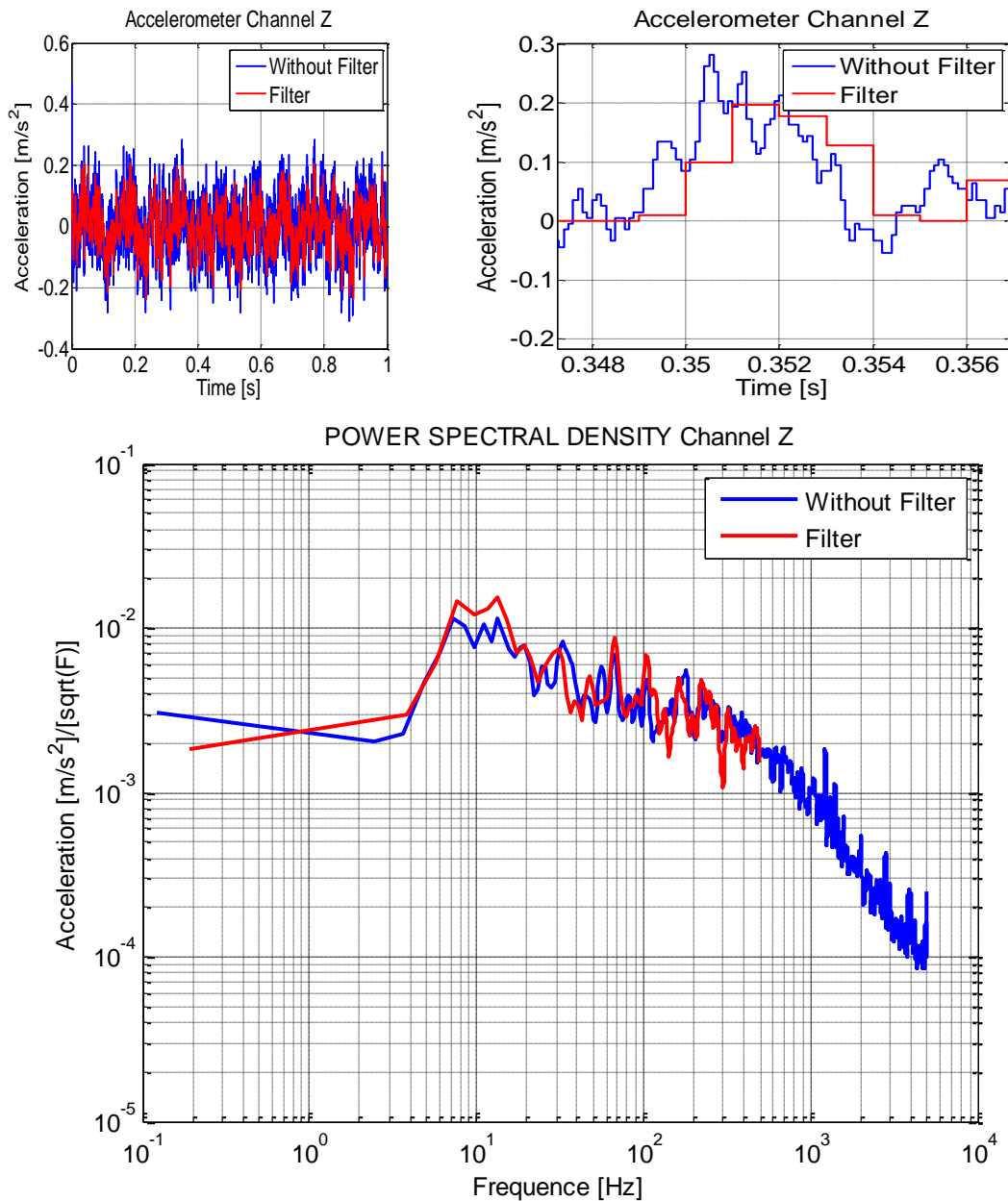| TEST	CHANNEL	ZERO [V]	ZERO[M/S^2]	STANDARD DEVIATION[M/S^2]	AVERAGE[M/S^2]
Left inclination	Y	0.1196	1.4670	0.0710	18.7662

From the figure above, we can see the output data in time and its power spectral density. We should notice that the sensor with the filter has less noise and, also has a quantization error similar with the theoretical (9.87m [m/s^2]). Moreover, here there are not some strong frequencies, like the side view. Nevertheless there are small frequencies that could be due to aliasing or could be due to vibration on the building or vibrations on the table where the sensor was.

However, in left inclination the Y-axis does not measure the gravity, but it present a similar standard deviation compared with the datasheet's value, which is 0.108 [M/S^2].

5.2.2.2 CHANNEL Z

5.2.2.2.1   SIDE VIEW

In blue we can see 10000 samples at 10kHz; in red we can see the filter which is 1000 samples at 1kHz.

TEST	CHANNEL	ZERO [V]	ZERO[M/S^2]	STANDARD DEVIATION[M/S^2]	AVERAGE[M/S^2]
Side view	Z	0.5234	6.4799	0.2796	23.6247

From the figure above, we can see the output data in time and its power spectral density. We should notice that the sensor with the filter has less noise and, also has a quantization error similar with the theoretical (9.87m [m/s^2]). Moreover there are some frequencies that the sensor sense with and without the filter. These frequencies could be due to aliasing or could be due to vibration on the building or vibrations on the table where the sensor was.

In side view the Z-axis does measure the gravity, this is the reason that the average value is 26.6247 m/s^2, which is bigger than the expect value. But it presents a big standard deviation compared with the datasheet's value, which is 0.108 [M/S^2].

5.2.2.2.2   BOTTOM VIEW

In blue we can see 10000 samples at 10kHz; in red we can see the filter which is 1000 samples at 1kHz.

POWER SPECTRAL DENSITY Channel Z
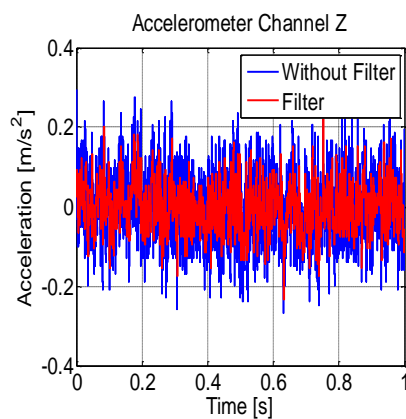
TEST	CHANNEL	ZERO [V]	ZERO[M/S^2]	STANDARD DEVIATION[M/S^2]	AVERAGE[M/S^2]
Bottom view	Z	0.3971	4.8691	0.0795	5.5541

From the figure above, we can see the output data in time and its power spectral density. We should notice that the sensor with the filter has less noise and, also has a quantization error similar with the theoretical (9.87m [m/s^2]). Moreover, here there are not some strong frequencies, like the side view. Nevertheless there are small frequencies that could be due to aliasing or could be due to vibration on the building or vibrations on the table where the sensor was.

In bottom view, the Z-axis does measure the gravity, this is the reason that the average value is 5.55 m/s^2, which is smaller than the expect value. But it present a similar standard deviation compared with the datasheet's value, which is 0.108 [M/S^2].

5.2.2.2.3   FRONT INCLINATION

In blue we can see 10000 samples at 10kHz; in red we can see the filter which is 1000 samples at 1kHz.

Accelerometer Channel Z

POWER SPECTRAL DENSITY Channel Z

TEST	CHANNEL	ZERO [V]	ZERO[M/S^2]	STANDARD DEVIATION[M/S^2]	AVERAGE[M/S^2]
Front inclination	Z	0.5284	6.4800	0.0801	13.7532

From the figure above, we can see the output data in time and its power spectral density. We should notice that the sensor with the filter has less noise and, also has a quantization error similar with the theoretical (9.87m [m/s^2]). Moreover, here there are not some strong frequencies, like the side view. Nevertheless there

96

are small frequencies that could be due to aliasing or could be due to vibration on the building or vibrations on the table where the sensor was.

However, in front inclination the Z-axis does not measure the gravity, but it present a similar standard deviation compared with the datasheet's value, which is 0.108 [M/S^2].

5.2.2.2.4   BACK INCLINATION

In blue we can see 10000 samples at 10kHz; in red we can see the filter which is 1000 samples at 1kHz.

TEST	CHANNEL	ZERO [V]	ZERO[M/S^2]	STANDARD DEVIATION[M/S^2]	AVERAGE[M/S^2]
Back inclination	Z	0.4453	5.4605	0.0784	14.7728

From the figure above, we can see the output data in time and its power spectral density. We should notice that the sensor with the filter has less noise and, also has a quantization error similar with the theoretical (9.87m [m/s^2]). Moreover, here there are not some strong frequencies, like the side view. Nevertheless there are small frequencies that could be due to aliasing or could be due to vibration on the building or vibrations on the table where the sensor was.

However, in back inclination the Y-axis does not measure the gravity, but it present a similar standard deviation compared with the datasheet's value, which is 0.108 [M/S^2].

5.2.2.2.5 RIGHT INCLINATION

In blue we can see 10000 samples at 10kHz; in red we can see the filter which is 1000 samples at 1kHz.

POWER SPECTRAL DENSITY Channel Z

TEST	CHANNEL	ZERO [V]	ZERO[M/S^2]	STANDARD DEVIATION[M/S^2]	AVERAGE[M/S^2]
Right inclination	Z	0.5481	6.7212	0.0782	13.5120

From the figure above, we can see the output data in time and its power spectral density. We should notice that the sensor with the filter has less noise and, also has a quantization error similar with the theoretical (9.87m [m/s^2]). Moreover, here there are not some strong frequencies, like the side view. Nevertheless there are small frequencies that could be due to aliasing or could be due to vibration on the building or vibrations on the table where the sensor was.

However, in right inclination the Z-axis does not measure the gravity, but it present a similar standard deviation compared with the datasheet's value, which is 0.108 [M/S^2].

5.2.2.2.6 LEFT INCLINATION

In blue we can see 10000 samples at 10kHz; in red we can see the filter which is 1000 samples at 1kHz.

TEST	CHANNEL	ZERO [V]	ZERO[M/S^2]	STANDARD DEVIATION[M/S^2]	AVERAGE[M/S^2]
Left inclination	Z	0.5870	7.1981	0.0918	13.0351

From the figure above, we can see the output data in time and its power spectral density. We should notice that the sensor with the filter has less noise and, also has a quantization error similar with the theoretical (9.87m [m/s^2]). Moreover, here there are not some strong frequencies, like the side view. Nevertheless there

are small frequencies that could be due to aliasing or could be due to vibration on the building or vibrations on the table where the sensor was.

However, in left inclination the Z-axis does not measure the gravity, but it present a similar standard deviation compared with the datasheet's value, which is 0.108 [M/S^2].

5.2.3 GYROSCOPE

As we see before, the gyroscope measures the angular acceleration that has every axes with respect to position. But the output data of the ADC is a digital word of 12bit, and then is necessary to converts this digital word into angular acceleration. If I multiply the digital word by the quantization error of the ADC, I obtain the voltage. This voltage divide by the sensitivity of the gyroscope gives me the angular acceleration. To obtain the Bias I make the difference between the voltage at zero acceleration from the datasheet and the mean value of the results I got from the ADC.

Finally I obtain the power spectral density of every channel. This basically is the power of the noise that will help me in the future when I make the control.

To test the gyroscope there are 2 different outputs. The first one is the output with an amplifier of 4.5, this output is more sensible. The second one is the normal output, without amplifier. Next we will see the result and plots of the 2 different tests, everyone with the Bias, standard deviation and the power spectral density of each channel.

5.2.3.1 WITHOUT AMPLIFIER

5.2.3.1.1   CHANNEL X

In blue we can see 10000 samples at 10kHz; in red we can see the filter which is 1000 samples at 1kHz.
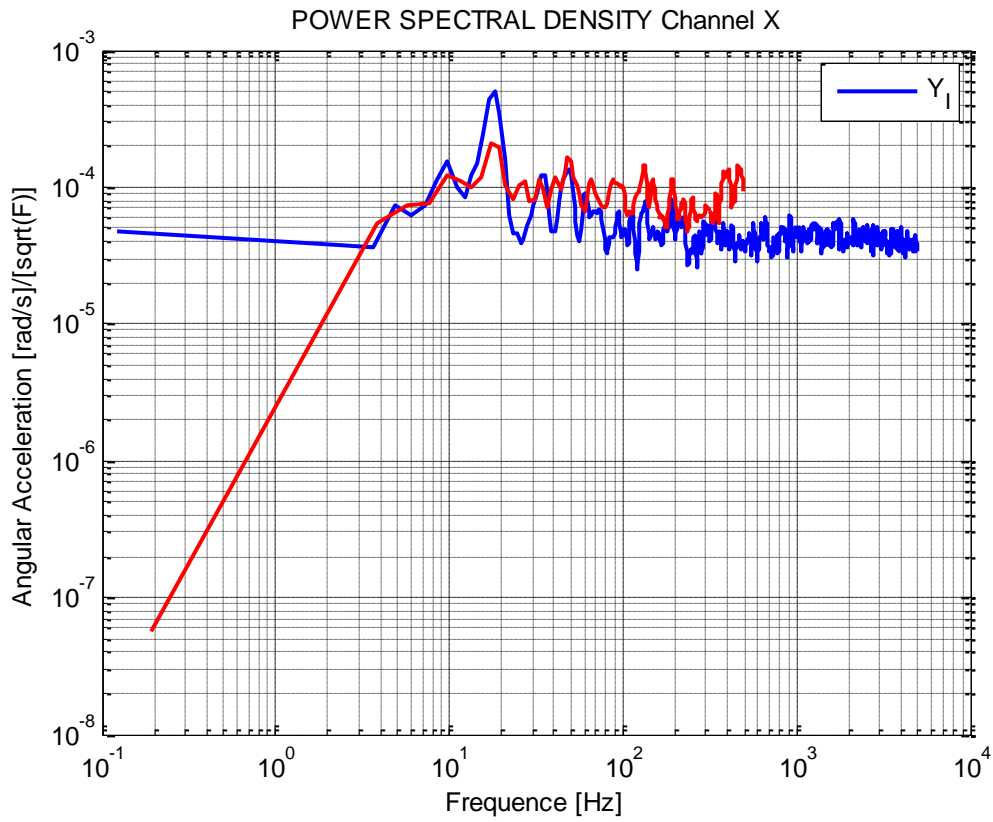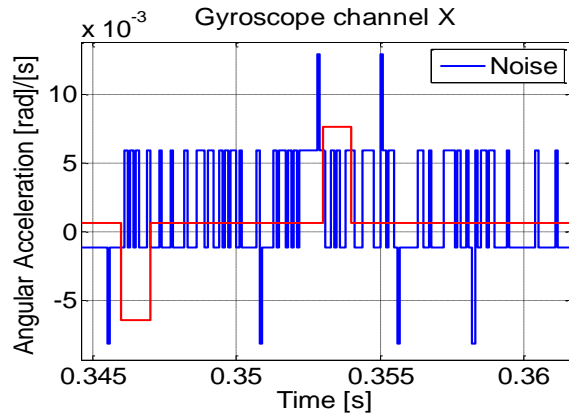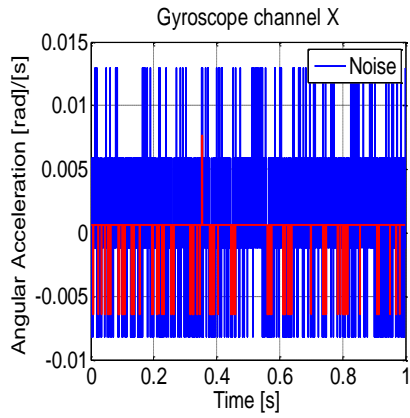
5.2.3.1.2 CHANNELY

In blue we can see 10000 samples at 10kHz; in red we can see the filter which is 1000 samples at 1kHz.
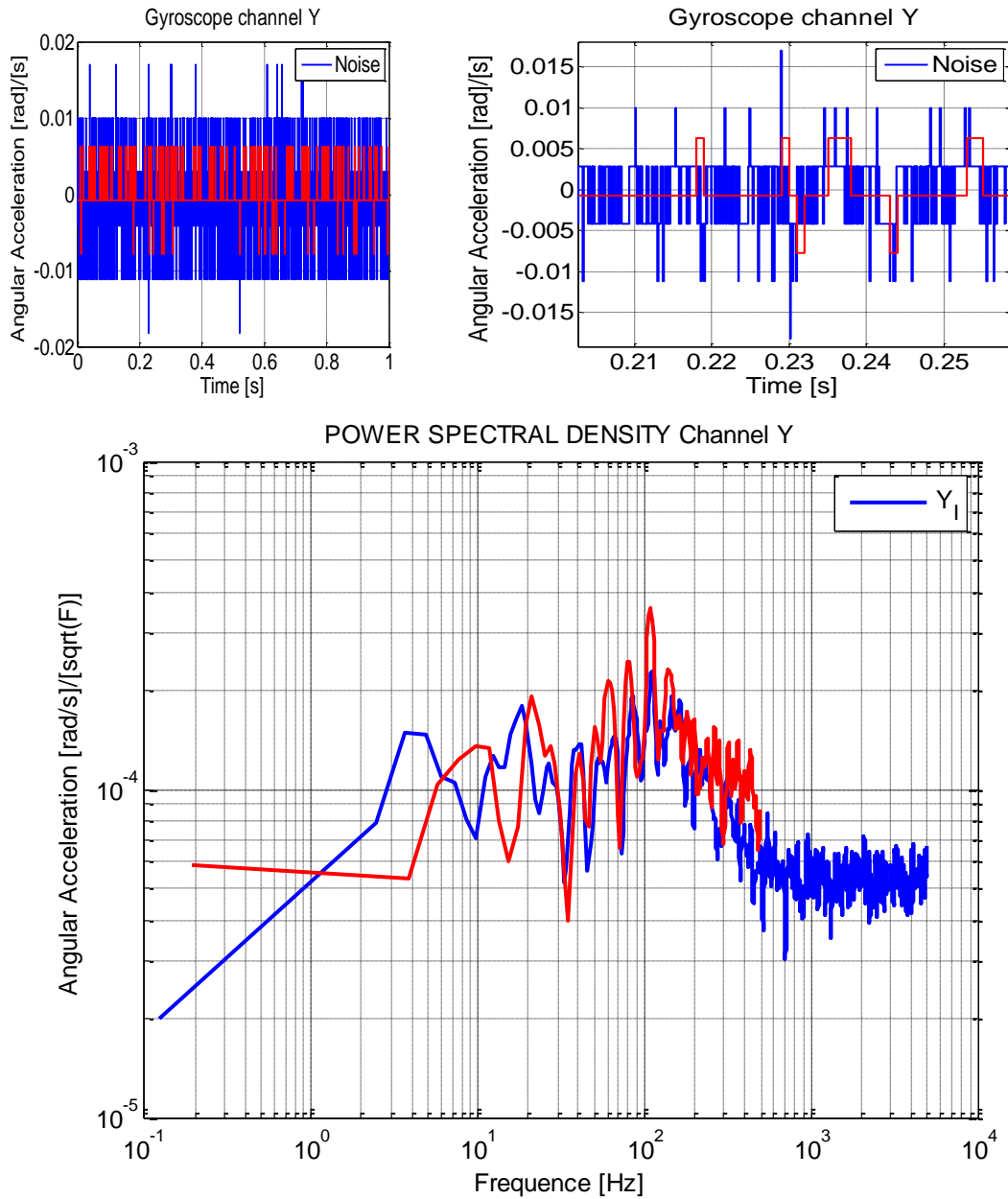
5.2.3.1.3 CHANNEL Z

In blue we can see 10000 samples at 10kHz; in red we can see the filter which is 1000 samples at 1kHz.
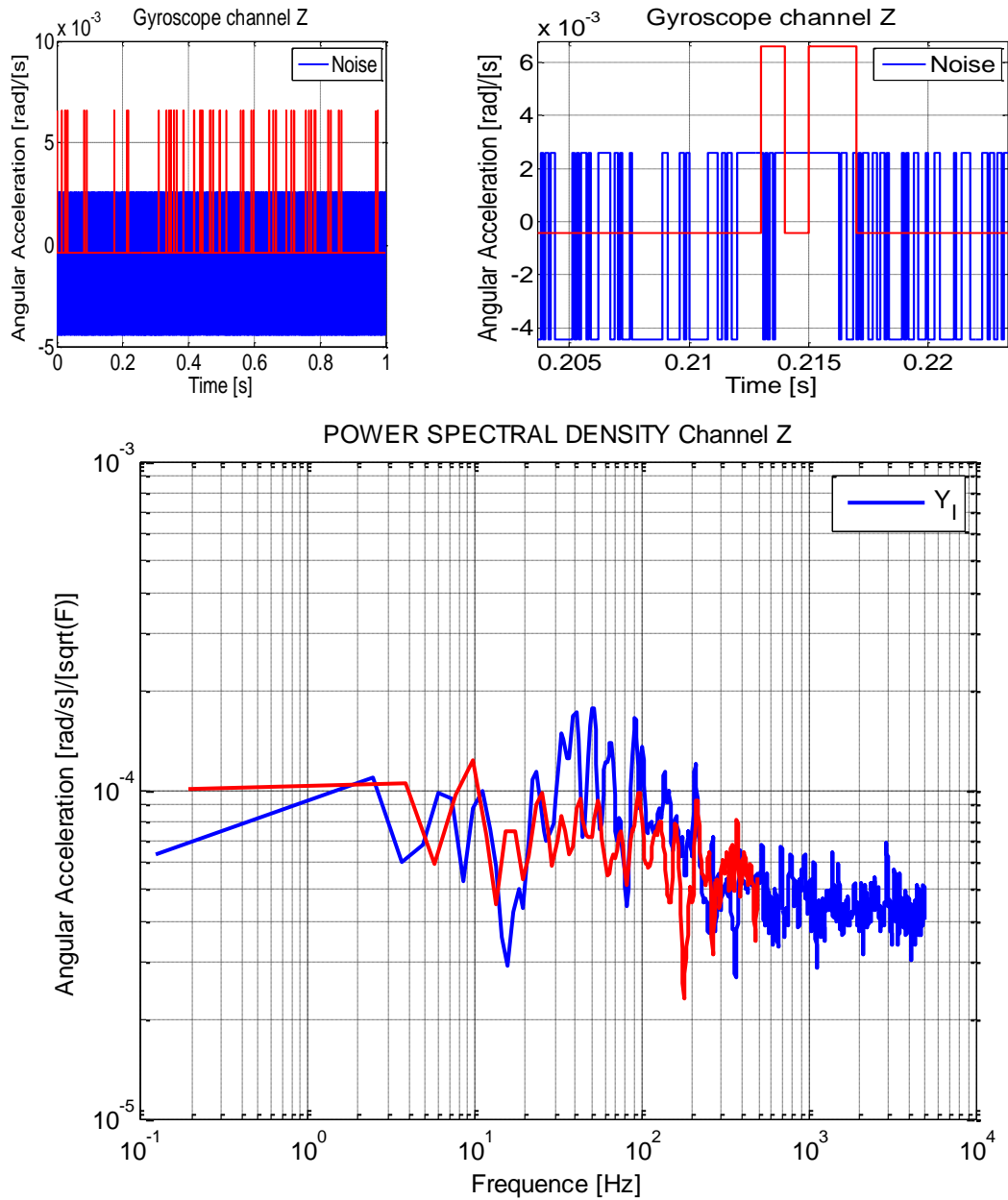
5.2.3.2 GYROSCOPE WITH 4.5 AMPLIFIER

5.2.3.2.1   CHANNEL X

In blue we can see 10000 samples at 10kHz; in red we can see the filter which is 1000 samples at 1kHz.
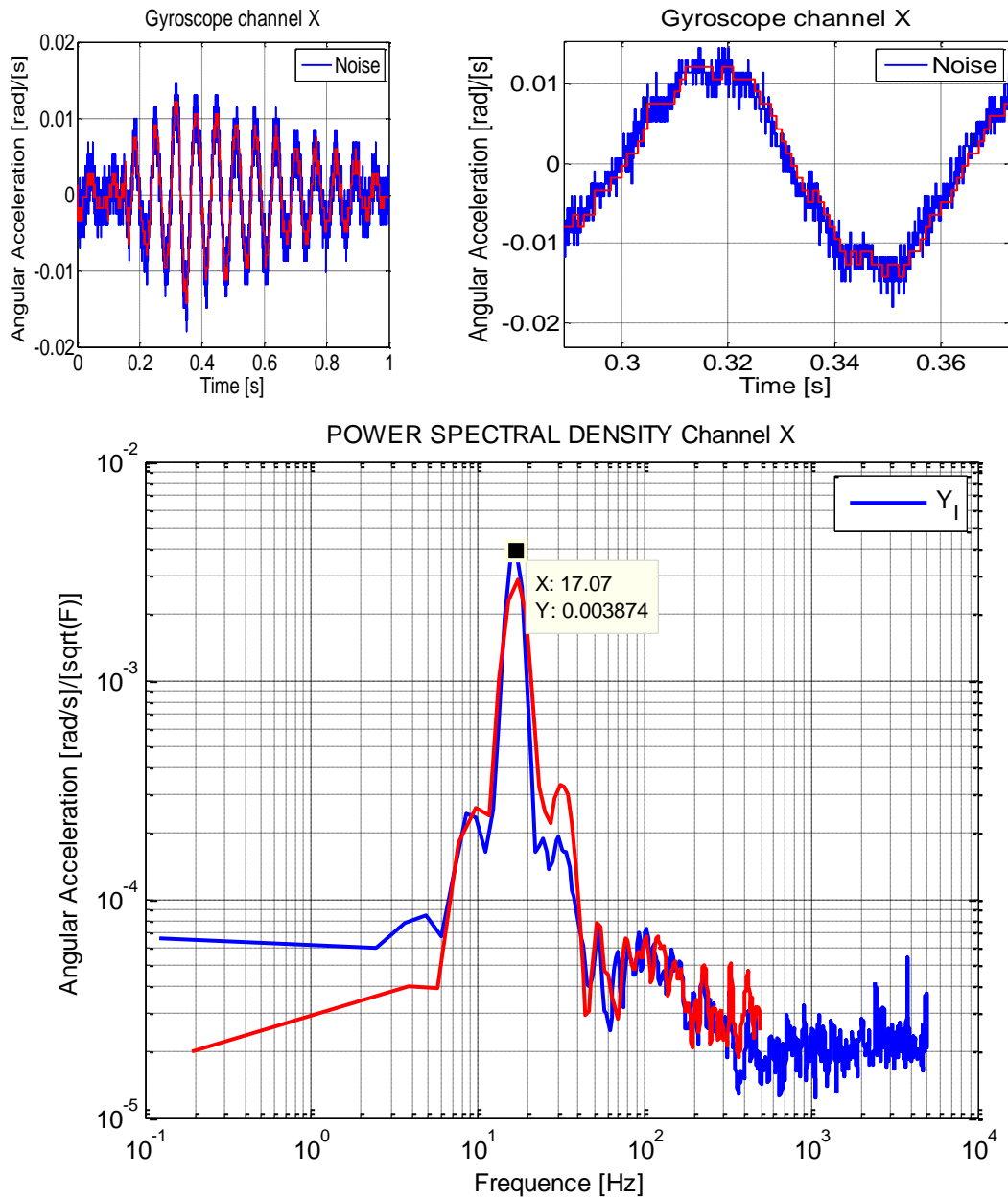
5.2.3.2.2   CHANNELY

In blue we can see 10000 samples at 10kHz; in red we can see the filter which is 1000 samples at 1kHz.
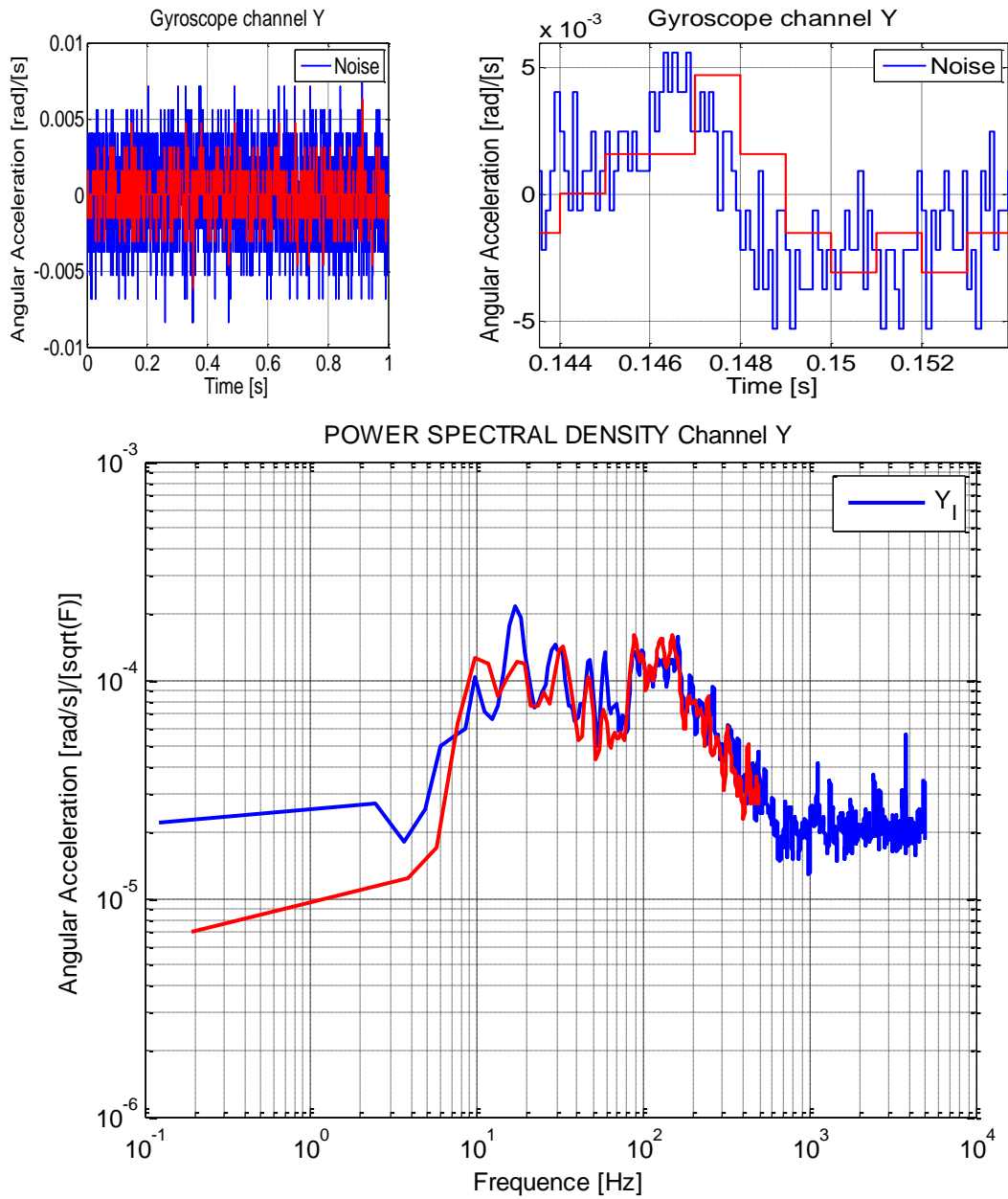
5.2.3.2.3   CHANNEL Z

In blue we can see 10000 samples at 10kHz; in red we can see the filter which is 1000 samples at 1kHz.
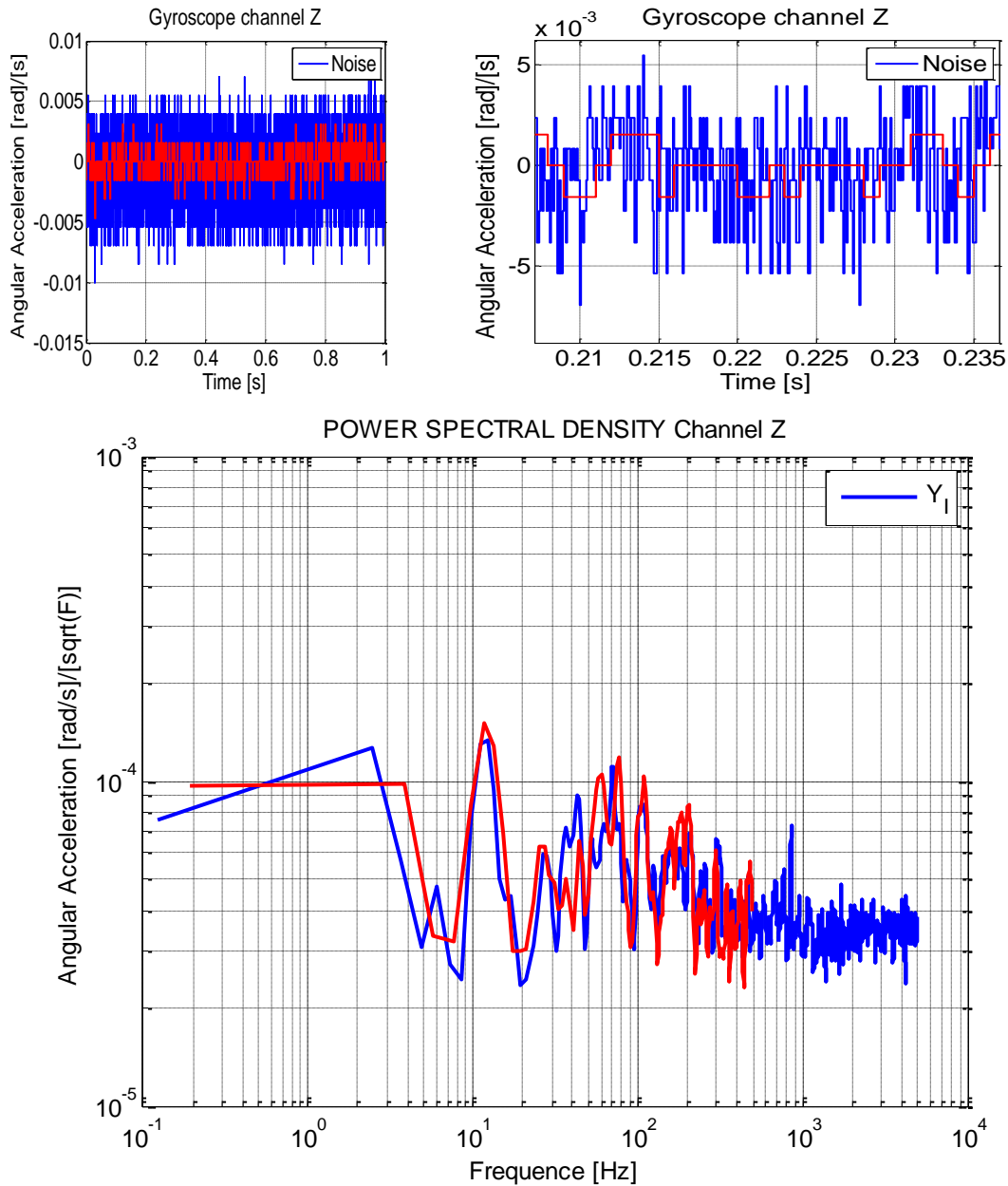
5.2.4   MAGNETOMETER

The magnetometer measure both the direction and the magnitude of Earth's magnetic fields from nano-Teslas to 8e-4 teslas .as mentioned before, the magneto resistive sensor circuit is a Trio of sensors that convert any incident magnetic field in the sensitive axis direction to a differential voltage output. The magnetometer

has a digital interface and 13 different register. There are 3 registers that can be read it or write it. In these registers I configured the magnetometer to have maximum possible sensitivity, 8 samples averaged and an output rate of 75Hz. This mean that every 13.33ms (75Hz) the magnetometer has a new measure loaded into the output register of every channel.

To test the magnetometer I uses the self test provide by the component itself. The test consists in: an internal current source generates DC current (about 10 mA) from the VDD supply. This DC current is applied to the offset straps of the magneto-resistive sensor, which creates an artificial magnetic field bias on the sensor. The difference of this measurement and the measurement of the ambient field will be put in the data output register for each of the three axes. This test is made with positive bias configuration and negative bias configuration.

5.2.4.1 POSITIVE BIAS SELFT TEST

5.2.4.1.1   CHANNEL X

1000 samples at 50Hz

POWER SPECTRAL DENSITY Channel X

5.2.4.1.2   CHANNEL Y

1000 samples at 50Hz

POWER SPECTRAL DENSITY Channel Y
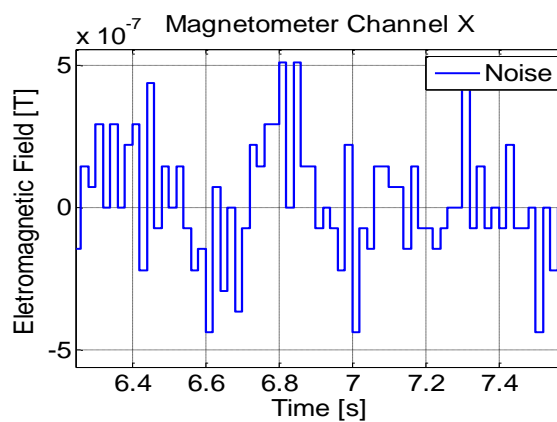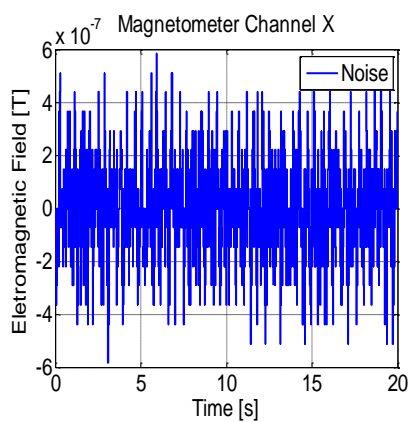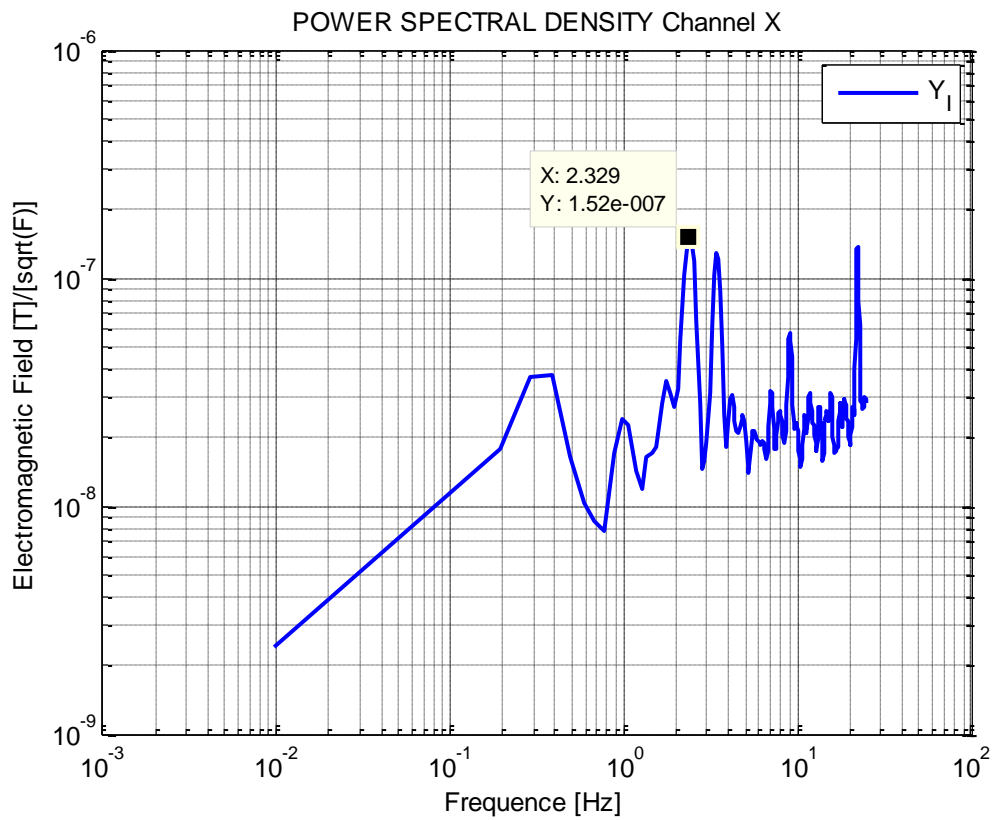
5.2.4.1.3   CHANNEL Z
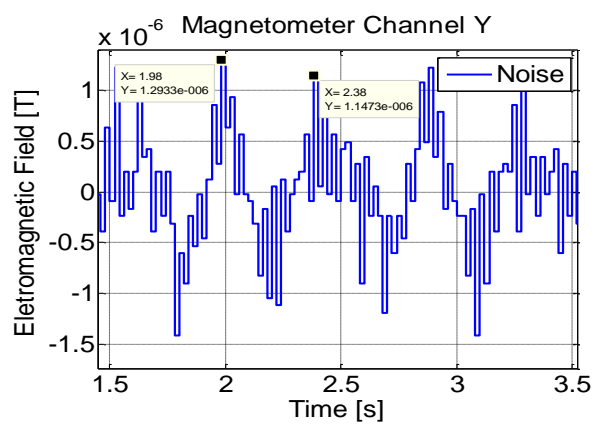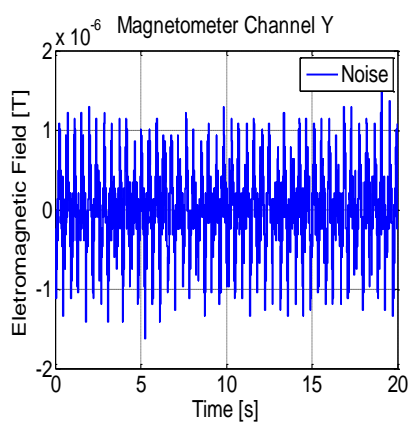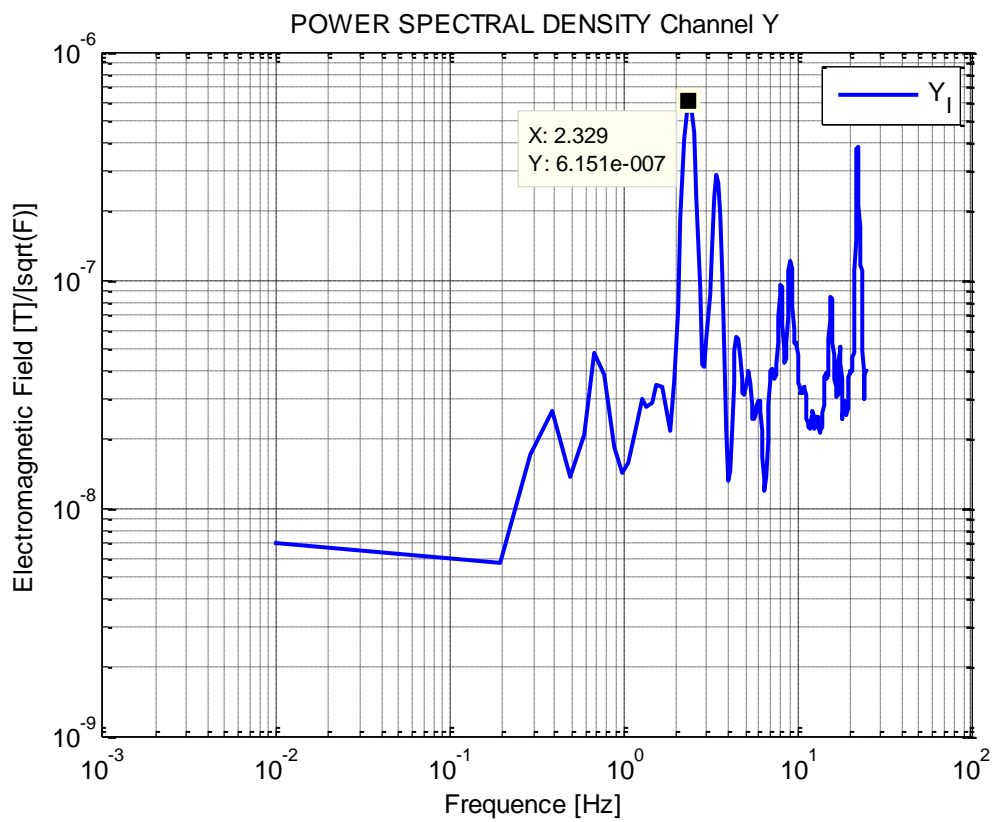
1000 samples at 50Hz

POWER SPECTRAL DENSITY Channel Z
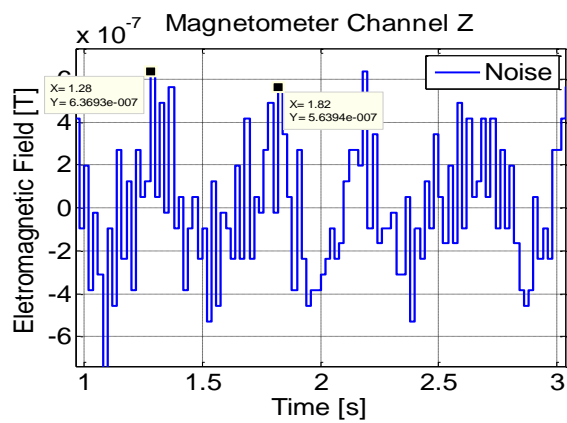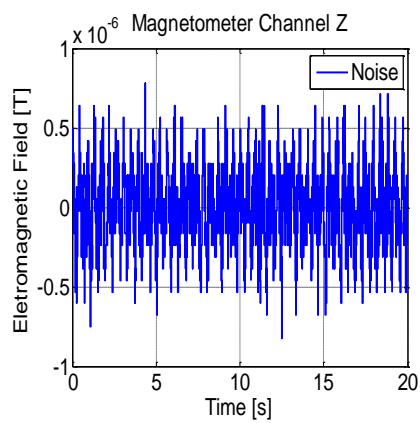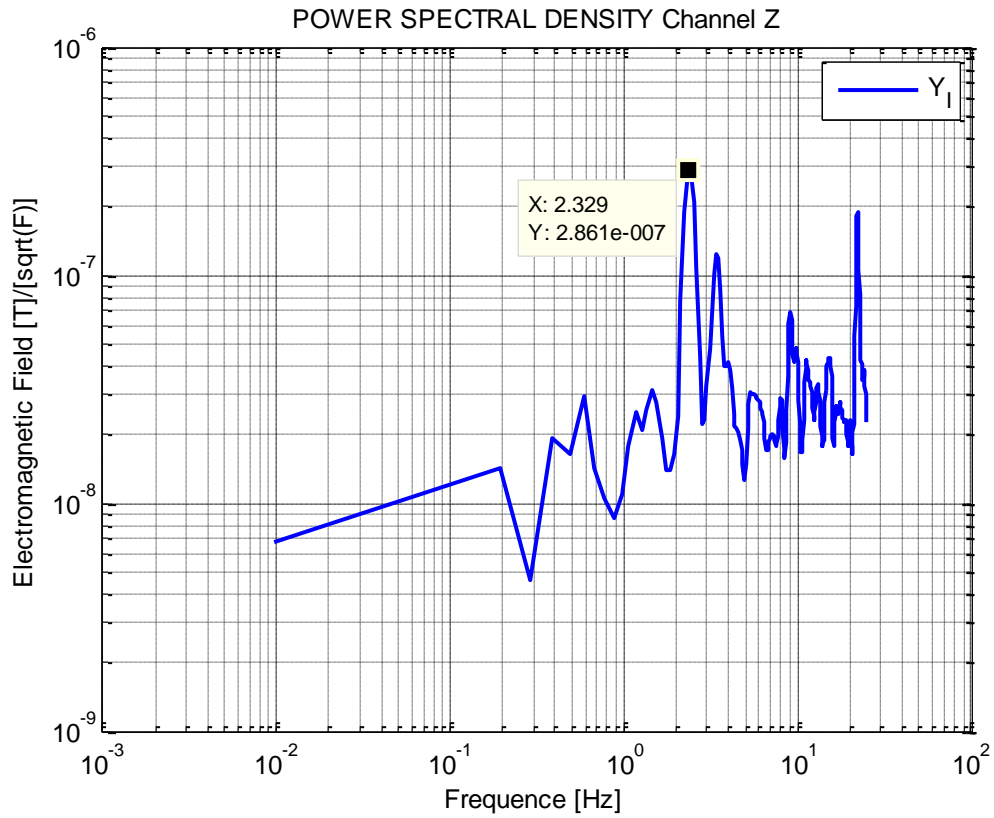
5.2.4.2 *NEGATIVE BIAS SELFT TEST*

5.2.4.2.1   CHANNEL X

1000 samples at 50Hz

POWER SPECTRAL DENSITY Channel X

5.2.4.2.2   CHANNEL Y

1000 samples at 50Hz

POWER SPECTRAL DENSITY Channel Y

5.2.4.2.3   CHANNEL Z

1000 samples at 50Hz

POWER SPECTRAL DENSITY Channel Z

X: 2.232
Y: 7.555e-007
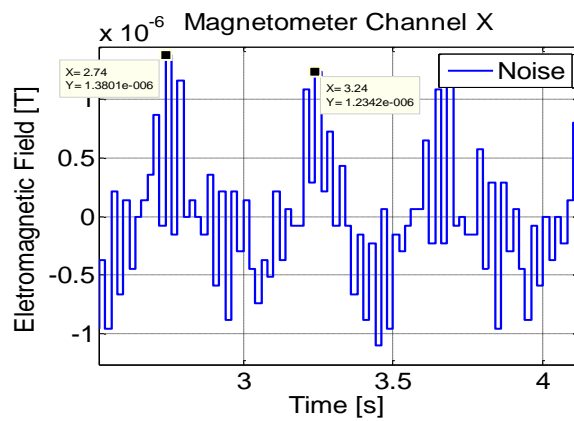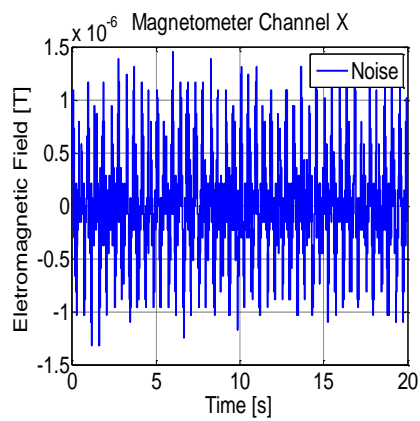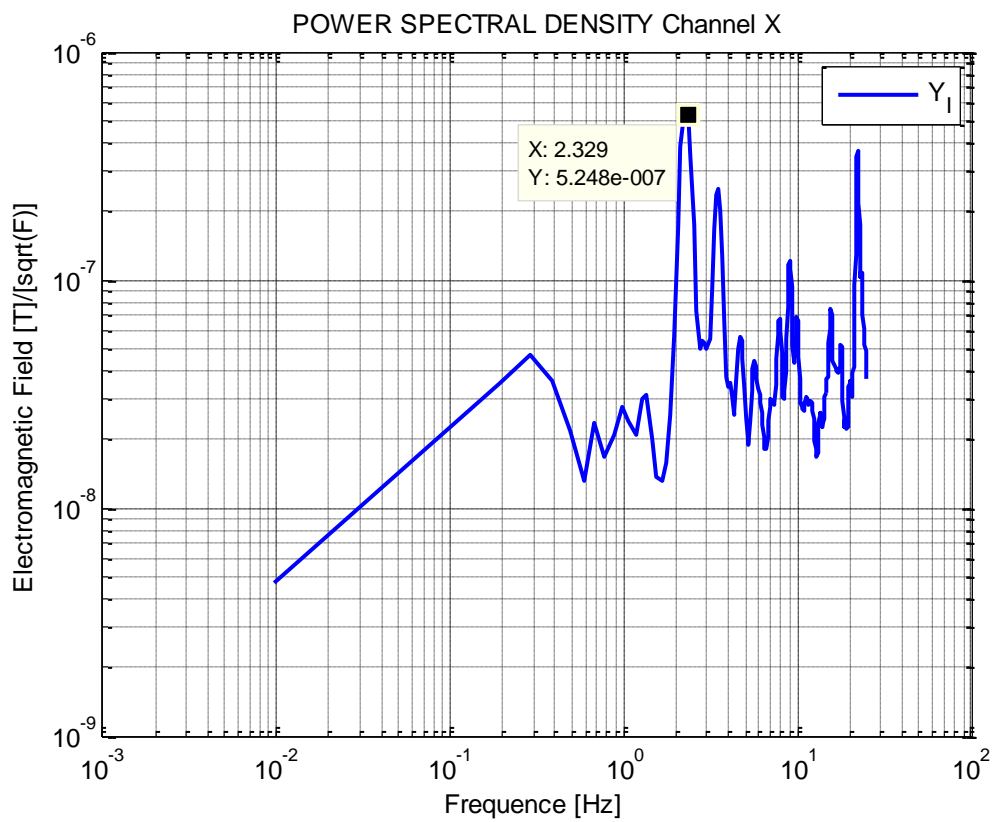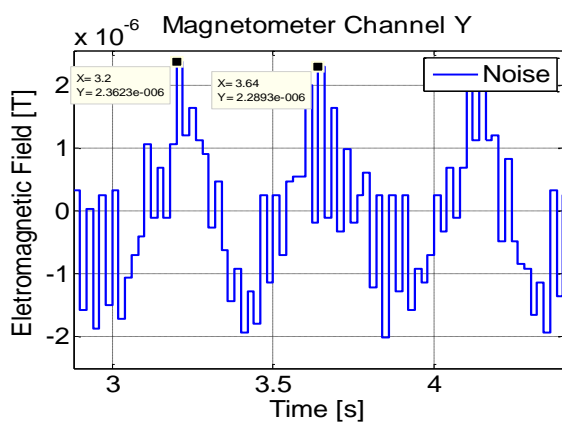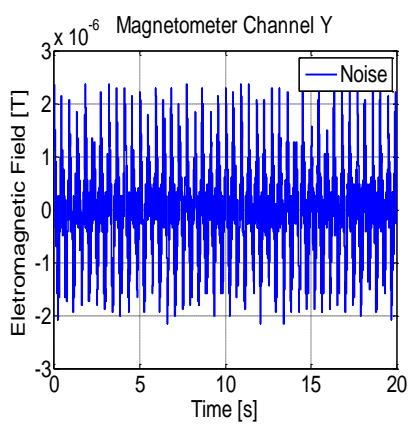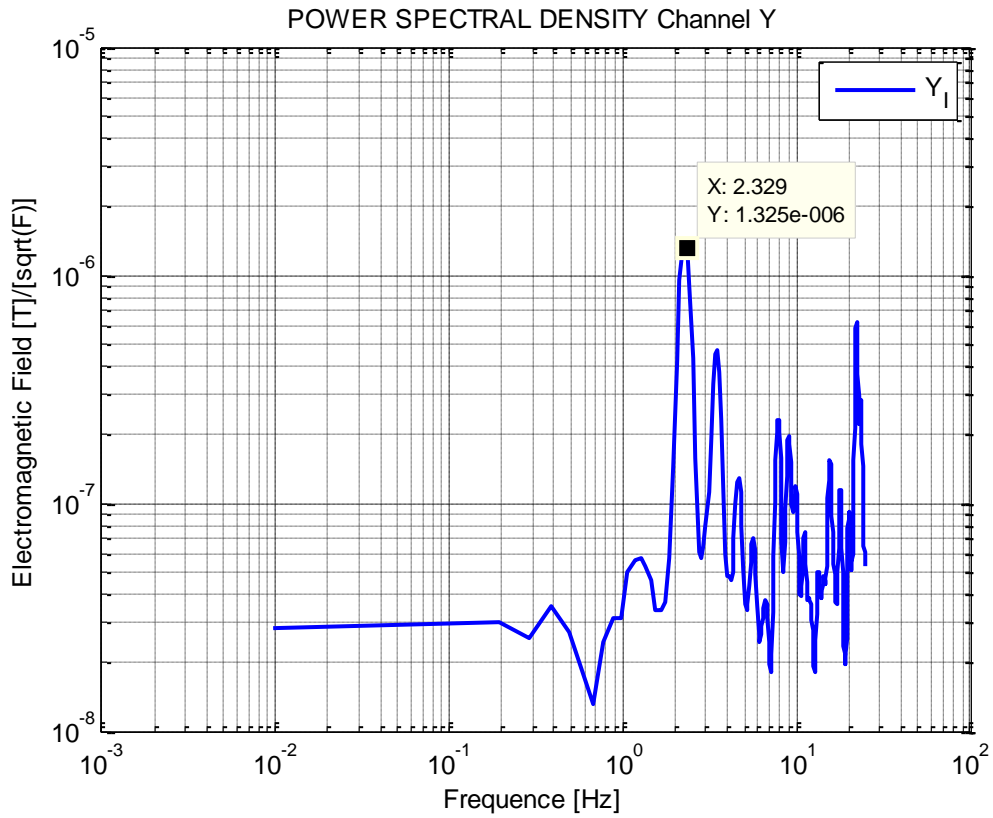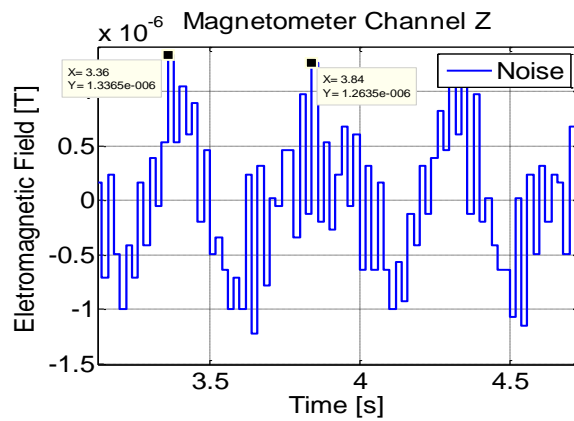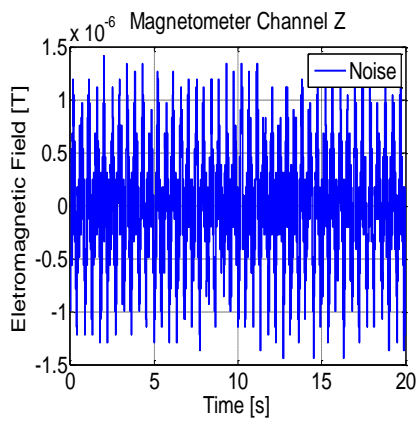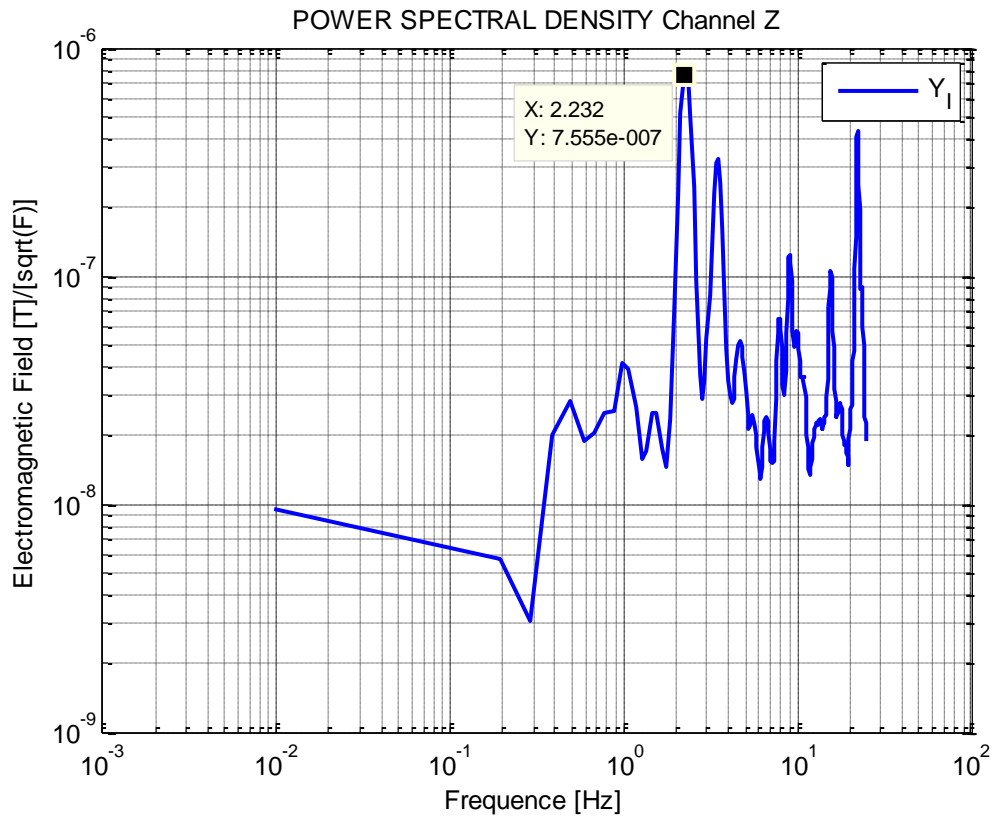
5.2.5 TABLE OF RESULTS

5.2.5.1 ACCELEROMETER

NUMBER	TEST	CHANNEL	ZERO [V]	ZERO[M/S^2]	STANDARD DEVIATION[M/S^2]	AVERAGE[M/S^2]
1.	Bottom view	X	0.2990	3.6661	0.0695	16.5671
2.	Bottom view	Y	0.1363	1.6717	0.0753	18.5615
3.	Bottom view	Z	0.3971	4.8691	0.0795	5.5541
4.	Side view	X	0.2417	2.9640	0.3222	17.2692
5.	Side view	Y	0.0057	0.0702	0.4064	20.1630
6.	Side view	Z	0.5234	6.4799	0.2796	23.6247
7.	Front inclination	X	0.3416	4.1889	0.0692	16.0443

8.	Front inclination	Y	-0.0076	-0.0936	0.0726	10.5168
9.	Front inclination	Z	0.5284	6.4800	0.0801	13.7532
10.	Back inclination	X	0.3249	3.9846	0.0721	16.2486
11.	Back inclination	Y	0.2549	3.1255	0.0745	26.9178
12.	Back inclination	Z	0.4453	5.4605	0.0784	14.7728
13.	Right inclination	X	0.1920	2.3545	0.0704	8.0687
14.	Right inclination	Y	0.1228	1.5061	0.0714	18.7271
15.	Right inclination	Z	0.5481	6.7212	0.0782	13.5120
16.	Left inclination	X	0.4820	5.9101	0.0731	24.1332
17.	Left inclination	Y	0.1196	1.4670	0.0710	18.7662
18.	Left inclination	Z	0.5870	7.1981	0.0918	13.0351

Table9. Results accelerometer.

From Table9 it is possible to obtain the measure of the gravity. It can be calculate making the difference between: the value of one axis when it is not subjected to gravity, and the value of the same axis when it is subjected to gravity. As an example I take the Z-axis. The Z-axis is subjected to gravity in side view or bottom view, and it is not subjected to gravity in the rest. I make the difference between the front inclination and the side view:

$$Z_{side-view} - Z_{front\ inclination} = 23.6247 - 13.7532 = 9.87\ m/s\char94 2$$

As we can see the measure for the gravity is 9.87 m/s^2.

5.2.5.2 GYROSCOPE

NUMBER	TEST	CHANNEL	ZERO[Rad/s]	STANDARD DEVIATION[Rad/S]	AVERAGE[Rad/S]
1.	GYROSCOPE WITHOUT AMPLIFIER	X	0.0385	0.0032	11.7416
2.	GYROSCOPE WITHOUT	Y	0.4151	0.0043	11.3650

	AMPLIFIER				
3.	GYROSCOPE WITHOUT AMPLIFIER	Z	0.0985	0.0034	11.6816
4.	GYROSCOPE WITH 4.5 AMPLIFIER	X	-0.0387	0.0053	2.6348
5.	GYROSCOPE WITH 4.5 AMPLIFIER	Y	0.3366	0.0022	2.2596
6.	GYROSCOPE WITH 4.5 AMPLIFIER	Z	-0.0710	0.0027	2.6672

Table10. Gyroscope's results.

5.2.5.3 MAGNETOMETER

NUMBER	TEST	CHANNEL	STANDARD DEVIATION[T]	AVERAGE[T]	AVERAGE[LSB]
1.	POSITIVE BIAS	X	2.0696e-007	1.1263e-004	1.5430e+003
2.	POSITIVE BIAS	Y	5.5958e-007	1.0586e-004	1.4503e+003
3.	POSITIVE BIAS	Z	2.8622e-007	1.1104e-004	1.5213e+003
4.	NEGATIVE BIAS	X	5.0709e-007	-1.1036e-004	-1.5119e+003
5.	NEGATIVE BIAS	Y	1.0545e-006	-1.0740e-004	-1.4714e+003
6.	NEGATIVE BIAS	Z	6.2351e-007	-1.0988e-004	-1.5053e+003

Table10. Magnetometer's results.

5.3 CONTROLLED ENVIRONMENT (Thales Alenia space)

In order to obtain the results of the controlled environment, the microcontroller with the sensors were putted into a special table. The table is a "StableTop 450 Optical tabletops ". It is an optical table enhanced with proprietary tuned and broadband dampers, where the outer skins are matched with the internal plate to minimize bowing due to thermal variations and cycling and to ensure the flatness of the tabletop is maintained. Moreover, the table has self-leveling vibration isolator that offers the highest performance of any pneumatic isolator. The special part of the table that permits us to have a controlled environment is the super damp isolators, which provide total vertical and horizontal isolation with extremely low resonant frequency and constant height.

The optical table was provided by Thales Alenia space. Next, I will present all the results of the measurements done with the special table.

5.3.1 ACCELEROMETER

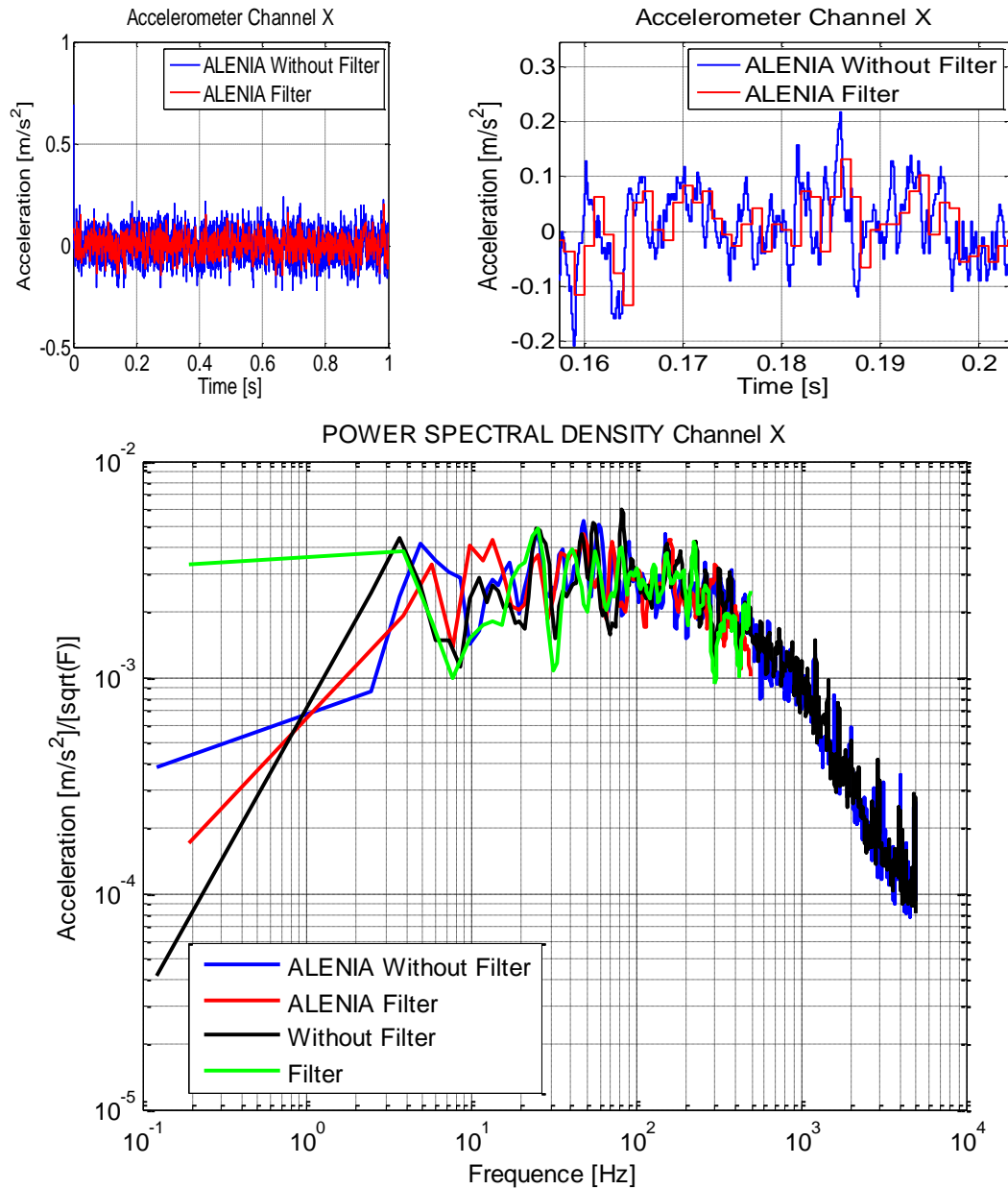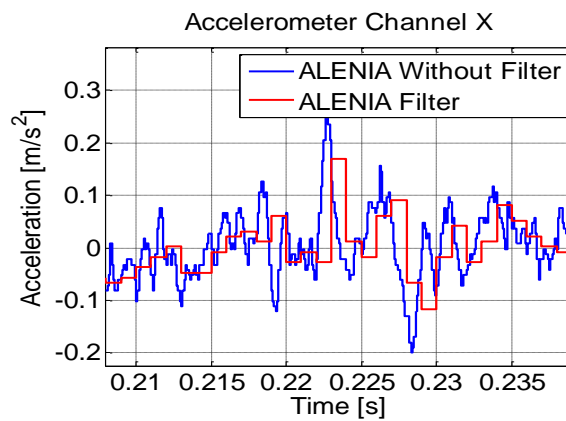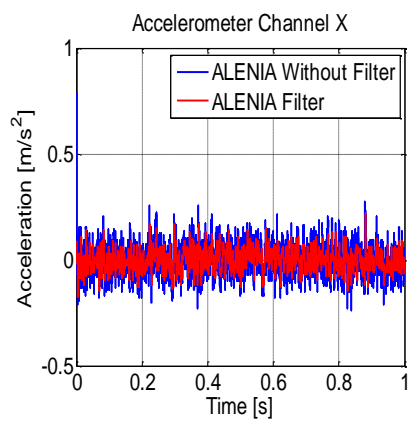#### *5.3.1.1 CHANNEL X*

5.3.1.1.1 SIDE VIEW

In blue we can see 10000 samples at 10kHz; in red we can see the filter which is 1000 samples at 1kHz.
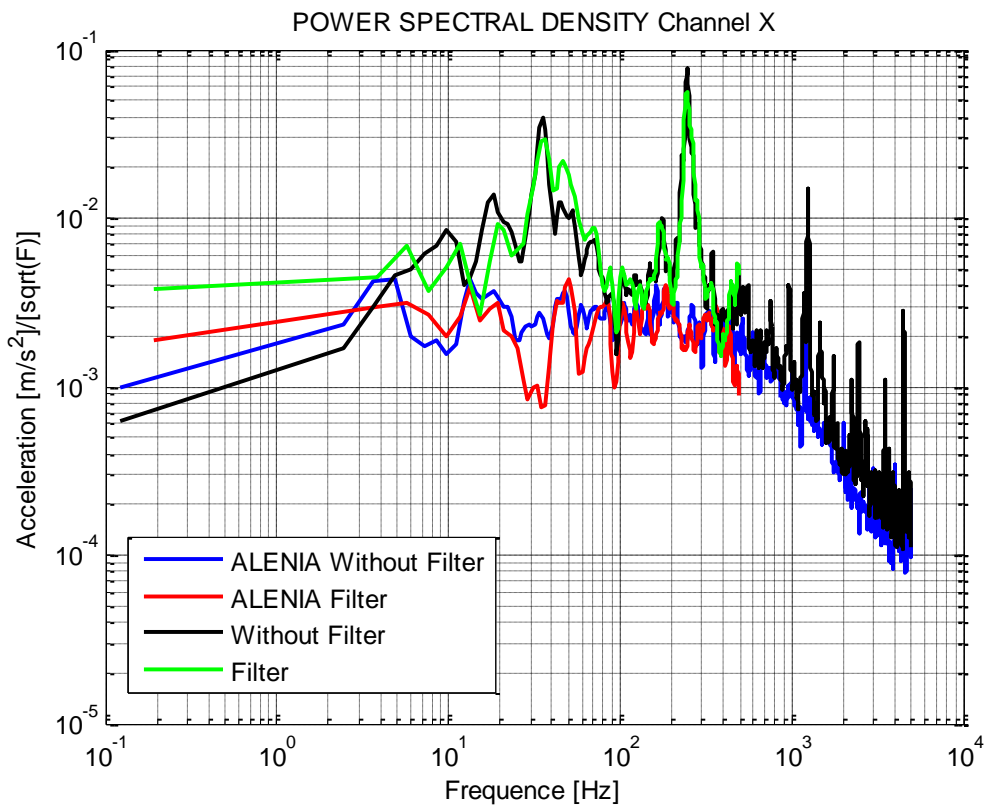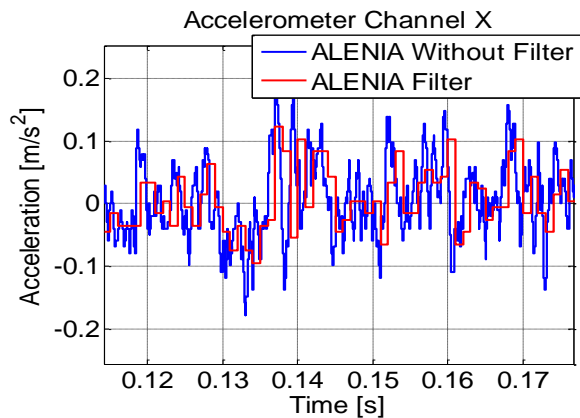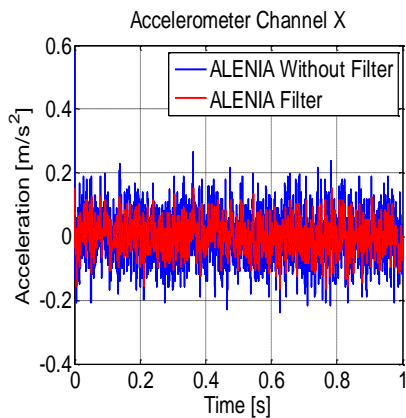
TEST	CHANNEL	ZERO [V]	ZERO[M/S^2]	STANDARD DEVIATION[M/S^2]	AVERAGE[M/S^2]
Side view	X	0.3319	4.0702	0.0676	16.1631

As we can see in the power spectral density figure, the noise is smaller in the ALENIA's test than in the normal test. It is important to notice that the frequencies due to aliasing or external vibrations are reduce notoriously because the special optical table.

5.3.1.1.2   BOTTOM VIEW

In blue we can see 10000 samples at 10kHz; in red we can see the filter which is 1000 samples at 1kHz.
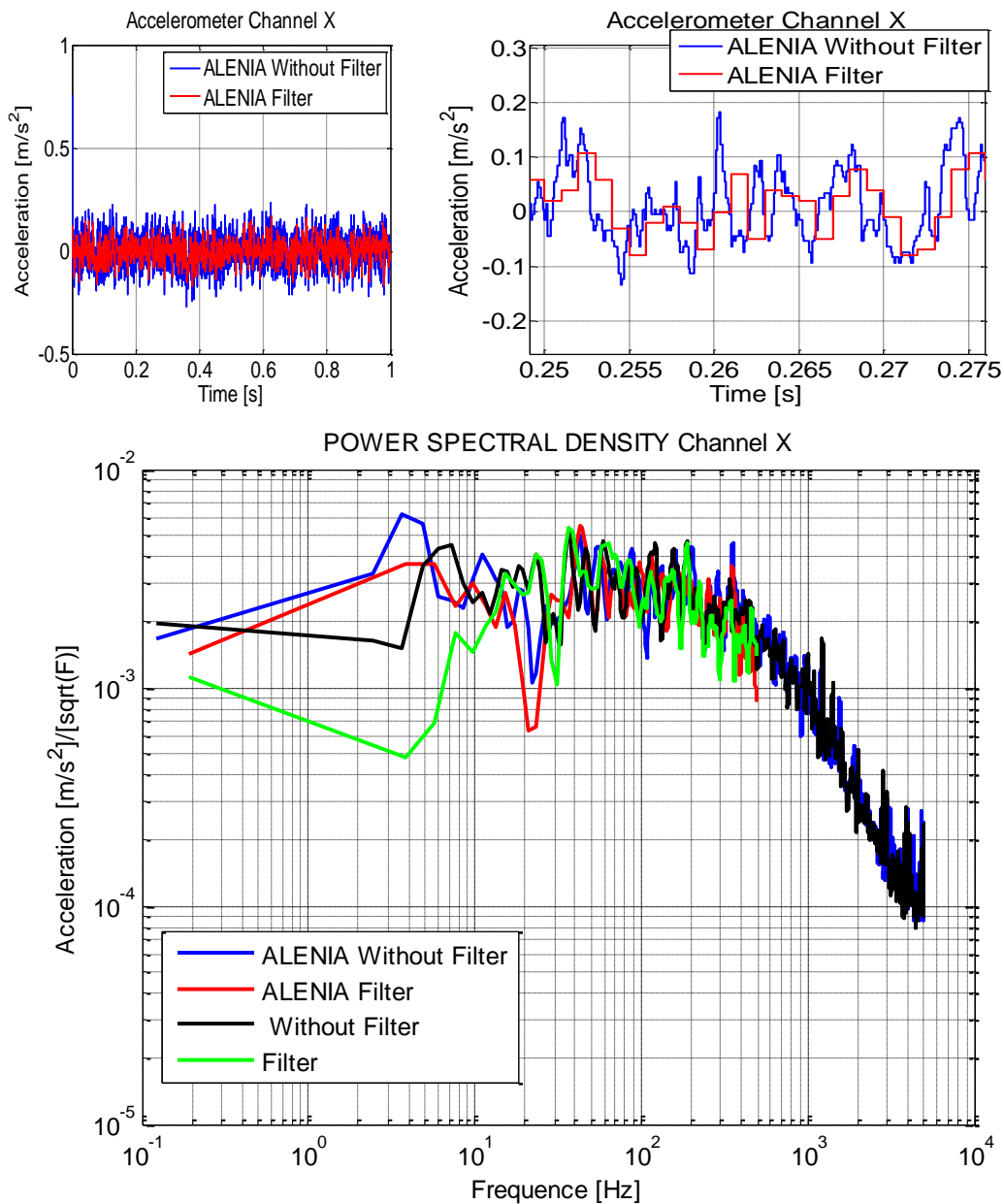
TEST	CHANNEL	ZERO [V]	ZERO[M/S^2]	STANDARD DEVIATION[M/S^2]	AVERAGE[M/S^2]
Bottom view	X	0.3074	3.7692	0.0714	16.4640

5.3.1.1.3   FRONT INCLINATION

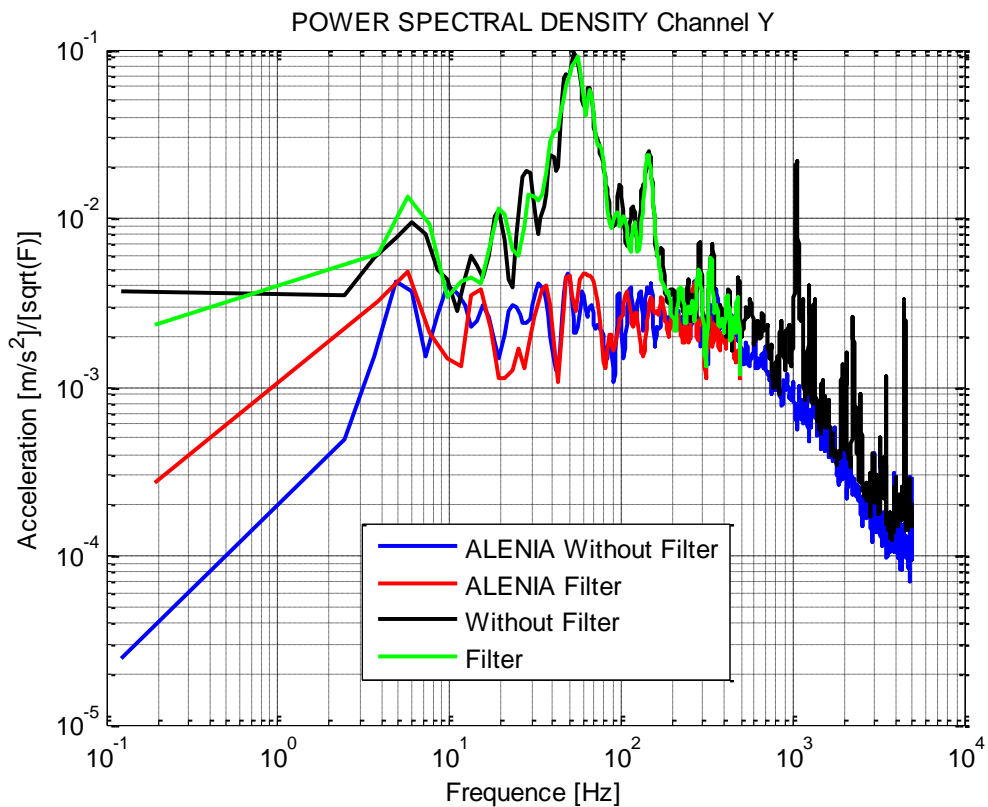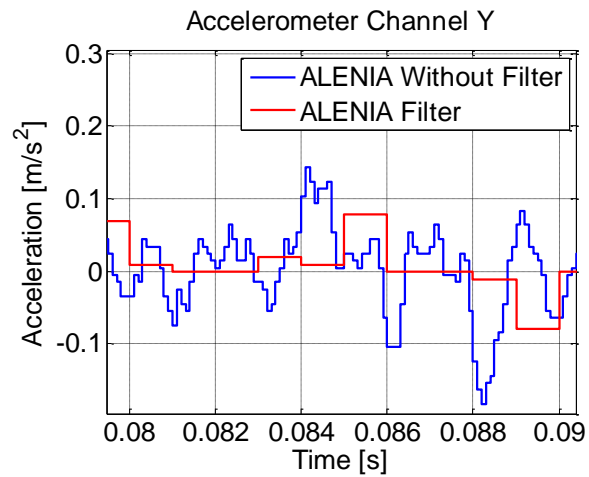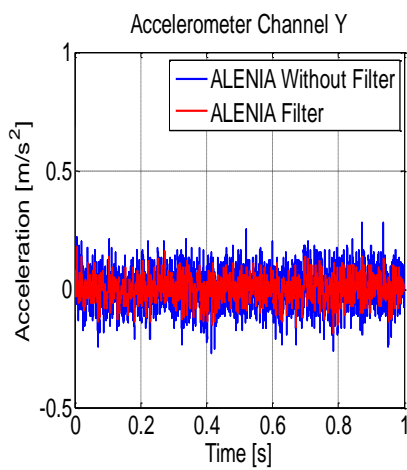In blue we can see 10000 samples at 10kHz; in red we can see the filter which is 1000 samples at 1kHz.

TEST	CHANNEL	ZERO [V]	ZERO[M/S^2]	STANDARD DEVIATION[M/S^2]	AVERAGE[M/S^2]
Front inclination	X	0.3367	4.1289	0.0665	16.1044

5.3.1.1.4   BACK INCLINATION

In blue we can see 10000 samples at 10kHz; in red we can see the filter which is 1000 samples at 1kHz.

POWER SPECTRAL DENSITY Channel X
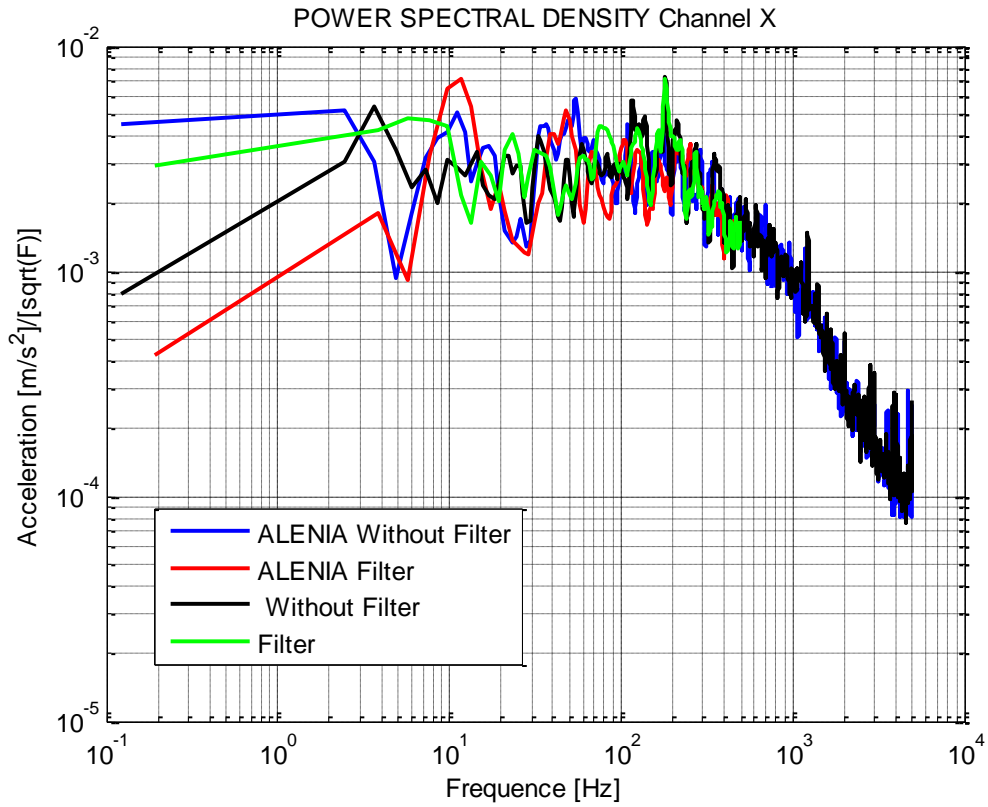
TEST	CHANNEL	ZERO [V]	ZERO[M/S^2]	STANDARD DEVIATION[M/S^2]	AVERAGE[M/S^2]
Back inclination	X	0.3181	3.9002	0.0685	16.3331

5.3.1.1.5 RIGHT INCLINATION

In blue we can see 10000 samples at 10kHz; in red we can see the filter which is 1000 samples at 1kHz.

POWER SPECTRAL DENSITY Channel X
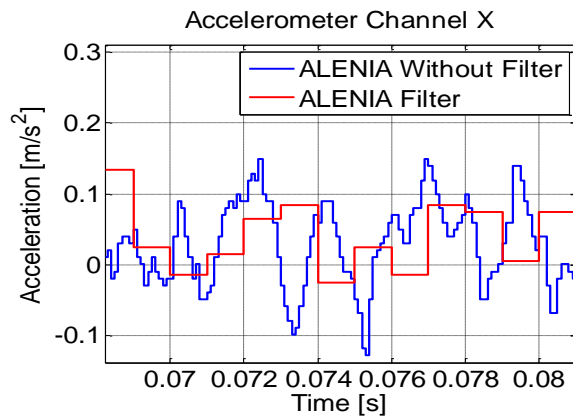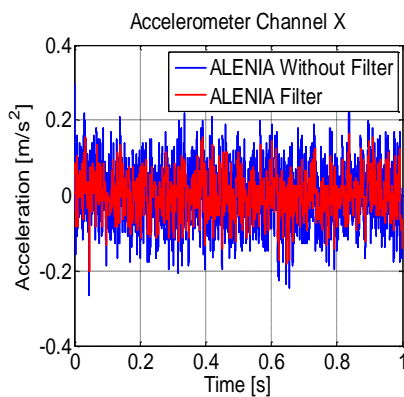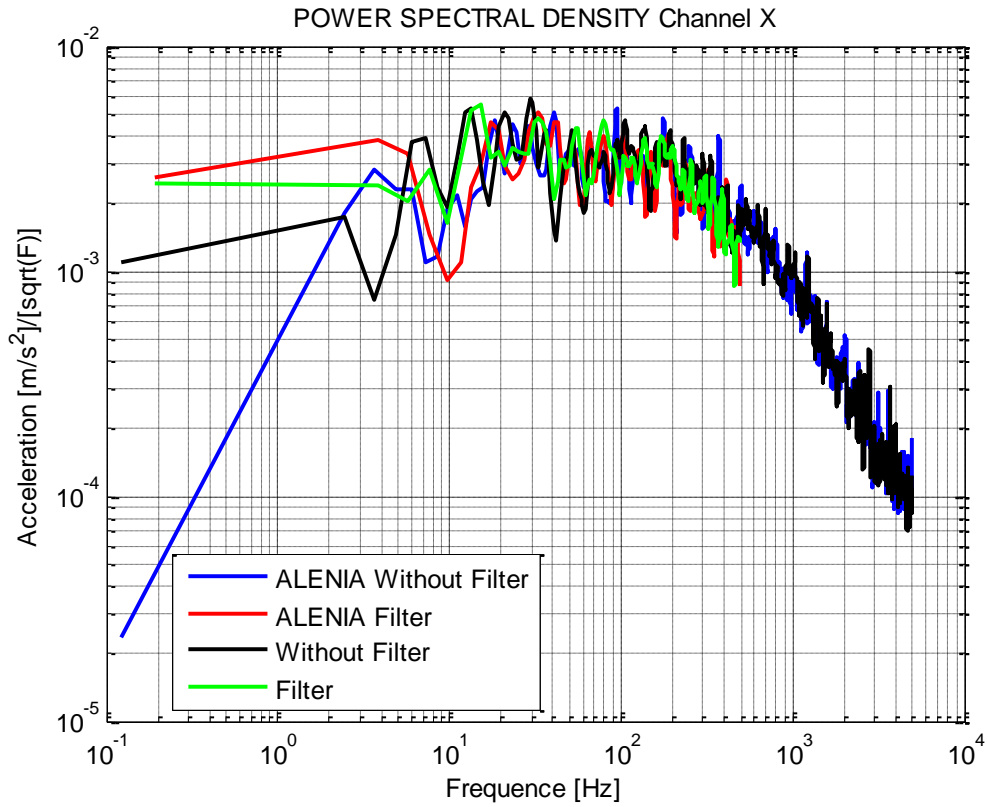
TEST	CHANNEL	ZERO [V]	ZERO[M/S^2]	STANDARD DEVIATION[M/S^2]	AVERAGE[M/S^2]
Right inclination	X	0.1838	2.2536	0.0686	8.1696

5.3.1.1.6 LEFT INCLINATION

In blue we can see 10000 samples at 10kHz; in red we can see the filter which is 1000 samples at 1kHz.

POWER SPECTRAL DENSITY Channel X
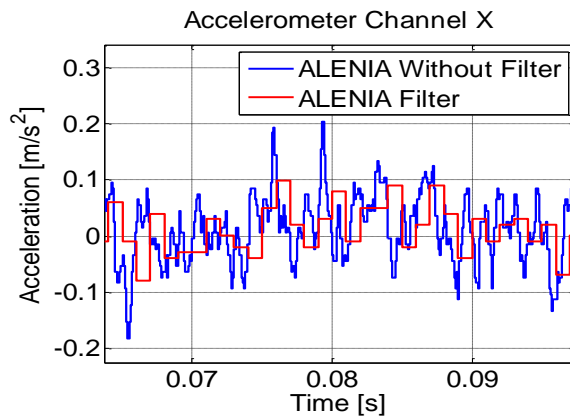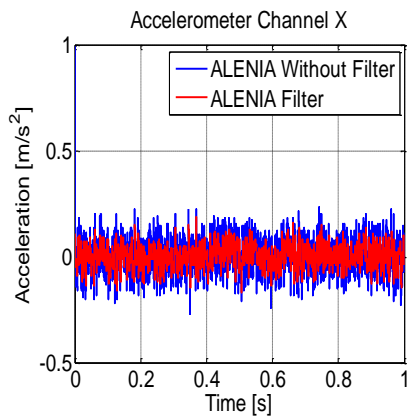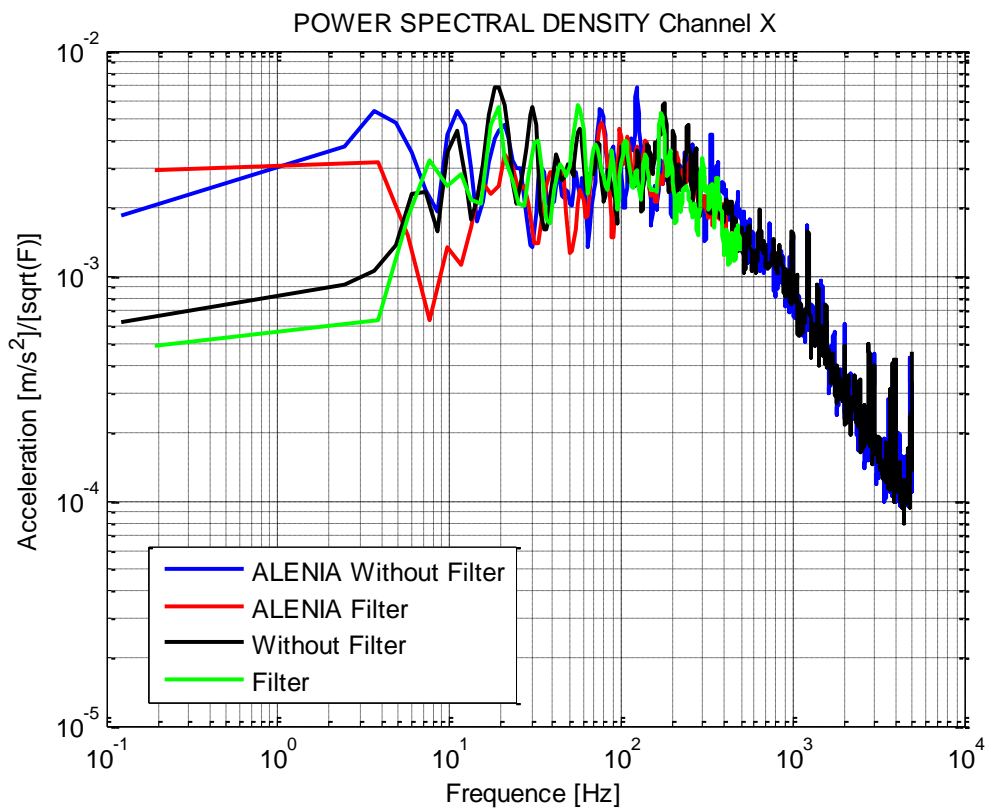
TEST	CHANNEL	ZERO [V]	ZERO[M/S^2]	STANDARD DEVIATION[M/S^2]	AVERAGE[M/S^2]
Left inclination	X	0.4798	5.8840	0.0714	24.1593

5.3.1.2 *CHANNEL Y*

5.3.1.2.1   SIDE VIEW

In blue we can see 10000 samples at 10kHz; in red we can see the filter which is 1000 samples at 1kHz.

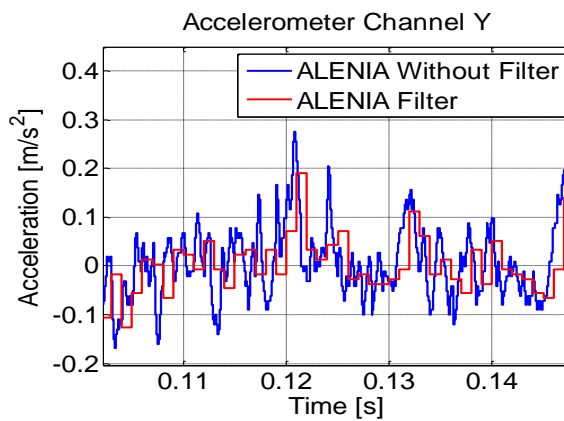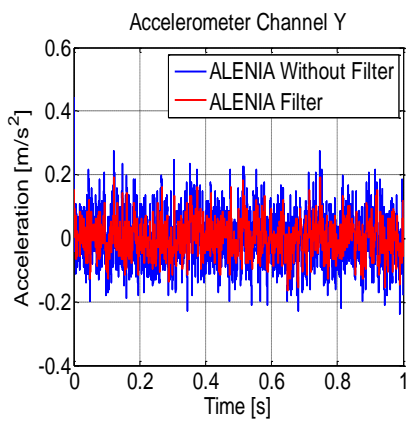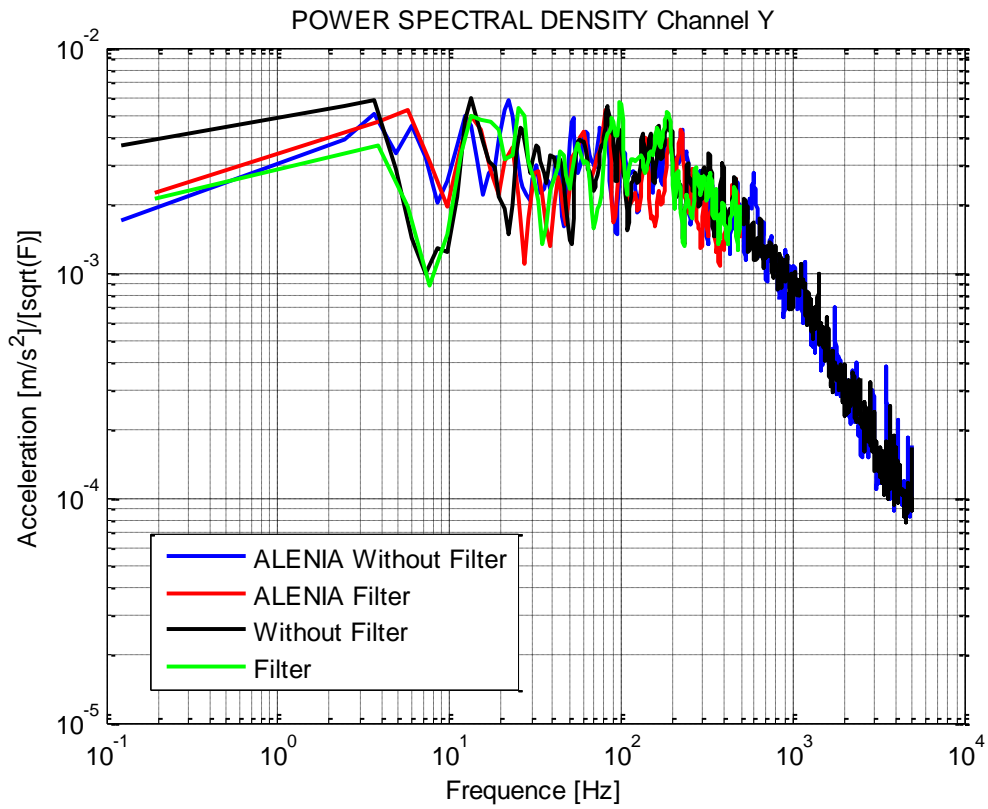| TEST	CHANNEL	ZERO [V]	ZERO[M/S^2]	STANDARD DEVIATION[M/S^2]	AVERAGE[M/S^2]
Side view	Y	0.0745	0.9137	0.0702	19.3195

As we can see in the power spectral density figure, the noise is smaller in the ALENIA's test than in the normal test. It is important to notice that the frequencies due to aliasing or external vibrations are reduce notoriously because the special optical table.

5.3.1.2.2 BOTTOM VIEW

In blue we can see 10000 samples at 10kHz; in red we can see the filter which is 1000 samples at 1kHz.

POWER SPECTRAL DENSITY Channel Y
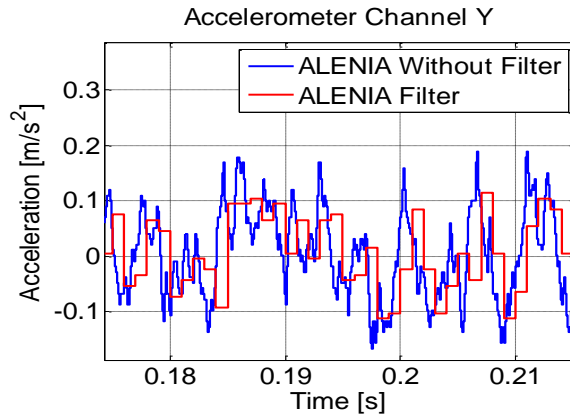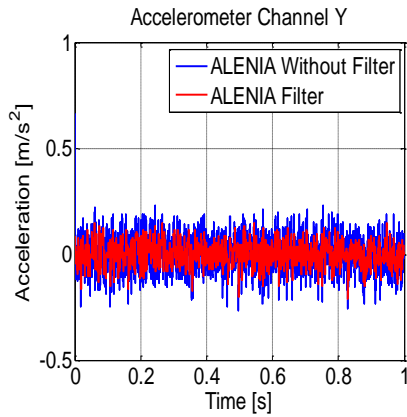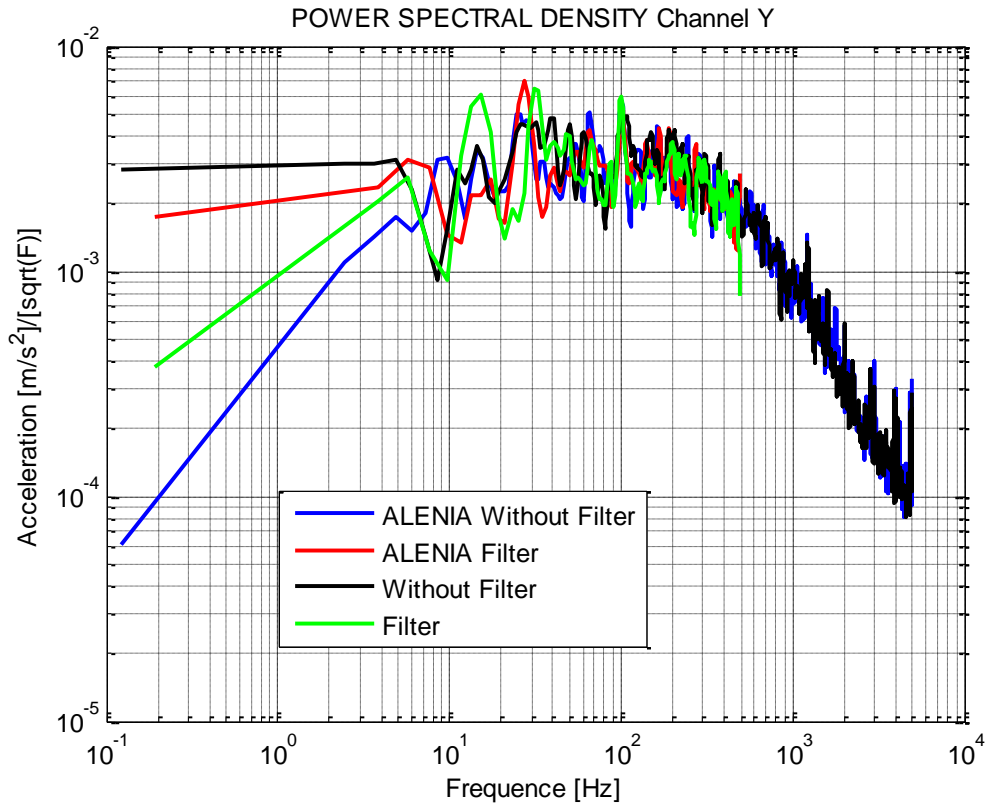
TEST	CHANNEL	ZERO [V]	ZERO[M/S^2]	STANDARD DEVIATION[M/S^2]	AVERAGE[M/S^2]
Bottom view	Y	0.0718	0.8804	0.0727	19.3528

5.3.1.2.3   FRONT INCLINATION

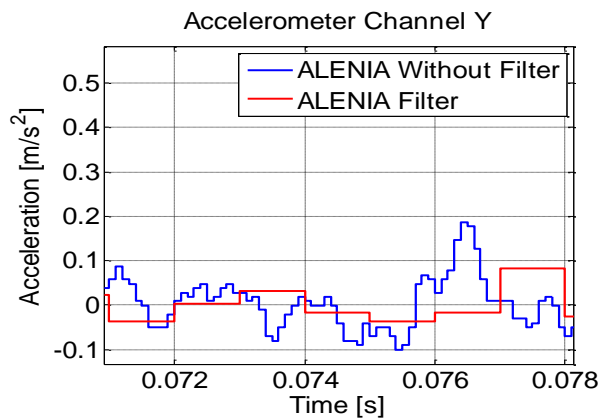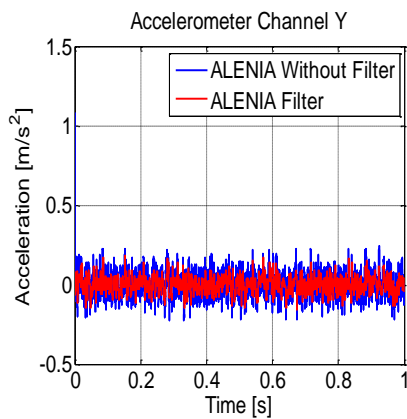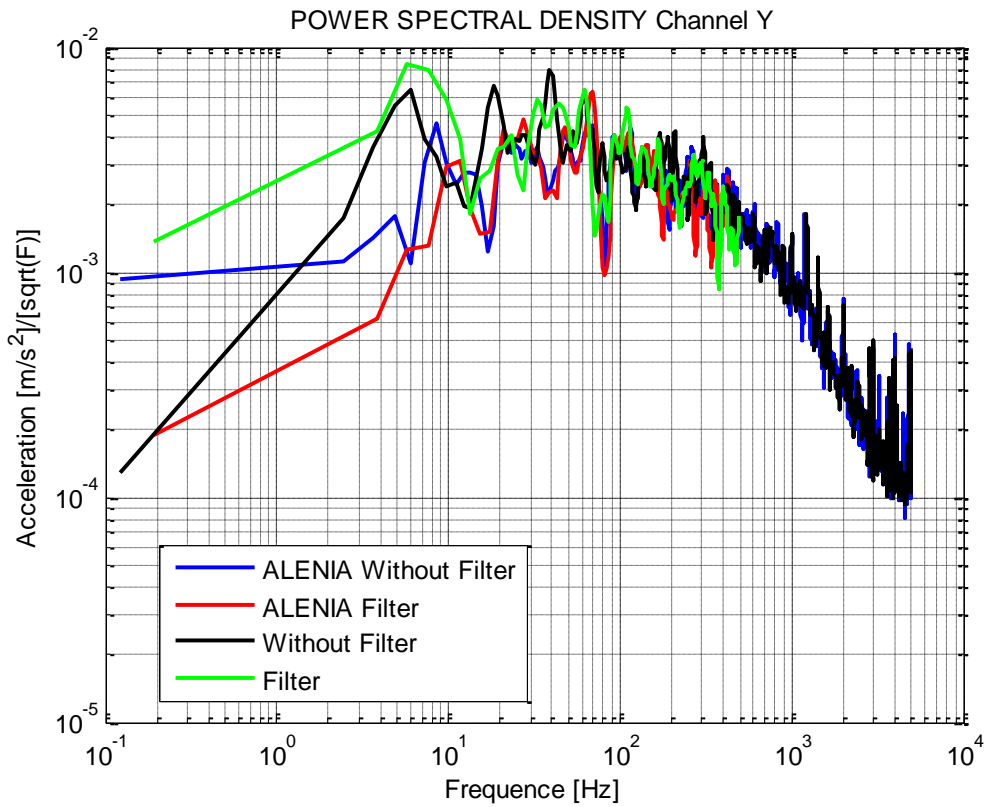In blue we can see 10000 samples at 10kHz; in red we can see the filter which is 1000 samples at 1kHz.

POWER SPECTRAL DENSITY Channel Y

TEST	CHANNEL	ZERO [V]	ZERO[M/S^2]	STANDARD DEVIATION[M/S^2]	AVERAGE[M/S^2]
Front inclination	Y	-0.0130	-0.1594	0.0697	10.5825

5.3.1.2.4   BACK INCLINATION

In blue we can see 10000 samples at 10kHz; in red we can see the filter which is 1000 samples at 1kHz.
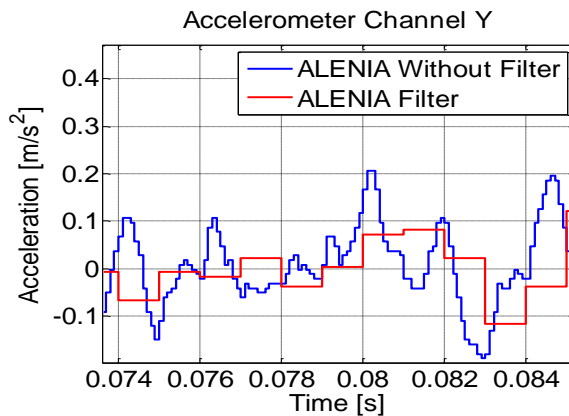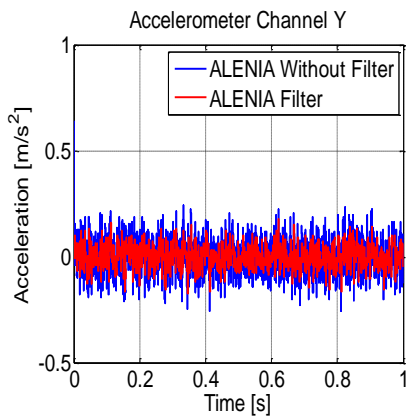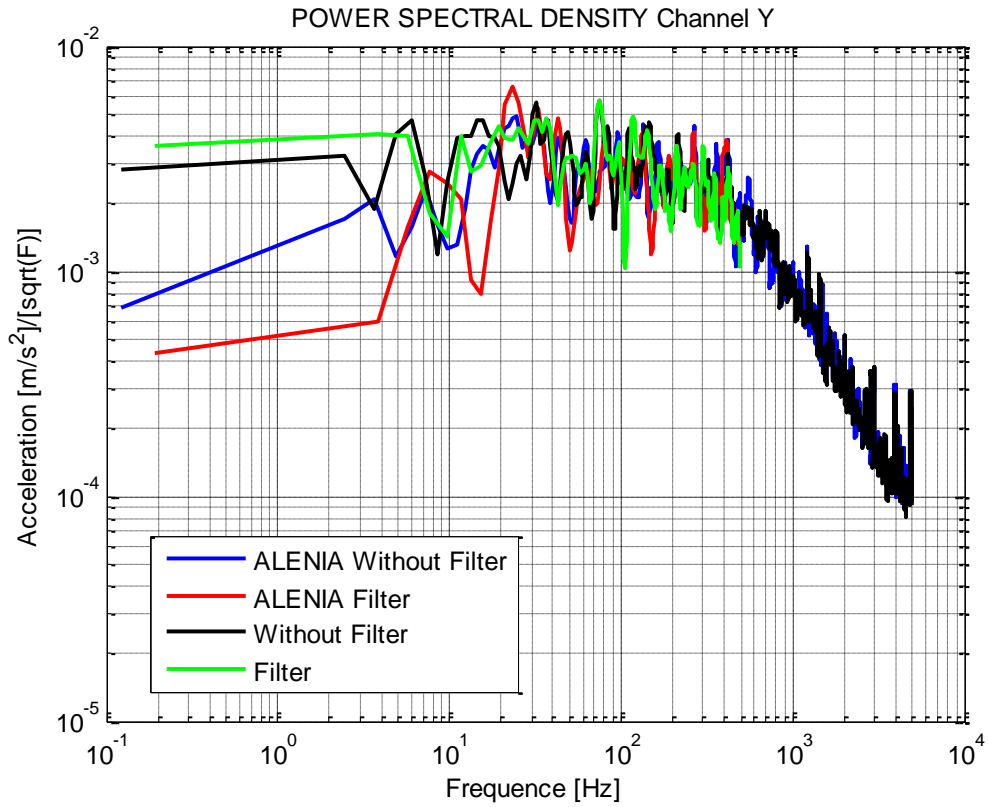
POWER SPECTRAL DENSITY Channel Y

TEST	CHANNEL	ZERO [V]	ZERO[M/S^2]	STANDARD DEVIATION[M/S^2]	AVERAGE[M/S^2]
Back inclination	Y	0.2521	3.0909	0.0705	26.9524

5.3.1.2.5   RIGHT INCLINATION

In blue we can see 10000 samples at 10kHz; in red we can see the filter which is 1000 samples at 1kHz.
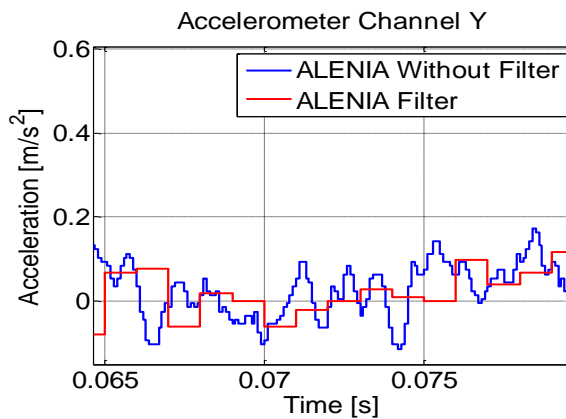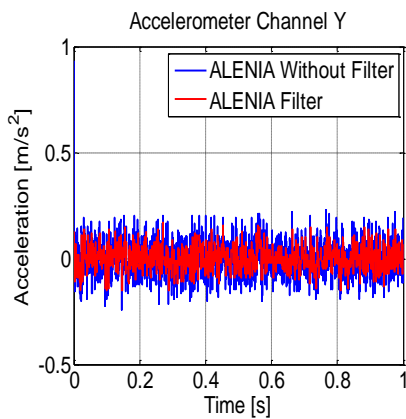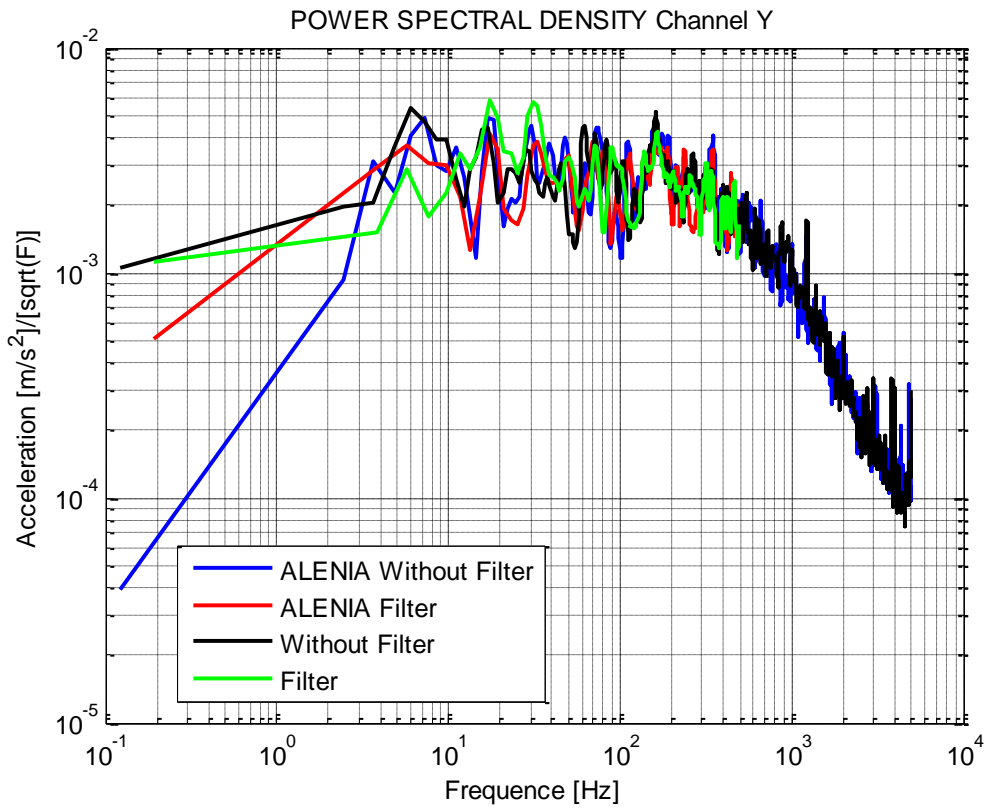
POWER SPECTRAL DENSITY Channel Y

TEST	CHANNEL	ZERO [V]	ZERO[M/S^2]	STANDARD DEVIATION[M/S^2]	AVERAGE[M/S^2]
Right inclination	Y	0.1239	1.5193	0.0712	18.7139

5.3.1.2.6 LEFT INCLINATION

In blue we can see 10000 samples at 10kHz; in red we can see the filter which is 1000 samples at 1kHz.
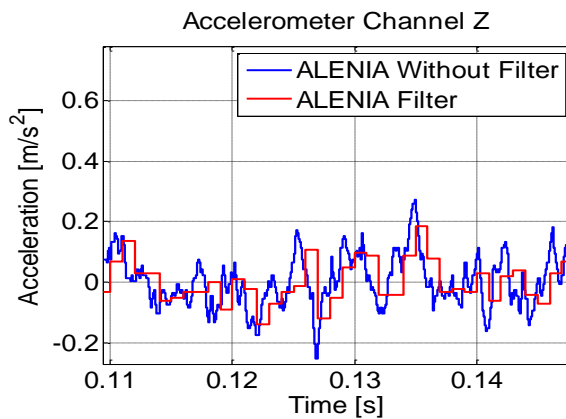
POWER SPECTRAL DENSITY Channel Y

TEST	CHANNEL	ZERO [V]	ZERO[M/S^2]	STANDARD DEVIATION[M/S^2]	AVERAGE[M/S^2]
Left inclination	Y	0.1228	1.5058	0.0695	18.7274

5.3.1.3 CHANNEL Z

5.3.1.3.1 SIDE VIEW

In blue we can see 10000 samples at 10kHz; in red we can see the filter which is 1000 samples at 1kHz.

POWER SPECTRAL DENSITY Channel Z
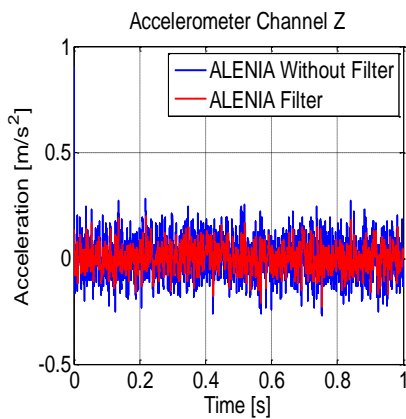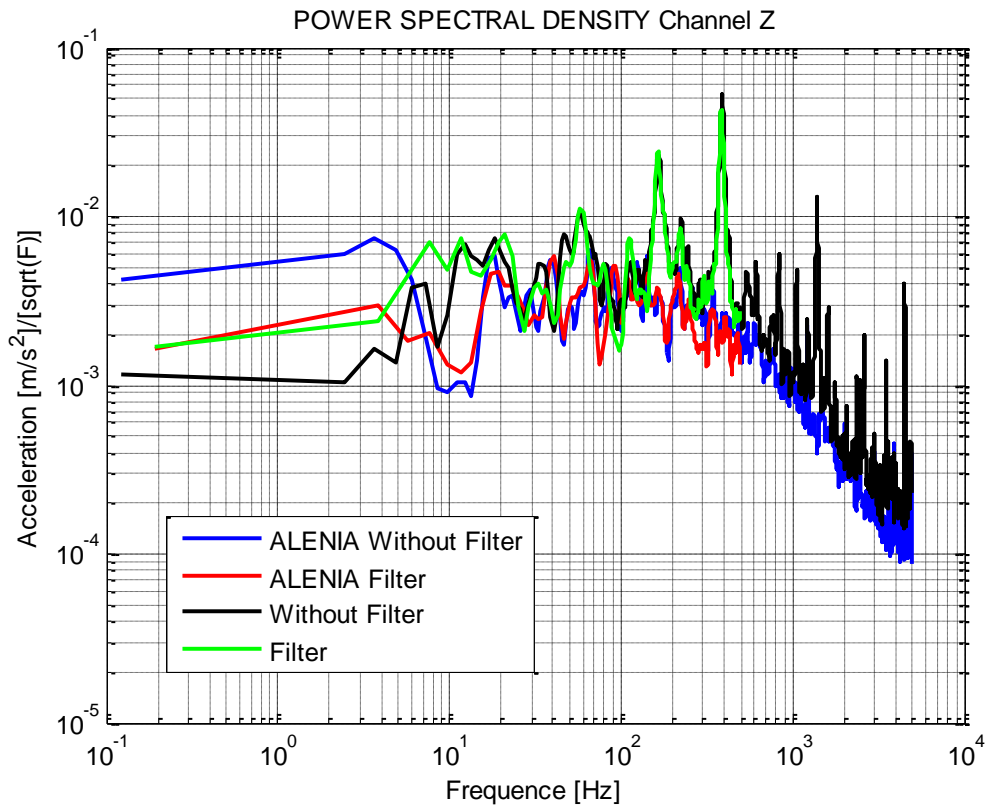
TEST	CHANNEL	ZERO [V]	ZERO[M/S^2]	STANDARD DEVIATION[M/S^2]	AVERAGE[M/S^2]
Side view	Z	0.6553	8.0973	0.0782	22.0073

As we can see in the power spectral density figure, the noise is smaller in the ALENIA's test than in the normal test. It is important to notice that the frequencies due to aliasing or external vibrations are reduce notoriously because the special optical table.

5.3.1.3.2   BOTTOM VIEW

In blue we can see 10000 samples at 10kHz; in red we can see the filter which is 1000 samples at 1kHz.

TEST	CHANNEL	ZERO [V]	ZERO[M/S^2]	STANDARD DEVIATION[M/S^2]	AVERAGE[M/S^2]
Bottom view	Z	0.3965	4.8622	0.0795	5.5610

5.3.1.3.3   FRONT INCLINATION

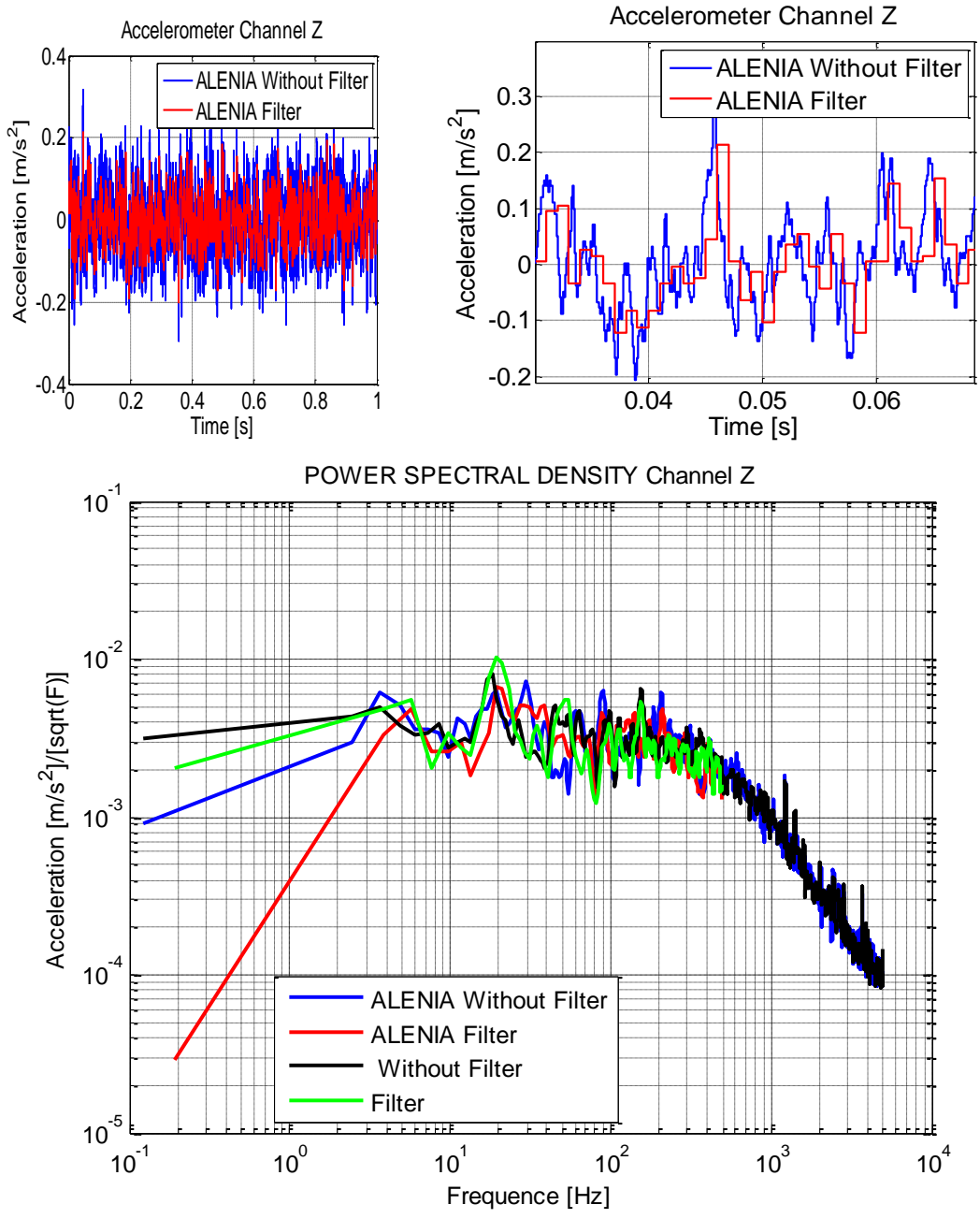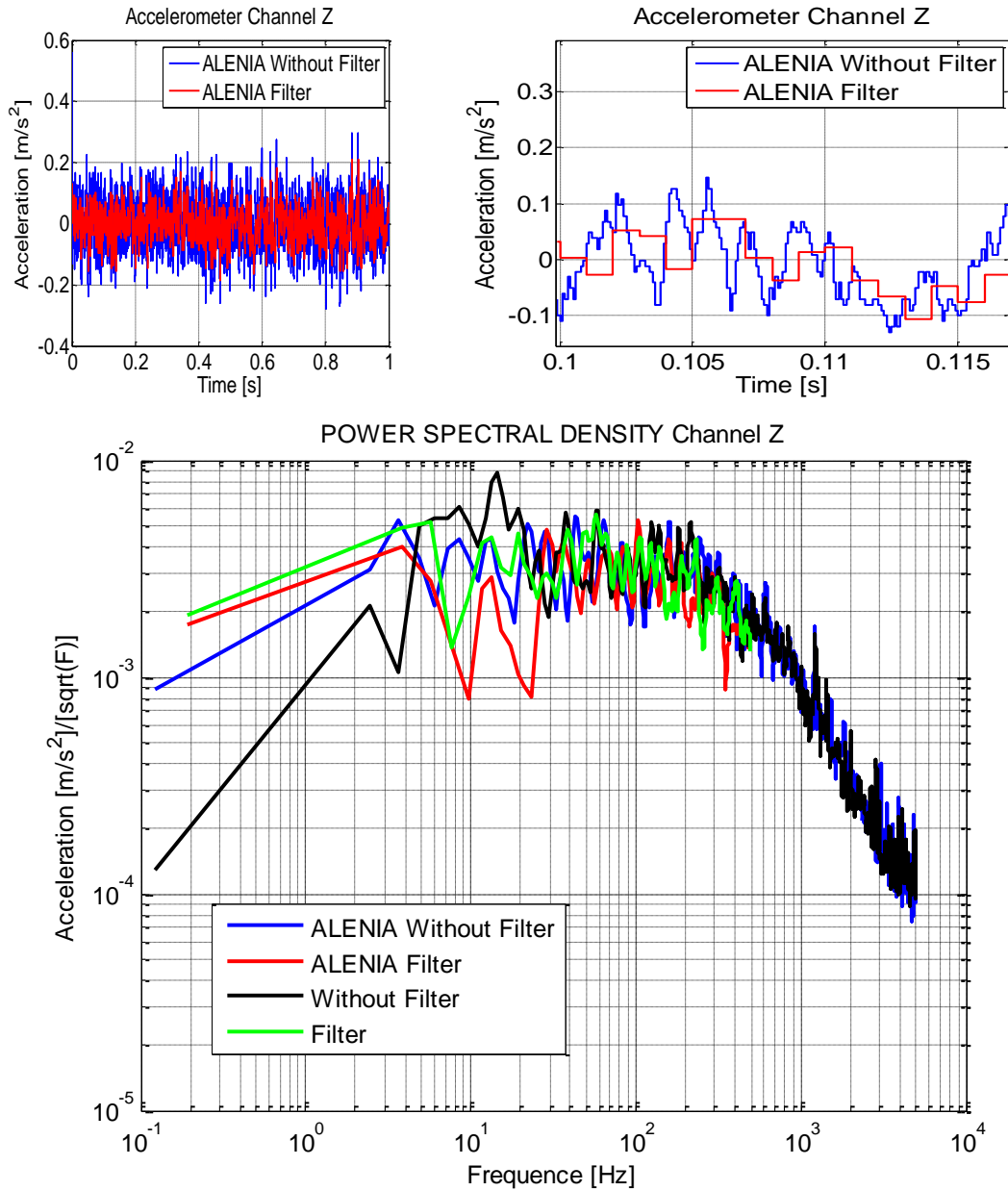In blue we can see 10000 samples at 10kHz; in red we can see the filter which is 1000 samples at 1kHz.

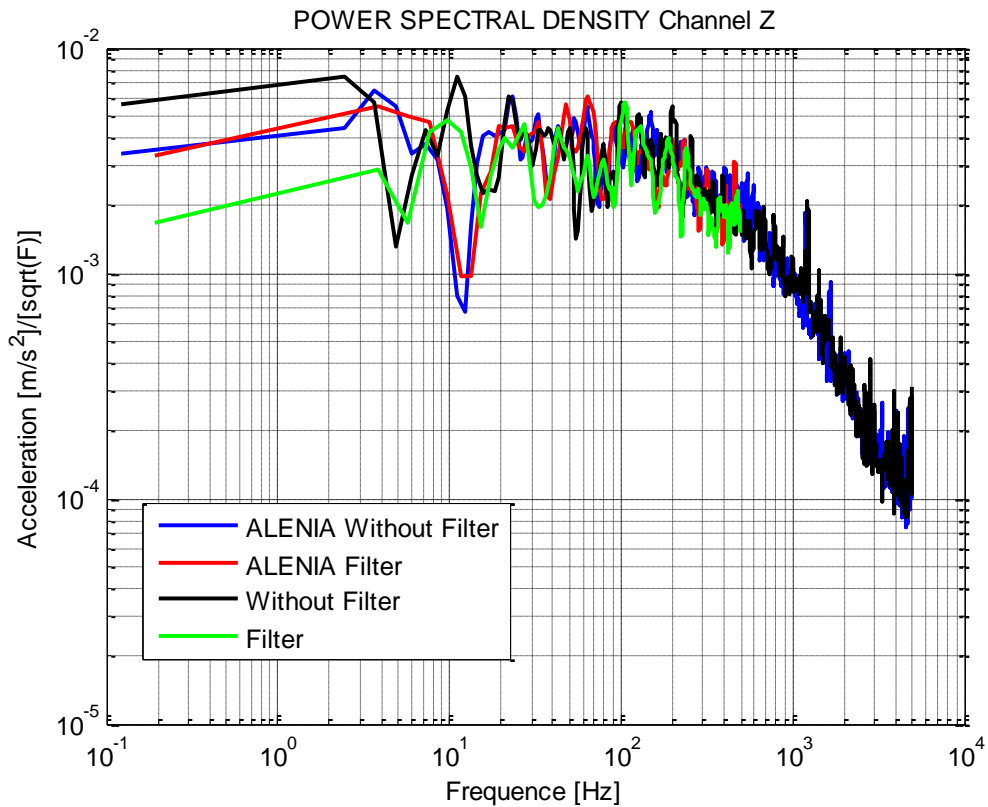| TEST	CHANNEL	ZERO [V]	ZERO[M/S^2]	STANDARD DEVIATION[M/S^2]	AVERAGE[M/S^2]
Front inclination	Z	0.5107	6.2621	0.0761	13.9711

5.3.1.3.4   BACK INCLINATION

In blue we can see 10000 samples at 10kHz; in red we can see the filter which is 1000 samples at 1kHz.

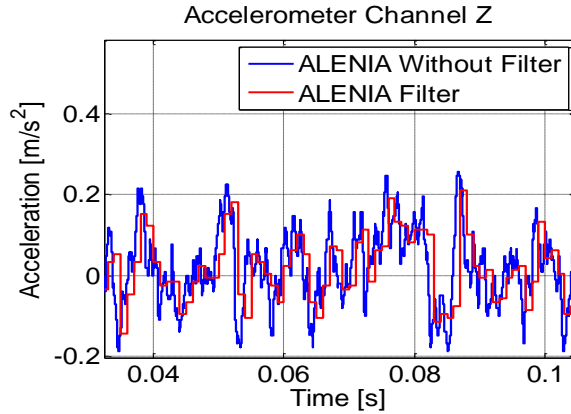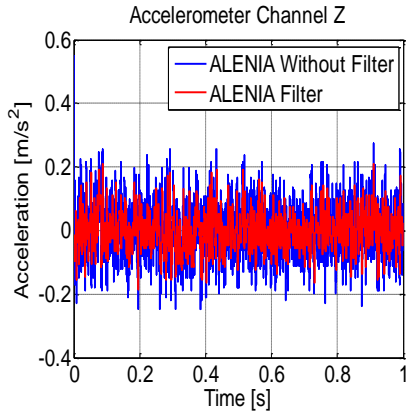| TEST	CHANNEL	ZERO [V]	ZERO[M/S^2]	STANDARD DEVIATION[M/S^2]	AVERAGE[M/S^2]
Back inclination	Z	0.5639	6.9144	0.0782	13.3189

5.3.1.3.5 RIGHT INCLINATION

In blue we can see 10000 samples at 10kHz; in red we can see the filter which is 1000 samples at 1kHz.

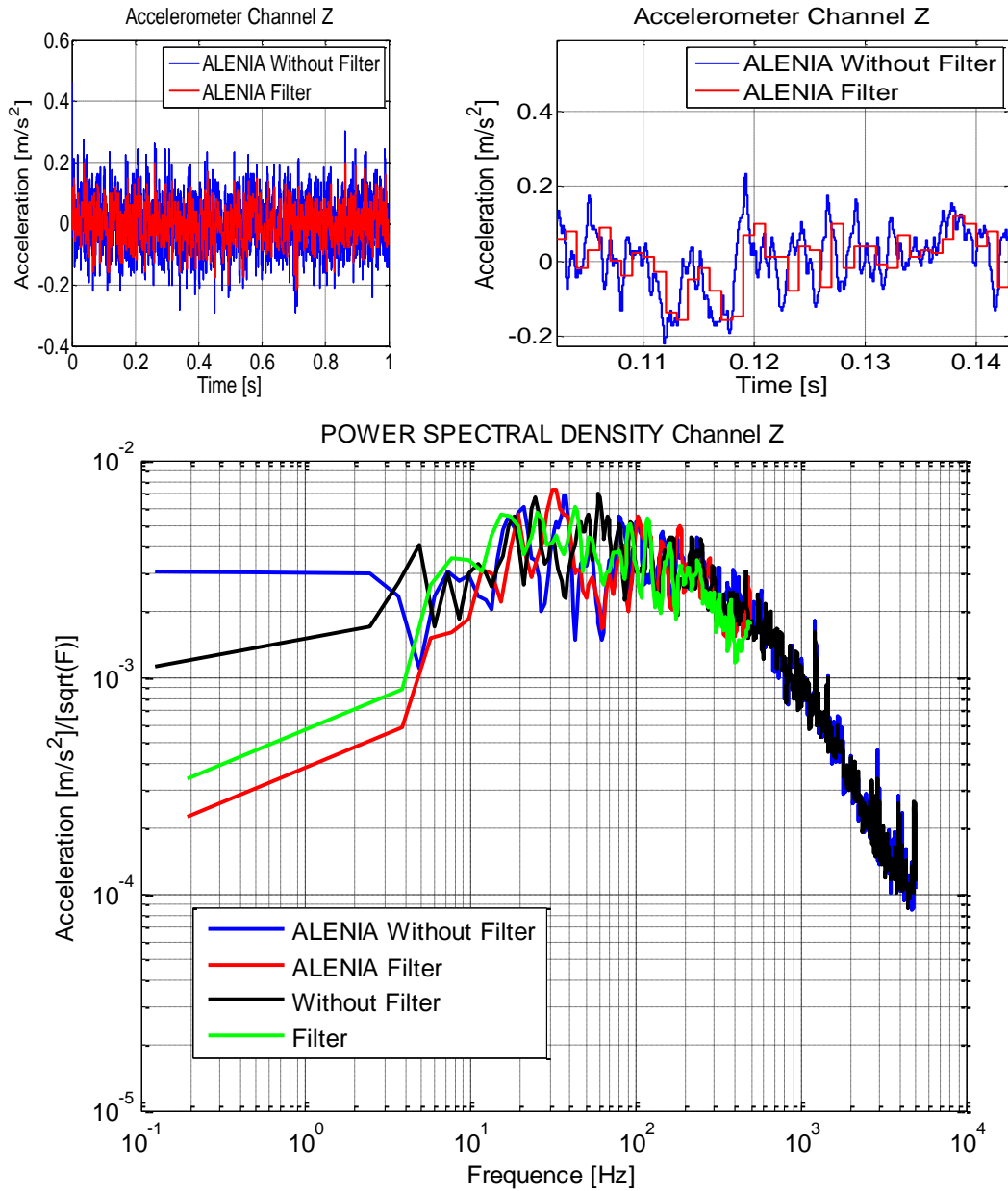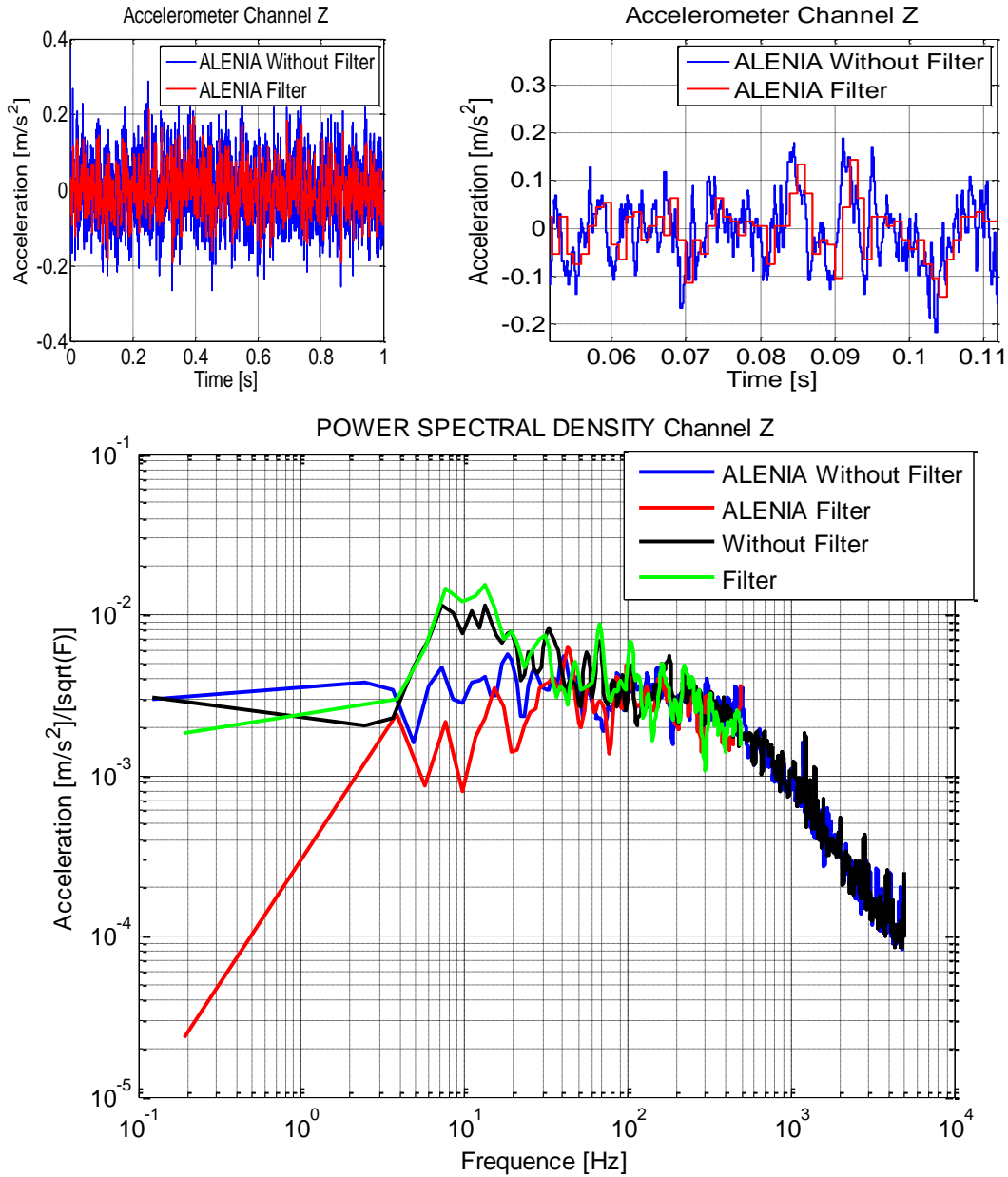| TEST	CHANNEL	ZERO [V]	ZERO[M/S^2]	STANDARD DEVIATION[M/S^2]	AVERAGE[M/S^2]
Right inclination	Z	0.5009	6.1418	0.0789	14.0914

5.3.1.3.6 LEFT INCLINATION

In blue we can see 10000 samples at 10kHz; in red we can see the filter which is 1000 samples at 1kHz.

TEST	CHANNEL	ZERO [V]	ZERO[M/S^2]	STANDARD DEVIATION[M/S^2]	AVERAGE[M/S^2]
Right inclination	Z	0.5481	6.7212	0.0782	13.5120

5.3.2 GYROSCOPE

5.3.2.1 GYROSCOPE WITH 4.5 AMPLIFIER

5.3.2.1.1 CHANNEL X

In blue we can see 10000 samples at 10kHz; in red we can see the filter which is 1000 samples at 1kHz.
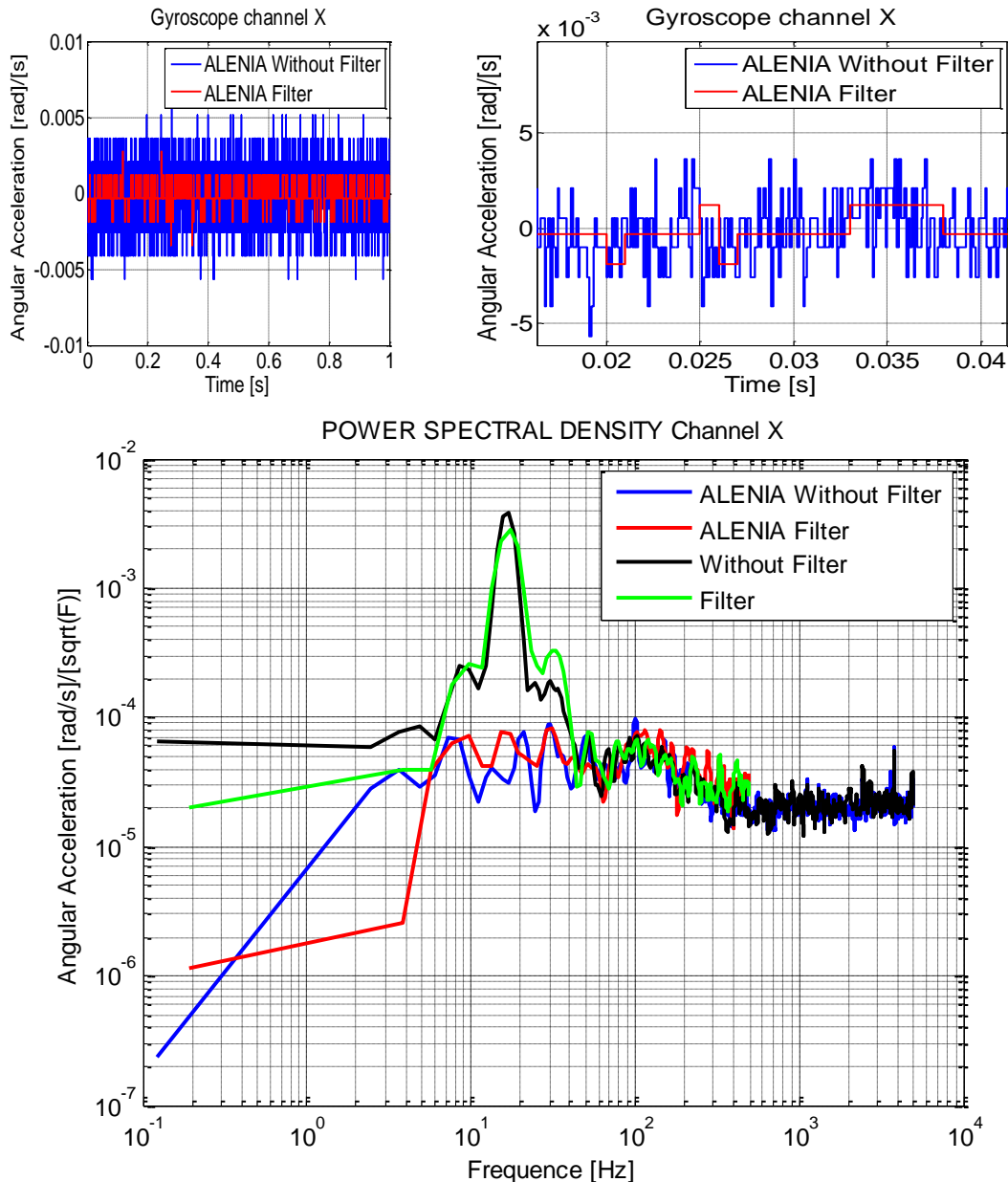
As we can see in the power spectral density figure, the noise is smaller in the ALENIA's test than in the normal test. It is important to notice that the frequencies due to aliasing or external vibrations are reduce notoriously because the special optical table.

In blue we can see 10000 samples at 10kHz; in red we can see the filter which is 1000 samples at 1kHz.
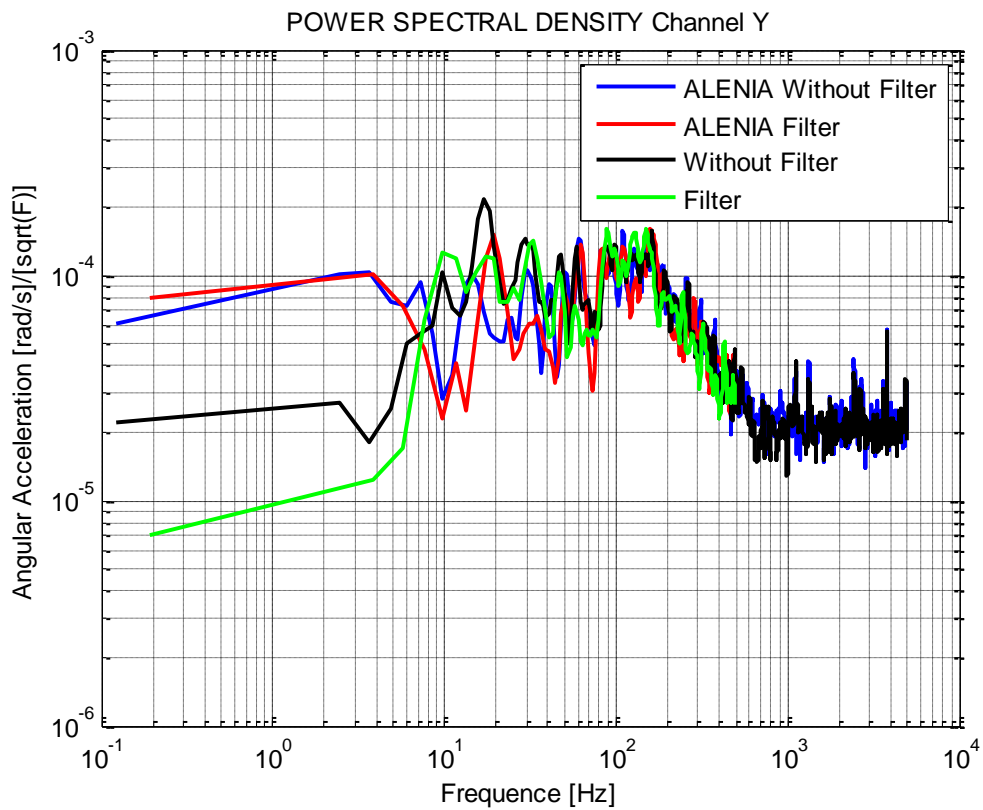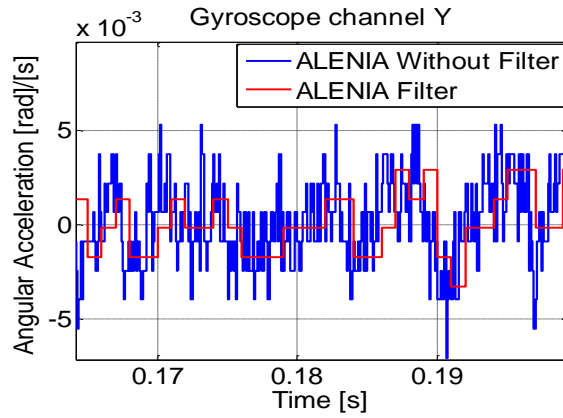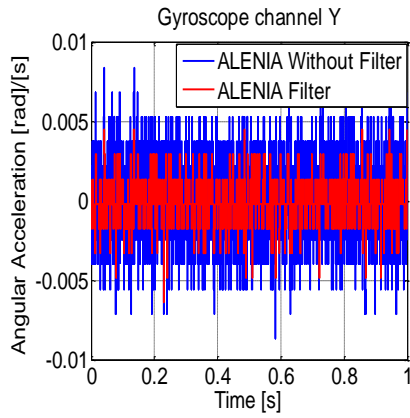
5.3.2.1.3 CHANNEL Z

In blue we can see 10000 samples at 10kHz; in red we can see the filter which is 1000 samples at 1kHz.

5.3.3 TABLE OF RESULTS
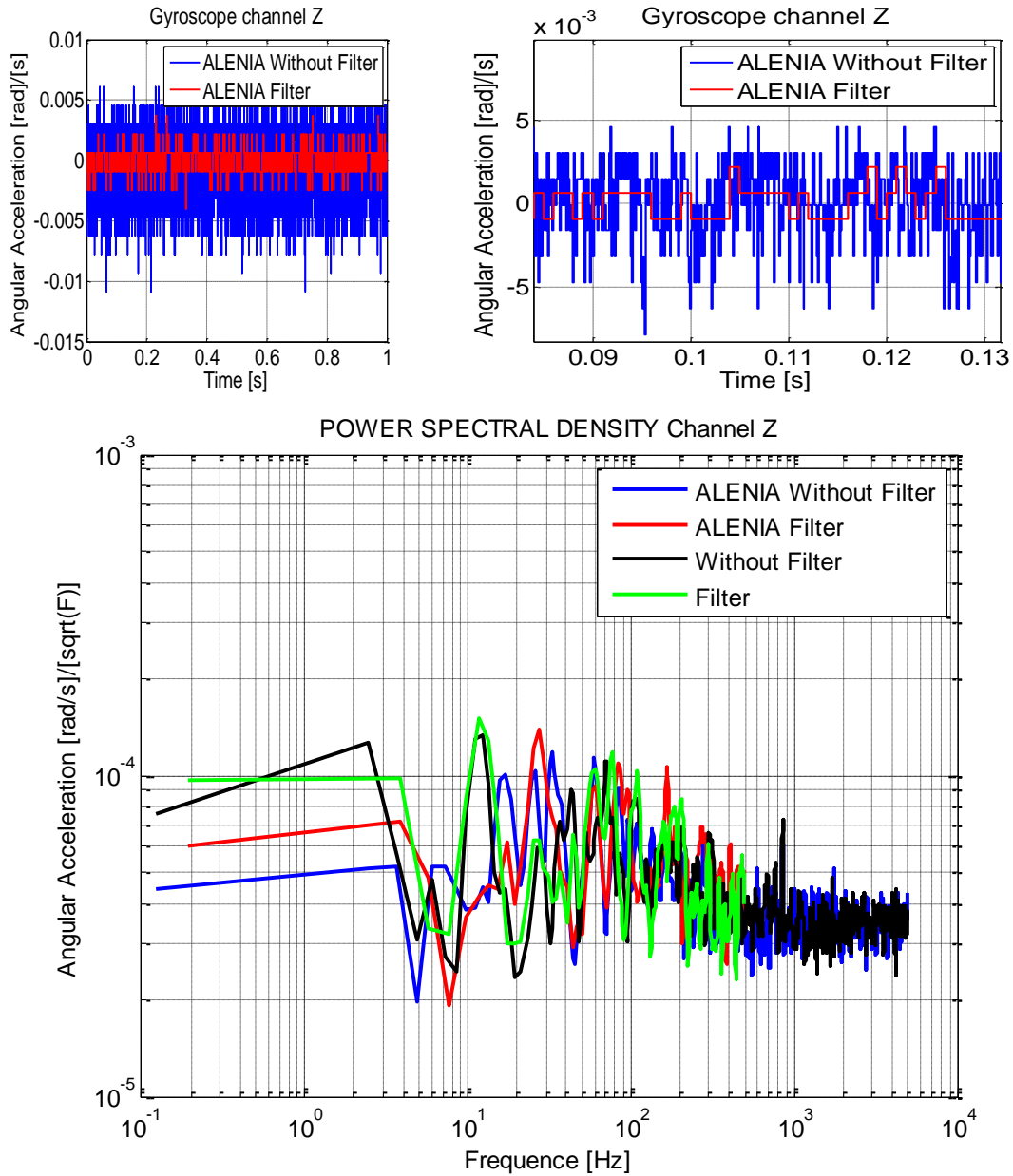
5.3.3.1 ACCELEROMETER

NUMBER	TEST	CHANNEL	ZERO [V]	ZERO[M/S^2]	STANDARD DEVIATION[M/S^2]	AVERAGE[M/S^2]
1.	Bottom view	X	0.3074	3.7692	0.0714	16.4640
2.	Bottom view	Y	0.0718	0.8804	0.0727	19.3528
3.	Bottom view	Z	0.3965	4.8622	0.0795	5.5610
4.	Side view	X	0.3319	4.0702	0.0676	16.1631
5.	Side view	Y	0.0745	0.9137	0.0702	19.3195
6.	Side view	Z	0.6553	8.0973	0.0782	22.0073
7.	Front inclination	X	0.3367	4.1289	0.0665	16.1044
8.	Front inclination	Y	-0.0130	-0.1594	0.0697	10.5825
9.	Front inclination	Z	0.5107	6.2621	0.0761	13.9711
10.	Back inclination	X	0.3181	3.9002	0.0685	16.3331
11.	Back inclination	Y	0.2521	3.0909	0.0705	26.9524
12.	Back inclination	Z	0.5639	6.9144	0.0782	13.3189
13.	Right inclination	X	0.1838	2.2536	0.0686	8.1696
14.	Right inclination	Y	0.1239	1.5193	0.0712	18.7139
15.	Right inclination	Z	0.5009	6.1418	0.0789	14.0914
16.	Left inclinat	X	0.4798	5.8840	0.0714	24.1593

	ion				
17.	Left inclinat ion	Y	0.12 28	1.5058	0.0695	18.7274
18.	Left inclinat ion	Z	0.60 83	7.4596	0.0759	12.7737

Table11. Accelerometer's result.

In table11 we can see that the standard deviation is smaller than the value of the datasheet, which is 0.108 m/s^2. Moreover, it is possible to calculate the measure of gravity, like mentioned before in **section 4.2.5.1.**

5.3.3.2 GYROSCOPE

NUMBER	TEST	CHANNEL	ZERO[Rad/S]	STANDARD DEVIATION[Rad/S]	AVERAGE[Rad/S]
1.	GYROSCOPE WITHOUT AMPLIFIER	X	0.0389	0.0029	11.7412
2.	GYROSCOPE WITHOUT AMPLIFIER	Y	0.4240	0.0041	11.3561
3.	GYROSCOPE WITHOUT AMPLIFIER	Z	0.0982	0.0033	11.6819
4.	GYROSCOPE WITH 4.5 AMPLIFIER	X	-0.0388	0.0017	2.6349
5.	GYROSCOPE WITH 4.5 AMPLIFIER	Y	0.3440	0.0023	2.2521
6.	GYROSCOPE WITH 4.5 AMPLIFIER	Z	-0.0719	0.0026	2.6680

Table12. Gyroscope's result.

The standard deviation expected for the gyroscope with amplifier is 0.015 rad/s for X -axis and Y-axis, and 0.0096 rad/s for Z-axis. As we can see in the table12, the standar desviation is very close to the expected one given by the datasheet. This means that the gyroscope works fine, and the data output will has small noise, then is a trust measure.

6. CONCLUSIONS

Despite of there are many sensors that are used by aircraft to make it more autonomous, the quadricopter Borea, because of its dynamics and ability to fly, uses the essential sensors to obtain the attitude of the aircraft on fly and has implemented control's algorithms to make the speed and flight path stabilization, making it unique in maneuverability providing a large capacity of flight.

The UBD4 was an optimum choice for the quadricopter Borea because its characteristics, contents the sensors and provide the connections to other devices, allow us to make software to simulate control algorithms for a soft landing.

Despite of there were some problems with the communication between the microcontroller and the EEPROM; because the communication introduce some errors to the lecture. The microcontroller allows us to obtain the sensor's lectures in the desired way, although there are many ways to program the microcontroller, we programmed it to make the instruction as fast as it can. The environment used to program is MPLAB IDE, it is an integrated development environment in which the user can write code, program PICs and even debug them in-circuit. Together with the in circuit debugger, the user can pretty much do everything the microcontrollers can offer.

The different acquisition times were possible to obtain due to the interruptions on the timer. There are 2 main interruptions; the first interruption is use to run the instruction where all data output of the ADC is save every 1ms; the second timer is use to run the instruction where all the data output of the magnetometer is save every 20ms.

This work has met the intended objectives of obtain in a synchronous way the lecture of all the sensors, with different acquisition time, to use them in the control of the quadricopter Borea.

In the result we can see that it is much better measure in a controlled environment because frequencies due to aliasing or external vibrations are reduced notoriously. For example, the next figure shows the power spectral density of one channel of the accelerometer.

POWER SPECTRAL DENSITY Channel Y
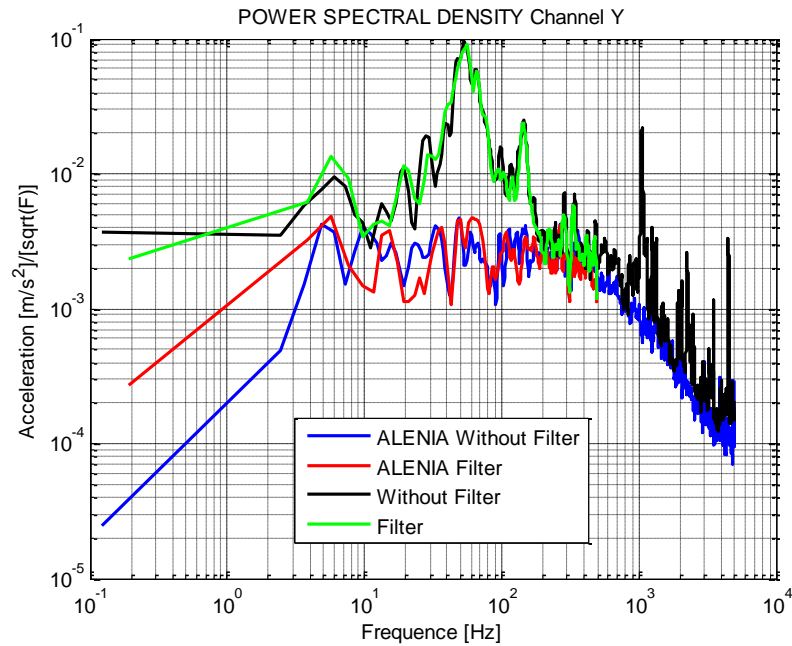
We can clearly see that the noise is smaller in the controlled environment (blue or red lines) than the uncontrolled environment, also the controlled environment does not present a peak of noise at 60 Hz like the uncontrolled environment. Moreover, if we compare the results of standard deviation of one measure in the two environments, we can see that the controlled environment has smaller standard deviation than the uncontrolled environment. For example, the next table shows the results of the gyroscope with amplifier channel X:

ENVIRONMENT	TEST	CHANNEL	ZERO[Rad/S]	STANDARD DEVIATION[Rad/S]	AVERAGE[Rad/S]
controlled	GYROSCOPE WITH 4.5 AMPLIFIER	X	-0.0388	0.0017	2.6349
Uncontrolled	GYROSCOPE WITH 4.5 AMPLIFIER	X	-0.0387	0.0053	2.6348

The standard deviation expected for the gyroscope with amplifier is 0.015 rad/s for X –axis.As we can see , the controlled environment presents 0.0017 rad/s, very close to the expected value , this means that the data from the gyroscope tends to be very close to the average. The gyroscope in an uncontrolled environment presents a bigger standard deviation due to the noise and vibration that affected it.

7. REFERENCE

1. http://www.theuav.com/. *http://www.theuav.com/*. [Online]

2. http://en.wikipedia.org/wiki/Abbe_error. *http://en.wikipedia.org/wiki/Abbe_error*. [Online]

3. **Enrico Canuto, Gianfranco Sechi.** *Spacecraft modelling and control.* 2012.

4. *SPACECRAFT SUN SENSORS .* s.l. : NASA, 1970. SP-8047.

5. **Needham, Joseph.** *Science and Civilization in China: Volume 4, Physics and Physical Technology; Part 2, Mechanical Engineering.* s.l. : Caves Books Ltd., 1986.

6. http://science.howstuffworks.com/gimbal1.htm. *http://science.howstuffworks.com/gimbal1.htm.* [Online]

7. **BASSI, DAVIDE.** *MISURA DELLA FUNZIONE DI DENSITA SPETTRALE DI UN SEGNALE ALEATORIO.* 1999.

8. http://cnx.org/content/m10656/latest/. *http://cnx.org/content/m10656/latest/.* [Online]

9. https://www.sparkfun.com/products/10582. *https://www.sparkfun.com/products/10582.* [Online]

10. **Keir, Hugh.** *UDB4 Quick START GUIDE.* 2012.

11. **Semiconductor, ON.** *NCP5500, NCV5500,NCP5501, NCV5501.* s.l. : Literature Distribution Center for ON Semiconductor, 2010.

12. *±1.5g, ±6g Three Axis Low-g Micromachined Accelerometer.* s.l. : Freescale Semiconductor, 2008. MMA7361L.

13. *ISZ-500 Single-Axis Z-Gyro.* s.l. : InvenSense Inc., 2010. PS-ISZ-0500B-00-06.

14. *Integrated Dual-Axis Gyro IDG-500.* s.l. : InvenSense, Inc., 1197 Borregas, Ave. Sunnyvale, CA 94089, USA, 2008. DS-IDG-0500B-00-01.

15. **Gill, A. E.** Atmosphere–Ocean Dynamics. [book auth.] J. R Holton. *An Introduction to Dynamic Meteorology, 3d edition.* s.l. : Academic Press, 1982.

16. *3-Axis Digital Compass IC HMC5883L.* s.l. : Honeywell, 2011. # 900405.

17. http://www.microchip.com/wwwproducts/devices.aspx?ddocname=en546064. *http://www.microchip.com/wwwproducts/devices.aspx?ddocname=en546064.* [Online]

18. *Section 7. Oscillator.* s.l. : Microchip Technology Inc, 2008. DS70186C.

19. *Section 11. Timers.* s.l. : Microchip Technology Inc., 2008. DS70205B.

20. *Section 10. I/O Ports.* s.l. : Microchip Technology Inc., 2008. DS70193C.

21. *Section 16. Analog-to-Digital Converter (ADC).* s.l. : Microchip Technology Inc., 2006. DS70183A.

22. *Section 19. Inter-Integrated Circuit™ (I2C™).* s.l. : Microchip Technology Inc., 2008. DS70195B.

23. **Gill, A. E.** Atmosphere–Ocean Dynamics. [book auth.] J. R Holton. *An Introduction to Dynamic Meteorology, 3d edition.* s.l. : Academic Press, 1982.